Aluminium Based Material Extrusion through Mathematical Contoured Die: Numerical & Experimental Investigation

Dissertation submitted in partial fulfilment

of the requirements of the degree of

Doctor of Philosophy

In

Mechanical Engineering

By

Sambit Kumar Mohapatra

(Roll Number-512ME1038)

Based on research carried out

Under the Supervision of

Prof. Kalipada Maity

July 2016

Department of Mechanical Engineering

National Institute of Technology Rourkela

Department of Mechanical Engineering

National Institute of Technology

July 27, 2016

Certificate of Examination

Roll Number: 512ME1038

Name: Sambit Kumar Mohapatra

Title of Dissertation: Aluminium Based Material Extrusion through Mathematical Contoured Die: Numerical & Experimental Investigation

We the below signed, after checking the dissertation mentioned above and the official record book (s) of the student, hereby state our approval of the dissertation submitted in partial fulfillment of the requirements of the degree of Doctor of Philosophy in Mechanical Engineering at National Institute of Technology Rourkela. We are satisfied with the volume, quality, correctness, and originality of the work.

Prof. Kalipada Maity
Supervisor

Prof. Susanta Kumar Sahoo
Member (DSC)

Prof. Bipin Bihari Verma
Member (DSC)

Prof. Swadesh Kumar Pratihar
Member (DSC)

Prof. Siba Sankar Mohapatra
Chairman (DSC)

Department of Mechanical Engineering
National Institute of Technology

Prof. Kalipada Maity
Professor

July 27, 2016

Supervisors' Certificate

This is to certify that the work presented in this dissertation entitled "*Aluminium Based Material Extrusion through Mathematical Contoured Die: Numerical & Experimental Investigation*" by "Sambit Kumar Mohapatra", Roll Number 512ME1038, is a record of original research carried out by him under my supervision and guidance in partial fulfillment of the requirements of the degree of *Doctor of Philosophy* in *Mechnical Engineering*. Neither this dissertation nor any part of it has been submitted for any degree or diploma to any institute or university in India or abroad.

Kalipada Maity
Professor

Dedication

to

“*My Parents*”

Sambit Kumar Mohapatra

Declaration of Originality

I, Sambit Kumar Mohapatra, Roll Number 512ME1038 hereby declare that this dissertation entitled "*Aluminium Based Material Extrusion through Mathematical Contoured Die: Numerical & Experimental Investigation*" presents my original work carried out as a doctoral student of NIT Rourkela and, to the best of my knowledge, it contains no material previously published or written by another person, nor any material presented by me for the award of any other degree or diploma of NIT Rourkela or any other institution. Any contribution made to this research by others, with whom I have worked at NIT Rourkela or elsewhere, is explicitly acknowledged in the dissertation. Works of other authors cited in this dissertation have been duly acknowledged under the section "Bibliography". I have also submitted my original research records to the scrutiny committee for evaluation of my dissertation.

I am fully aware that in case of any non-compliance detected in future, the Senate of NIT Rourkela may withdraw the degree awarded to me on the basis of the present dissertation.

July 27, 2016

NIT, Rourkela *Sambit Kumar Mohapatra*

Acknowledgement

The journey of reaching any milestone is never easy without a determined ambition, sincere dedication and a perfect person who can torch your path of ignorance. I am obliged to Prof. Kalipada Maity for being an embodiment of the constant source of inspiration and knowledge. Under his guidance, I have learnt the art of doing research.

I am thankful to Prof. Ranjit Kumar Sahoo, Director, NIT Rourkela and Prof. Siba Sankar Mohapatra, HOD, ME NIT Rourkela for their kind support and cooperation for the fulfilment of the work.

I must thank Prof. Sunil Kumar Sarangi, former Director, NIT Rourkela for his motivational speeches at regular interval of my tenure. At the same time, I am thankful to the teaching staffs of the department, whose valuable suggestions at the right time helped me reaching the goal.

I sincerely acknowledge the helping hand of the laboratory staffs and other nonteaching staffs of NIT Rourkela, for their timely help and support. My friends, whose consolation during the bad days and encouraging words, helped me maintain the equilibrium during the course of fulfilling my ambition.

After all, the love of family and relatives whose blessings are like the rays of sunshine help me seeing my inner strength and march towards the goal.

Lastly, I must thank the invisible force which we define as the almighty God for giving me patience and driving me towards a never ending process of learning.

July 27, 2016

NIT, Rourkela *Sambit Kumar Mohapatra*

Abstract

The metal forming process is preferable for manufacturing the parts of moderate complexity and greatly diversified profiles for the larger volume of productions to reduce the tooling cost. Energy saving, less scrap generation and near net shape production with better mechanical properties along with high production rate have enhanced the specific forming process, extrusion, for the production of long straight metal products. The huge demand of aluminium alloy in the extrusion industry for fulfilling the market requirements in the sector of building and architecture, construction, automobile and transport system, electrical and electronics, aerospace, and heat exchangers tends to optimize the process for improved process efficiency as well as product quality.

Prediction of the influence of process parameters is very difficult owing to the concealed material deformation during extrusion. Due to this reason, an illustrious finite element analysis tool (DEFORM ^{TM}) was adopted to investigate the process. The simulations were performed to ascertain extrusion load, effective stress, effective strain and temperature distribution for square to square extrusion process. To decipher the effect of die length, ram velocity and extrusion ratio in the process, simulations were carried out by varying the variables in a wide range with different types of dies. The process was also employed for the investigation of the round to square extrusion considering the same parameters along with punch shape for Al-6063 alloy. Influence of die profile plays a predominant role in predicting the ultimate load requirements and flow characteristics. Considering the die profile an important component, the profile for round to square shape has been developed by following cosine, linear converging, elliptic, hyperbolic and 3rd order polynomial laws. Considering the above die profiles the simulations were conducted with optimised process parameters to find out a suiatable die profile. The simulations were validated with high-temperature experimentations. To improve the product properties, aluminium metal matrix composites (AMMC) prepared by powder metallurgy (PM) route has been extruded. Four different reinforcing elements of 2 wt. % (Zn, Ti, Soda lime silica glass and ZrO2) were added to Al / 5 wt. % of Mg / 1 wt. % of Gr matrix. To avoid the product defects, mathematically contoured cosine profiled die was used for the thermo-mechanical treatment. The improvement of the product properties has been studied.

The optimum parameters before experimentation can be set by utilising the finite element tool successfully. Computerised finite element techniques are the best suitable

technique to understand the concealed operations like extrusion. The optimum ranges for the extrusion of simple square bar section from the same shape billet and round to square extrusion has been established. The cosine profiled die for both kinds of extrusion as well as PM composite was found suitable as it generates lesser velocity relative difference at die exit. A significant amount of property improvement was observed in the AMMC after thermo-mechanical treatment.

Keywords: Extrusion; Die-profile; FEM; DEFORM; VRD

Contents

Certificate of Examination ..... **ii**

Supervisors' Certificate ..... **iii**

Dedication ..... **iv**

Declaration of Originality ..... **v**

Acknowledgement ..... **vi**

Abstract ..... **vii**

Contents ..... **ix**

List of figures ..... **xiii**

List of tables ..... **xvii**

Nomenclature ..... **xviii**

1. Introduction **1**

1.1 Background 1

1.2 Motivation to the research 3

1.3 Research objective 4

1.4 Organization of the thesis 4

2. Literature Survey **6**

2.1 Overview 6

2.2 Process control 6

2.2.1 Die length or semi-angle 7

2.2.2 Friction condition 7

2.2.3 Temperature and ram velocity 9

2.3 Tooling developments 11

2.4 Material developments 15
2.5 Summary 21
3. Investigation of square bar extrusion from same shape billet using FEM Analysis 22
3.1 Overview 22
3.2 Finite element analysis 23
3.2.1 Formulation of a new problem 24
3.2.2 Thermal conditions formulation 25
3.2.3 Boundary conditions 26
3.2.4 Pre-processor 27
3.2.4.1. Simulation control 27
3.2.4.2. Materials 27
3.2.4.3. Object definition 27
3.2.4.4. Inter-object relation 28
3.2.4.5. Boundary condition 28
3.2.5 Simulation engine 28
3.2.6 Post processor 29
3.3 Die profile design and modelling 29
3.4 Results and discussion 32
3.4.1 Effect of die profile and die length 34
3.4.2 Effect of ram velocity and extrusion ratio 38
3.4.3 Study of flow pattern and velocity relative difference 42
3.5 Conclusions 43
4. Extrusion Analysis of Al-6XXX through Linear Converging Die 45
4.1 Overview 45

4.2 Determination of flow stress and friction factor 46
4.3 Modelling of extrusion 48
4.4 Results and discussion 48
4.4.1 Flow stress and friction condition 48
4.4.2 FEM analysis 50
4.4.2.1 Effect of friction 51
4.4.2.2 Effect of die length 54
4.4.2.3 Velocity relative difference (VRD) 55
4.4.2.4 Effect of punch shape 56
4.4.3 Experimental investigation 58
4.4.3.1. The test rig 59
4.4.3.2. Study of microstructural effect and microhardness 65
4.5 Conclusions 67
5. Round to Square Extrusion through Converging Die 69
5.1 Overview 69
5.2 Development of mathematically contoured die profiles 70
5.3 Finite element modelling 75
5.4 Results and discussion 76
5.5 Experimental investigation 79
5.5.1 The test rig 81
5.5.2 Experimental procedure 86
5.5.3 Flow pattern study 87
5.6 Conclusions 89
6. Extrusion of Aluminium MMC through Cosine Die 91
6.1 Overview 91

6.2 Sample fabrication and characterisation 92
6.2.1 Powder selection and characterisation 92
6.2.2 Blending of the mixture 94
6.2.3 Double axial cold compaction 95
6.2.4 Controlled atmospheric sintering 96
6.2.5 Characterisation of sintered samples 97
6.2.5.1 Density 97
6.2.5.2 Hardness test 98
6.2.5.3 Wear test 98
6.2.5.4 Three point flexural test 100
6.2.5.5 Scanning electronic microscopy 100
6.3 Secondary Processing (Hot extrusion) and characterisation 101
6.3.1 Hot extrusion 101
6.3.2 Characterisation of extruded specimen 101
6.4 Results and discussion 102
6.4.1 Physical characteristics of the powders 102
6.4.2 Density analysis 103
6.4.3 Microstructural studies 106
6.4.4 Mechanical testing 108
6.4.4.1 Compression test of sintered specimen 108
6.4.4.2 Micro-hardness 110
6.4.4.3 3-point bend test and factography 110
6.4.4.4 Wear test 113
6.4.4.5 Wear microscopy 116
6.4.4.6 Load requirement 119
6.5 Conclusions 120

7. Closure..... 122

References 125

List of figures

Figure 1.1: (a) Passenger carrier design of high-speed train ICE 1 of Deutsche Bahn AG (b) bus body (c) high-efficiency heatsink (d) window frame with thermal brake [4] 2
Figure 3.1: Major variable parameters of DEFORM-3D 26
Figure 3.2: Comparative die profile curves 30
Figure 3.3: Solid model cross section view of (a) Cosine, (b) LC and (c) shear die. 30
Figure 3.4: Load versus punch stroke/billet diameter for T shaped compression 33
Figure 3.5: Compression test comparison. 33
Figure 3.6: Variation of comparative load versus stroke 34
Figure 3.7: Variation of load versus stroke (cosine profiled die) 35
Figure 3.8: Variation of load versus stroke (linear converging die) 35
Figure 3.9: Variation of load w.r.t die length for (a) 3.30-R and (b) 9.47-R. 36
Figure 3.10: Effective stress Distribution & Load prediction graph for 9.47-R by (a) cosine (b) LC and (c) shear faced die 37
Figure 3.11: Effective (a) stress, (b) strain and (c) temperature distribution for 9.47-R by cosine die 38
Figure 3.12: (a) Effective stress, (b) effective strain and (c) temperature distribution for 9.47-R by L.C die 39
Figure 3.13: Variation of load versus stroke at different ram velocities 40
Figure 3.14: Variation of load versus stroke at different ram velocities 40
Figure 3.15: Variation of load versus stroke at different ram velocities 41
Figure 3.16: Maximum load versus extrusion ratio 41
Figure 3.17: Flow pattern study of (a) shear faced (b) cosine profile and 42
Figure 3.18: VRD (%) versus Extrusion ratio for cosine as well as LC dies 43
Figure 4.1: Pre-tested specimen along with the tested specimen 47
Figure 4.2: (a) The hot compression set up during operation (b) Inside view of the furnace . 47
Figure 4.3: Initial ring specimen along with the tested specimen 47
Figure 4.4: True stress versus true strain at a strain rate of 0.1 s^{-1} 49
Figure 4.5: Standard calibration curve for ring specimen of 6:3:2 dimension 50
Figure 4.6: Variation of load versus stroke for extrusion ratio-2 52
Figure 4.7: Variation of load versus stroke for extrusion ratio-3.33 52
Figure 4.8: Variation of load versus stroke for extrusion ratio-10 53

Figure 4.9: Variation of maximum extrusion pressure w.r.t frictional co-efficient..... 53
Figure 4.10: Variation of maximum load w.r.t die length..... 54
Figure 4.11: VRD versus shear friction coefficient 55
Figure 4.12: Variation of max pressure w.r.t VRD..... 56
Figure 4.13: (a) 2D drafting of punch shapes and (b) flow grid pattern 57
Figure 4.14: Variation of Load w.r.t stroke by different punch shape..... 58
Figure 4.15: Variation of load versus stroke by different punch shape 59
Figure 4.16: 2-D drafting as well as the setup during experimentation 60
Figure 4.17: Punch holder 61
Figure 4.18: Punch 61
Figure 4.19: Container..... 62
Figure 4.20: Linear converging round to square split die 63
Figure 4.21: Die holder 63
Figure 4.22: Support plate 64
Figure 4.23: Variation of load w.r.t stroke 64
Figure 4.24: Experimented samples..... 65
Figure 4.25: Microstructural effect 65
Figure 4.26: Micro-hardness testing 66
Figure 4.27: Hardness of the product across the extrusion direction..... 66
Figure 4.28: Hardness of the product along the extrusion direction..... 67
Figure 5.1: Round to square line diagram of cosine profiled die (a) isometric view in one quadrant and (b) front view with 18 divisions, 10 degrees each. 70
Figure 5.2: Three-dimensional coordinates of the cosine die profiles in one quadrant. 72
Figure 5.3: Three-dimensional coordinates of the linear converging die profiles in one quadrant. 73
Figure 5.4: Three-dimensional coordinates of the hyperbolic die profiles in one quadrant. .. 73
Figure 5.5: Three-dimensional coordinates of the elliptic die profiles in one quadrant. 74
Figure 5.6: Three-dimensional coordinates of the 3rd order polynomial die profiles in one quadrant. 75
Figure 5.7: Simulated extrusion of the alloy by DEFORM-3D..... 76
Figure 5.8: Strain-rate distribution across the billet through (a) cosine (b) linear converging (c) hyperbolic (d) elliptic (e) 3rd order polynomial die profile..... 77
Figure 5.9: Effective-strain distribution across the billet through (a) cosine (b) linear converging (c) hyperbolic (d) elliptic (e) 3rd order polynomial die profile. 78

Figure 5.10: Load versus stroke for extrusion through different die profile. 79
Figure 5.11: Sequences of die making process (a) SolidWork's model (b) copper tool (c) Split cosine die. 80
Figure 5.12: 2 D drafting of the tooling setup. 81
Figure 5.13: The assembled tooling setup 82
Figure 5.14: Punch holder 83
Figure 5.15: Punch 84
Figure 5.16: Container 84
Figure 5.17: Cosine profiled split die 85
Figure 5.18: Die holder 85
Figure 5.19: Support plate 86
Figure 5.20: Extruded specimen 87
Figure 5.21: Variation of load w.r.t stroke 87
Figure 5.22: Experimental study flow pattern. 88
Figure 5.23: Extrusion Flow pattern analysis by FEM grid lines through (a) cosine (b) linear converging (c) hyperbolic (d) elliptic and (e) 3rd order polynomial die. 89
Figure 6.1: Detailed work plan for the study 93
Figure 6.2: Centrifugal blender 95
Figure 6.3: (a) Hydraulic press used for compaction (b) 2-D drafting of the process. 96
Figure 6.4: Controlled atmospheric furnace. 96
Figure 6.5: Variation of temperature w.r.t time 97
Figure 6.6: Density measurement kit with analytical balance. 98
Figure 6.7: Schematic layout of pin-on-disc wear testing apparatus. 99
Figure 6.8: Wear testing apparatus 100
Figure 6.9: 3-point bend test set-up 100
Figure 6.10: SEM images of (a) Al (b) Mg (c) Gr (d) Zn (e) Glass (f) Ti and (g) ZrO2 powder 104
Figure 6.11: Comparative density analysis 105
Figure 6.12: Relative porosity of the specimen 105
Figure 6.13: Microstructures of materials after extrusion 107
Figure 6.14: Stress strain plot for (a) sample-1, (b) sample-2, (c) sample-3, (d) sample-4 .. 109
Figure 6.15: Micro-Hardness of the samples 110
Figure 6.16: TRS of the sintered specimen 111
Figure 6.17: TRS of the extruded specimen 112

Figure 6.18 Factography of the extruded specimen (a) for sample-1(b) for sample-2 (c) for sample-3 (d) for sample-4 112
Figure 6.19: Wear rate for sample type-1 114
Figure 6.20: Wear rate for sample type-2 114
Figure 6.21: Wear rate for sample type-3 115
Figure 6.22: Wear rate for sample type-4 115
Figure 6.23: FESEM immages of the worn surfaces 119
Figure 6.24: Variation of load w.r.t stroke 120

List of tables

Table 3.1: Parameters considered for simulation 31
Table 3.2: Properties of AA-6063 32
Table 3.3: Flow stress data for AA-6063 at different strain and strain rates 32
Table 4.1: Parameters considered for simulation 48
Table 4.2: Properties of AA-6063 48
Table 4.3: list of individual tooling components 60
Table 5.1: List of individual components 81
Table 6.1: List of machineries used during this work 94
Table 6.2: Compositional details of the MMC 94
Table 6.3: variable parameters selected for experimentation 99
Table 6.4: Physical characteristics of the powders 102
Table 6.5: Density analysis for four specimen 105
Table 6.6: L9 orthogonal array 113

Nomenclature

A	Half width / depth of the extrudate
L	Length of the die
m	Shear friction coefficient
n	Strain hardening coefficient
R	Radious of the billet
T	temperature
V	Ram velicity
W	Half width / depth of the billet
σ	Flow stress of the billet material
τ	Shear stress
$\bar{\varepsilon}$	Effective strain
$\dot{\bar{\varepsilon}}$	Effective strain rate
k	Thermal conductivity
$\dot{r}$	Heat generation rate
T	Temperature
ρ	Density
c	Specific heat
α	Coefficient of conversion of mechanical energy to heat energy
q_n	Heat flux
Δv_n	Penetrating velocity
Δv_s	Sliding velocity
v_a	Average velocity
v_i	Velocity of individual component
RPM	Revolution per minute
w.r.t	With respect to
VRD	Velocity relative difference
LC	Linear converging

Chapter 1

Introduction

1.1 Background

The process of manufacturing a long straight product having a determined cross section by inducing a severe compressive stress in the object and confining the flow through a designed die profile, which closely resembling the product cross section is cognised as extrusion. Depending on the process variables or flexibility provided by the process it is recognized as hot, warm or cold extrusion, direct, indirect or hydrostatic extrusion, lubricated or unlubricated extrusion, metal, plastic or ceramic extrusion, etc.. The process pertained to assorted variables which need to be restrained by the optimum ranges during extrusion for the improvement of process efficiency and product quality. The demand of aluminium alloy in the extrusion industry for fulfilling the market requirements in the sector of building and architecture, construction, automobile and transport system [1], electrical and electronics, aerospace [2], and heat exchangers is due to its unlimited possibilities in product design. The 25% of the wrought aluminium semi-finished products are extruded. A better formability condition is satisfied by aluminium alloys due to their face-cantered cubic structure with twelve slip planes combined with high stacking fault energy. The demand for extruded aluminium products are rising significantly because of the abundant availability of raw material, better performance characteristics, improved production volume and finishing of the product. An illustration has been presented in Figure 1.1 which shows the versatile applications of extrusion products and the complexity involved with the profile.

In case of few special demands the softer aluminium alloys like 1XXX, 6XXX series and 3003,5152,5052 are cold extruded [3] But most of the products are hot extruded due to improved flow characteristics at high-temperature conditions. A number of variable parameters either state variable or internal variables are involved with the process. Few state variables having a significant effect on the process are operating temperature, extrusion ratio, friction condition, die geometry and ram velocity. Few internal variables (chemical composition of the work material, prior strain history, grain size, metallurgical structure, etc.) having the influence on the process need prerequisite treatments. All these

variables are significant in response to process and product importance. Not only these variables but also the die profile which controls the flow characteristics directly, must be investigated for the improvement of the product as well as process.

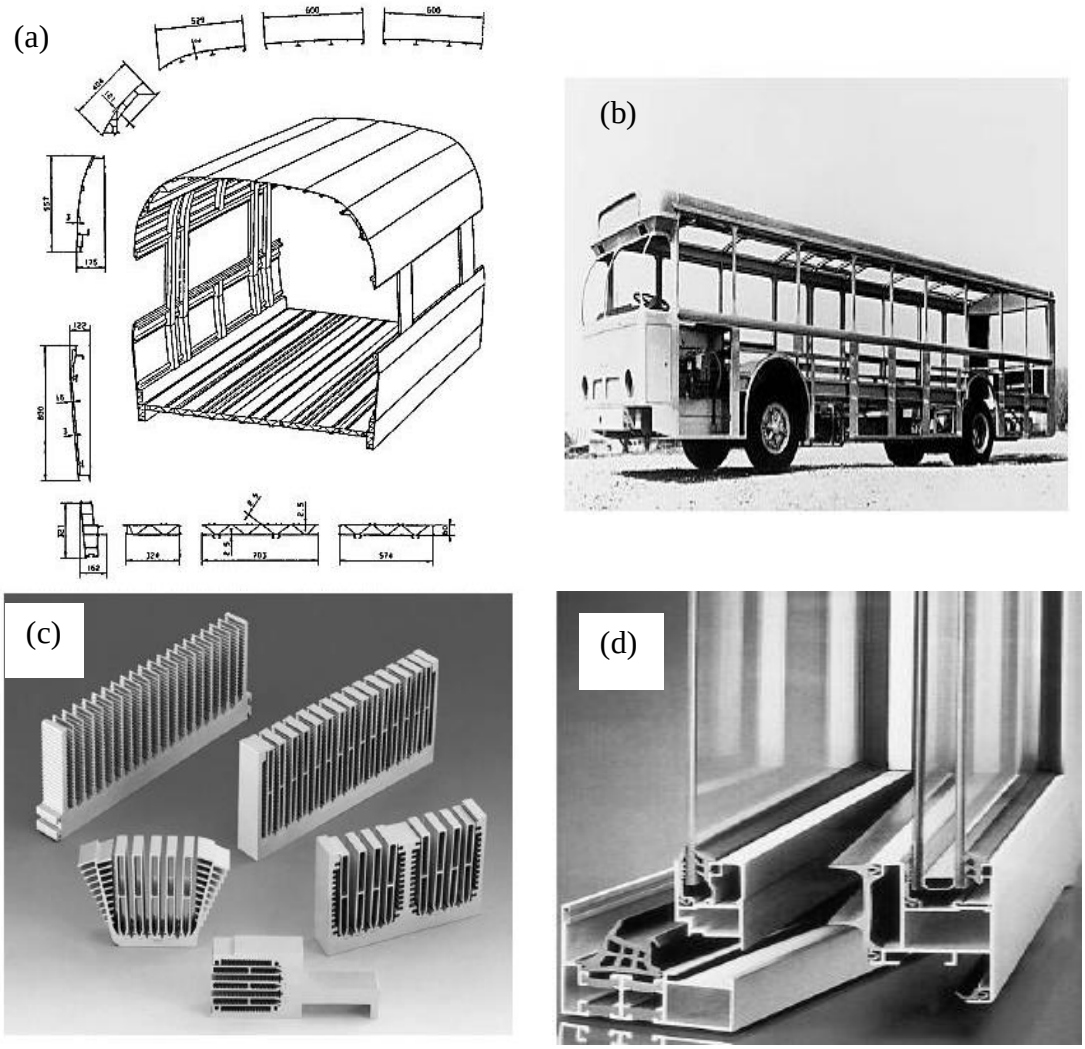

Figure 1.1: (a) Passenger carrier design of high-speed train ICE 1 of Deutsche Bahn AG (b) bus body (c) high-efficiency heatsink (d) window frame with thermal brake [4]

The application of computerised finite element analysis (FEA) nowadays assists to simulate the metal forming problems to anticipate the effects of the variables on the outcomes. The current trend is to investigate the process by FEA for improvement and optimisation of the process by avoiding traditional expensive experimental trials. There are a number of commercial finite element codes such as FORGE^{TM}, HyperXtrude [5, 6], LS-DYNA, SUPER-FORGE^{TM}, Q-FORM^{TM}, ABAQUS^{TM} [7], DEFORM^{TM} [8-10] which have been employed for the metal forming analysis successfully. The user defined local mesh density, user-friendly graphical interface, automatic remeshing facility available with DEFORM^{TM} has already been proved to be robust and accurate in industrial applications.

The internal variables, associated with the billet used in the process need to be concentrated before the experimentation. Among the state variables extrusion ratio and die length is predefined during the die design stage for the tooling as per the product desired. Other variables like ram velocity, operating temperature and friction condition need the instant care during experimentation. The afore-mentioned three parameters are interrelated each other. The optimal set of the process variables after FEA can be implemented during extrusion but to design a die profile remains a major challenge to the designer. Die profile has a major role in preventing redundant work by avoiding dead metal zone to improve the process efficiency as well as to improve the uniformity of velocities across the extrudate at die exit [11].

1.2 Motivation to the research

Aluminium is the second highest abundant metal present in the lithosphere of the earth. The most of the aluminium products are manufactured by forming process. The dominant percentage of aluminium based products is produced by extrusion [12] and the process of near net shape manufacturing disburses more power. To save energy by improving production efficiency with the proper concern of product quality, the variable process parameters need to be optimised. The complete research under extrusion can be focused into three categories to accomplish the objective. Those may be study of the effect of variable process parameters, study and development of the tooling setup and improvement of the billet material.

It is evident from the exhaustive literature survey that most of the work are concentrated on estimating the extrusion load by implementing numerical mathematical models. In few of the works die profile has also been designed and comparative analysis has been carried out for improving the die profile. However, no concrete work have been reported yet which relates the state variables with the energy requirement of extrusion process. A comparative flow analysis of the metal inside the die is necessary to observe the effect of die profile. But no experimental validation of the effect through designed die profile was carried out.

Extrusion of the metal matrix composites manufactured by powder metallurgy (PM) route is the emerging area of research these days. Trials have always been made to ameliorate the product property by reinforcing the various types of ingredients in the aluminium matrix because of its excellent mechanical, tribological and thermal properties. For improving the mechanical and surface properties of extruded composites, the die

profile plays a major role. But there is no work reported till date where extrusion of the MMC by PM route through mathematical contoured die has been experimented.

1.3 Research objective

The objective of the research is to improve the cold as well as hot extrusion process efficiency for aluminium alloy by investigating the influence of the process parameters by finite element modelling and simulation technique. The three broad areas of the research i.e., variable parameters, tooling set-ups and billet material have been concentrated to improve the product quality with lesser energy consumption. In the present investigation, a number of developments in the numerical simulation of extrusion as well as an experimental trial are reported. Attention is focussed on the following specific descriptions:

- Effect of the variable process parameters for the square to square extrusion of Al-6063 by FEA.
- Effect of variable process parameters by FEA as well as experimental validation for the round to square extrusion of Al-6063 using linear converging die-profile.
- Investigation of the effect of various 3-dimensional die profiles on round to square extrusion with experimental validation using non-linear converging die profile.
- Improvement of aluminium MMC prepared by powder metallurgy route by extruding through the best effect die profile.

1.4 Organization of the thesis

In the earlier sections of this chapter, the basic introduction, motivation, and objective of the work is adumbrated. The detailed contribution of the dissertation is structured with total number of seven chapters and as follows:

Chapter 2: Literature Survey

The systematic exhaustive literature review focused on the work already available was presented. The review is typically divided into three primary sections: the first pertains to the previous knowledge on the effects of variable process parameters, the second is based on the die profile and tooling setup development and the third is established on the development of product quality by improving billet material property.

Chapter 3: FEM Investigation of Square Bar Extrusion from Same Shape Billet

This chapter describes the finite element investigation of the effect of various process parameters on square to square extrusion through linear converging as well as cosine profiled die. The modelling was conducted by DEFORM^{TM} software package. The investigation was focused to improve the process efficiency by studying the role of different parameters in response to the maximum load requirement.

Chapter 4: Extrusion Analysis of Al-6XXX through Linear Converging Die

Effect of process parameters on the round to square extrusion of aluminium alloy by FEA has been performed. The simulation result is validated by experimentation through linear converging die profile.

Chapter 5: Round to Square Extrusion through Converging Die

To investigate the effect of die profile on round to square extrusion of aluminium alloy, several mathematical contoured die profiles have been developed by following cosine, linear converging, elliptic, hyperbolic and 3rd order polynomial law. The optimum profile i.e by following cosine law was manufactured for the experimental validation of the FEA.

Chapter 6: Extrusion of Aluminium MMC through Cosine Die

In this chapter the effect of extrusion through cosine die profile of round to square section, on aluminium metal matrix composite manufactured by PM route has been reported. The effect of extrusion through the die was analysed by comparing the properties before and after extrusion.

Chapter 7: Closure

Concluding remarks along with the future scope of the research are outlined in this section.

Chapter 2

Literature Survey

2.1 Overview

Due to the increasing demand for extruded products in many sectors such as automobile and transport, Electrical and electronics, construction and architecture, marine and aerospace, heat sinks, door and window frames, stair and landing ramps etc., an emerging direction to contribute research has been opened to improve the process efficiency as well as product quality. Extrusion is the only economical way of manufacturing such long straight complex cross-sectioned products. Aluminium alloy has the dominance over other materials in forming industry because of its better mechanical, tribological and thermal properties along with good formability.

The process that involves with many state variables which improve the complexity of the process is to be considered for a better production. The effect of the variables like ram velocity, die length, die profile, operating temperature, friction condition for both cold and hot extrusion process has been studied and reported from the past research works. Effect of die profile is mainly responsible for the formation of dead metal zone and redundant work by controlling the flow of material. Hence, it is the most critical area of consideration from the tooling design point of view. Apart from this to satisfy the requirements with better product quality, the billet material compositions and type is a new focus in this decade. Based on these requirements an exhaustive literature review has been carried out in different areas that only focusing the primary objective is described in this chapter. To fulfil the objective of the total research, it is classified into three categories focusing on three different zones such as:

1. Process control
2. Tooling developments
3. Material developments

2.2 Process control

Involvement of various operational variables needs to be restrained within the optimal range during operations to have better control over the process. To find the optimal range,

the effect of the particular variable need to be investigated substantially. As the change in metal during forming operation is concealed by the tooling setup or machinery, it's hard to know the effects of the variable parameters by experimental investigations. So most of the research in previous work are based on computerised finite element and analytical investigations.

2.2.1 Die length or semi-angle

Effect of deformation on stress-strain distribution as well as the effect of die semi-angle has been observed by Chen et al. [13] by rigid plastic simulation modelling. Dyi-Cheng et al.[14] studied the influence of state variables like die semi-angle, extrusion ratio and friction factor for plastic deformation of AA-6062. The extrusion force increases with the increase of die semi-angle ($10° \leq \alpha \leq 35°$) for a reduction of 1.562 and minimum shear friction coefficient of 0.1. But in practical approach with larger frictional resistances, lesser semi angle dies with larger die length need more power to overcome frictional resistances. So to optimize the die length a variation of frictional resistances with the involvement of usefulness is necessary [15]. The optimum die length in terms of relative die length (L/R) remains under 0.5 to 1 for a round to square bar extrusion studied by Karami et al.[16]. They found a good agreement between the analytical, experimental and FEM results. Gbenebor et al. [17] investigated the strain rate distribution to decipher its influence on deformation zone. They achieved the fastest extrusion with encountering the lowest flow-stress with a die of 15° semi-angle.

Effect of extrusion variables for a Al/Cu cladding bimetallic extrusion has been investigated by Khosravifard et al. [18]. In this case the velocity difference at the vicinity of the interface boundary by using a die with semi angle of 25° is less which leads to a proper bonding. The use of this die angle is also requiring less amount of maximum extrusion load.

2.2.2 Friction condition

Most of the FEM tools require friction as input variables whereas in experimental process the frictional value is not known incisively. So the friction value needs to be determined by some different procedures at the interface boundary. Frictional resistance depends on several factors like local temperature, relative velocity, geometry and tooling surface and contact pressure. Numerous research work were there to estimate and model the frictional parameter [19]. Different techniques like ring compression test [20] (the most popular

one), T-shaped compression test [21] and from the barrelling curvature of the compression test [22], different extrusion friction testing [20], double backward extrusion process [23] backward extrusion type forging [24] can be employed for the successful determination of friction condition. Hwu et al. [25] investigated the friction condition of steel by using ring compression test developed by Male and Cockcroft [26]. They studied the process by three ways by varying strain and strain rate to study their effects on frictional conditions. It was concluded, no significant effect of strain on the friction condition whereas effect of strain rate is there over the frictional value. The sensitivity of surface roughness is very much significant for the friction condition which is investigated by Hartlay et al. [27] using split Hopkinson pressure bar technique. Orangi et al. [28] have investigated the effect of frictional coefficients and reduction area on extrusion pressure and product velocity by ABAQUS/explicit finite element software. The power required to overcome friction in extrusion is directly related to the area of contact so the billet length and die length is restricted depending on the condition. High friction condition is responsible for heat generation, and the heat generation also improves friction and flow characteristics. Recent developments of various friction testing techniques that support aluminium extrusion process was elucidated by Liliang et al. [20]. They also did comparative analysis between classical, empirical and physically based friction models [29]. Trials were made to model the bearing channel friction condition, and the effects were studied by Ma et.al. [19, 30].

A process of forward-backward-radial extrusion by utilizing FEM simulation tool with experimental validation was investigated by Farhoumond and Ebrahimi [31] for estimating the effect of parameters like die geometry and friction. There is a significant influence of friction on strain distribution hence affects flow characteristics in metal forming operations. With increase in friction condition the forward flow of the metal reduces and the difference of heights between forward and backward cup decreases. Jooybari [32] studied a theoretical friction model for the analysis of a forward extrusion of aluminium as well as steel. The model works well with the dry aluminium extrusion but it fails to model hot lubricated steel extrusion. Friction condition directly influences flow characteristics, energy consumption, product quality, tooling life and thermal control during extrusion. Frictional resistances causes the heat generation in the billet at the boundary zone because of which it is difficult to maintain a proper temperature at the maximum deformation zone [33]. Frictional heat generation is directly depending on ram velocity, extrusion ratio and initial billet temperature. A very simple and sensitive barrel

compressive test was established for the determination of friction condition at the interface boundary by Ebrahimi and Najafizadeh [34]. A quantitative value of coefficient of friction is desired for the process. The friction model is either Coulomb friction model or Tresca friction model depending on the process conditions. If the mean normal stress component is smaller than flow stress of the material or for low contact pressure conditions like in rolling, sheet metal operations and wire drawing then the Coulombs friction model is applied. In other hand where the mean contact pressure is much higher than the normal stress there Tresca's friction model remains suitable. A slight more complex model i.e Wanheim and Bay's model which smoothens the curve of Coulomb's model and Tresca's model curve is less applied in forming investigations. The following expression is used for the coulombs law.

$$\tau = \mu p \tag{2.1}$$

where τ is the tangential stress (frictional stress), p is pressure between die billet interface and μ is the constant known as coefficient of friction.

In case of extrusion, the induced normal stress is much more than the flow stress of the soft material (billet). In this case, the higher asperity of peaks of the softer material is filled in the roughness valley or depressions of the harder material and an intimate contact zone is established at higher pressures in case of lesser lubrications. In this case sliding will not take place at the interface boundary, but it shifts to a layer below the interface by shearing of the soft metal which is known as subsurface sliding. The Tresca's friction model is expressed as follows.

$$\tau = mk \tag{2.2}$$

$$\text{where } k = \frac{\sigma_0}{\sqrt{3}} \tag{2.3}$$

and m is known as friction factor. It varies within 0-1. If value of m remains 0, then there is no friction condition and if 1 then there is sticking friction condition [35, 36].

2.2.3 Temperature and ram velocity

Temperature management is the key factor in aluminium extrusion which decides product quality and life of the die. During extrusion, the temperature at die exit is high which decides the microstructure and surface property of the product and improves the die abrasion that causes the error in shape and dimensional tolerances of the extrudate. Higher metal temperature improves the metal flow, but too high temperature induces over burning phenomena. With the increase of extrusion speed maximum temperature generation

increases and the time duration to dissipate the heat decreases accordingly, which introduces a new problem. The billet temperature can be estimated by the following relation:

$$T_1 = T_0 + \Delta T_D + \Delta T_F - \Delta T_T \qquad 2.4$$

The mentioned abbreviations are followed:

T_0 is the initial billet temperature.

ΔT_D is the increase in temperature due to energy dissipation during deformation.

ΔT_F is the raise in temperature due to friction at the die-billet interface.

ΔT_T is the heat removed from the billet through die.

As ΔT_F at the boundary is higher and ΔT_D at the maximum deformation zone is higher and the maximum amount of heat flows with the extruded product so the heat dissipation is nonuniform throughout the billet during extrusion [37]. A high-speed low-temperature extrusion of aluminium alloy was investigated by utilising DEFORM 2-D package by Meng-jun et al.[38]. A comparative higher dead metal zone is induced, and a higher strain value is observed at the die entry during the operation. Temperature distribution in the billet across the die is highly strain-rate dependent. The effect of ram speed on the heat generation of Al-7075 alloy is investigated by Zhou et al. [39]. Flow stress of a metal is both temperature and strain-rate dependent. Flow stress increases with decrease in temperature and increase in strain rate. With the increase in extrusion velocity, strain-rate as well as maximum extrusion temperature increases significantly which directly affect the mechanical properties of the product [40]. Ketabchi et al. [8] studied the role of temperature and punch speed on effective stress distribution, effective strain distribution and force estimation of a backward extrusion of Al-7075 alloy. To explore the response of metals to deform, to be extruded is highly essential as it affects the life of the tooling (die, container, punch) used, production efficiency and quality of the product. Zhao et al. [41] analysed the effect of deformation velocity on mechanical properties and microstructure of AA6063 in the continuous extrusion process.

Liu et al. [42] have investigated the effect of initial billet temperature and ram velocity on the temperature generation of extrudate at die exit. The process was analysed for the cross shaped extrusion of a wrought magnesium alloy by DEFORM finite element simulation technique. Among both types of combination low billet temperature with high ram speed and high billet temperature with low ram speed the latter one is responsible for

the isothermal extrusion and the earlier one supports to achieve the high throughput. For the condition of industrial extrusion both the parameters must be selected with respect to each other.

T sheppard [43] investigated the effect mean equivalent strain rate (speed) in relation to temperature on the extrusion of aluminium alloy. He related the mean equivalent strain rate (Z) for the grain effect due to various recrystaline phases with surface quality and breakthrough pressure.

Fang et al [44] analysed the effect of different state variables like ram speed and die bearing length on the extrusion of AA-7075 for a shaped profile by DEFORM finite element simulation technique. Effect of ram velocity has a significant effect on the temperature generation. Larger die bearing length helps to releasing heat from the extrudate and supports to achieve a greater dimensional accuracy. This case study also confirms the prediction of FEM results with the experimentation.

Jin et al. [45] have investigated the hot deformation behaviour of AA-7150 at a temperature and strain-rate range of 300-450℃ and 0.01-10 S^{-1} respectively. At a critical strain value, the material achieves peak stress and with increase in strain the stress decreases monotonically for all condition of temperatures. The flow softening is mainly depending on the dynamic recovery and recrystallization caused due to lower Zener-Hollomon constant (z).

For the improvement of the metal properties, it can be deformed at a controlled cryo temperature condition. Immanuel et al. [46] investigated the effect of cryogenic rolling on the mechanical and tribological behaviour of the Al-Si alloy. Cryo treatment during deformation reduces the grain size and improves the properties.

2.3 Tooling developments

Extrusion through the shear faced die is presently convenient in extrusion industries only because of chasteness in manufacturing. Formation of the dead metal zone, undesirable internal shear deformations, non-uniform metal flow, caused due to the use of this kind of die necessitates additional power . As a result, the process efficiency decreases. To avoid this energy loss, various types of curved dies were analysed for square to square extrusion by Maity et al. [47] and concluded that under sticking friction condition linear converging die remain better whereas, cosine die of same die length under zero friction condition. Square to square extrusion by a mathematical contoured die with an upper bound method for extrusion of lead was analysed by Maity et al. [48]. Similarly Narayanasamy et al. [49]

designed a streamlined die based on the uniform reduction of the area through die length to overcome the problems caused by shear faced die. Implementation of round die is more favourable than square dies for higher reductions with same operating conditions. Non-uniform metal flow occurs at die exit due to inhomogeneous temperature distribution and high-temperature generation at corners [50].

For uniform metal flow at die exit, the bearing length has been optimized for two hole die by Ulysse [51], using finite element method combining with optimization technique. The plastic stress, strain and flow field is affected by the die contour. To investigate the distributions, dies of equal strain rate, Richmond curve, sine curve, conic and elliptic curves are employed for the die design. Dies of equal strain rate has the great influence to achieve the uniform flow and less extrusion pressure [52].

An optimum combination of parameters to get a uniform metal flow at die exit for aluminium profile extrusion was obtained by using Taguchi analysis by Cunsheng Zhang et al. [53]. Effect of die semi-angle on surface property, maximum load requirement and relative sliding velocity of cold extrusion of Al-1100 was studied by Syahrullail et al.[15]. Effect of die shape (entry angle), punch load, energy absorption capacity and strain-rate on extrusion of AA-6063 has been studied by Gbenebor et al. [17] to know the responses mentioned above. By interpreting experimental data and FEM analysis, a new relation has been developed between strain rate and barrelling effect to know the friction coefficient [22] as of its significant participation in metal extrusion. Material flow characteristics at various stages along with dead zone were investigated using HyperXtrude for 6063 type aluminium alloy and validated with experiments for a porthole complex shape extrusion [5]. Not only die profile but also punch shape influence the flow characteristics of the metal [54]. The flow behaviour of the metal was investigated during hot extrusion of Al-7050 alloy by Li et al. [10]. Use of inner-cone punch transforms the central tensile stress into compressive which eliminates the dead metal zone and promotes uniform metal flow. By using MSC SuperForm the flow of the strip extrusion was investigated for obtaining a solution to avoid buckling by Halvorsen et al. [55]. They designed a feeder system to get different velocities at different zones of die for getting a uniform flow velocity at die exit.

Total work required for metal extrusion is the aggregate of the work needed to overcome friction, work required for homogeneous deformation and work required to overcome redundant work [56, 57]. Frictional work and redundant work both antagonize each other in relation to die land length. For shear faced die the die-billet interface friction is minimum with the maximum amount of redundant work and dead metal zone. Frictional

work increases with increase in die length, and it leads to reduction in redundant work. Friction and redundant work both have a great impact on the flow characteristics of metal in extrusion. The uniform flow velocity of metal at die exit, which depends on die profile and friction condition, for getting better product quality in extrusion has a great significance [6]. The process parameters such as stem speed, container temperature, and extrusion ratio have been optimised to achieve a minimum velocity relative difference at die exit and minimizing the extrusion force requirement [53, 58]. A number of numerical trials have been accomplished to determine a streamlined die for efficient extrusion [16, 59]. Various types of curved dies like concave and convex types of elliptic, circular, parabolic, etc. have been investigated by means upper-bound analysis for the square to square extrusion by Maity et al. [47]. The upper-bound analysis also has been carried out to investigate the circular shape extrusion from circular billet by Narayanasamy et al.[60] for different types of die profile. Extrusion through cosine die was found superior to linear converging and concave circular die. The streamlined die has been designed for extrusion of the square bar from round billet by Ponalagusami et.al. [61] based on third and fourth order polynomial as well as Bezier equation. Relative extrusion pressure for bezier curved die compared to linear converging, 3rd and 4th order polynomial die for the round to square extrusion was found lower. The investigation has been made to determine the velocity components in each direction of extrusion in a polynomial equation based die of fifth order having zero entry and exit die angle [62], and an optimum die profile has been developed by updated sequential quadratic programming. A die design methodology was proposed in conjunction with upper bound mathematical modelling to provide minimum distortion [63].

The design of a tooling setup must fulfil the uniform and stable metal flow at its die exit to avoid warped deformation and bending of the product. Zhang et al. [53] optimized the process parameters by considering 32 combinations of parameters for a hollow and complex cross-section of AA-6063 to get a minimum velocity relative difference (VRD) at die exit. Extrusion ratio, friction condition, and ram speed have the greatest influence on the VRD. Effect of ram speed on several variables along with VRD has been investigated [58, 64]. A number of trials have been made to study the flow behavior of the metal in order to minimize the power losses, but a few have manufactured the mathematically contoured 3-D die for its practicality test.

The material those are highly strain-rate sensitive, like Ti alloys, superplastic materials and MMCs can only be deformed suitably within a range of strain rate zone.

Keeping these factors point of view Kim et al. [65] has investigated various die profiles. The average strain-rate and volume deviation (V.D) is estimated by the following relations

$$\dot{\bar{\varepsilon}}_{avg} = \frac{\sum \dot{\bar{\varepsilon}} v_i}{V_{total}} \tag{2.5}$$

$$V.D = \frac{\sum (\dot{\bar{\varepsilon}} - \dot{\bar{\varepsilon}}_{avg})^2 v_i}{V_{total}} \tag{2.6}$$

where $\dot{\bar{\varepsilon}}$ and V_i are the effective strain-rate and volume of i_{th} element and V_{total} indicates for total volume.

By using bezier curve for a particular extrusion ratio all possible die profiles have been investigated. With increasing iteration number towards convergence the effective strain-rate distribution becomes more uniform. As the extrusion ratio increases, the iteration number need to be increased for the uniform strain-rate distribution. Uniform strain-rate directly affect the microstructure of the product. For a homogeneous property distribution across the product, uniform microstructure distribution is necessary which can be achieved by the designed equal strain-rate die. The process was numerically verified and validated through experimentation by Lee et al. [66].

Noorani-Azad et al. [67] have investigated to minimize the maximum load requirement, die life and metallurgical properties of the product. By utilizing slab method they found out the optimum die profile for the forward rod extrusion of the aluminium rod. Finite element code ABAQUS has been used for the numerical analysis. Optimum die semi-angle for the conical die has been found out and for the same reduction an optimum curved die was proposed. Maximum load required to accomplish extrusion through curved die is comparably lesser than the conical die whereas manufacturing of the curved die is quite difficult. Similar investigation by Saboori et al. [68] has been carried out for the comparative analysis of two different types of materials such as: lead and aluminium. Optimum die semi-angle for the conical die profile is considered as 30°. By considering both types of die profile (conical and curved) both kinds of extrusion, forward as well as backward has been performed. For all the conditions the load-stroke plot shows the minimum energy consumption with the use of curved profile.

A combined upper-bound and slab technique was proposed by Bakhshi-jooybari et al. [69] for estimating the extrusion load of aluminium and lead by an optimum curved die profile. After development of the die profile, the process was analysed by finite element code ABAQUS by implementing Coulomb friction model. All three numerical,

experimental and combined slab and upper-bound analytical technique in the load-stroke plot agrees each other with close tolerance.

To reduce the product defects, the die bearing length must be optimised to achieve an uniform exit velocity of the product. Die bearing length is the most significant parameter for controlling the exit velocity of the product. A novel approach has been presented by Lin et al. [70] which uses the medial axis transformation empirical bearing length design formula to design an optimal die in response to bearing length. A non-steady thermo-rigid-viscoplastic approach for three dimensional flat die hot extrusion process with automatic remeshing has been analysed by Lee et al.[71]. Various deformation parameters have been investigated for the process. Relative velocity of the product at the exit cross-section was found dependent on cross sectional area of the product as well as the die bearing design.

2.4 Material developments

Over the last few decades, there has been considerable attention to the evolution of Al-based MMCs developed by powder metallurgy (PM) route of manufacturing. The main advantage of this kind of manufacturing process is the good distribution of reinforcing particles, low processing temperature and the ability to produce near net shape products with intricate designs [72, 73]. This process is involved with very complex procedures and many areas need to be focused before manufacturing to have a better defect free product. The procedure starts form the powder production and ends with the heat treatment of the product followed by number of steps. Number of different steps involved with the manufacturing procedure is discussed below.

2.4.1. Powder production

Production of different metal powders is the most important base for the entire powder industry. The consumption of iron and steel, copper base, Nickel, tungsten, aluminium and tin are the most important in the industry. The various production techniques are specified beneath

- Grinding and milling :- The formation of powders is performed by mechanical means in the form of solid state. Among various processes ball and vibration milling, attritor milling, roller milling, the Hametag process and jet milling, are the popular processing of metal chips. The minimum particle size depends on the condition of the process and the metal type. The efficiency of the process is very low. In this case the produced particle shape are mostly irregular.

- Atomisation :- Melt atomization is the most used technique for the production of metal powders which follow melting, atomization and solidification and cooling. Depending on the solidification process these may be liquid atomization or gas atomization. Depending on the process conditions it may be of centrifugal, ultrasonic or vacuum atomization process. In this process the powders produced are in spherical form.
- Chemical process :- The reduction of metal compounds like oxides, nitrates, carbonates and halogenides with gasses and solids is the main chemical process. Hydrogen reduction, hydro chemical reduction, carbon reduction and various electrochemical processes are the important procedures for the production of powders.

2.4.2. Powder characterization

Powder properties and characteristics carry a major role for the product property. Few of them are discussed below:

- Particle size :- the particle size is expressed with the dimension of length. The distribution of the particle size varies from less than a micron to several hundred microns. The equivalent dimension of a sphere having similar properties can be represented as the particle size. Microscopy, LASER diffraction, sedimentation and sieve analysis are the most popular ways to determine particle size. The wide particle size distribution directly affect the density of the compact product as the smaller particles fill the inter particle gaps.
- Particle shape :- particle shape is responsible for the flowability of the powder during compaction process. The shape analysis is carried by the image analysis technique. There are various types of the shapes like nodular, acicular, fibrous, flaky, dendritic, angular, granular and irregular depending on their production method. The shape analysis is usually applied in linear, two- or three dimensional parameters.
- Flowability :- the behaviour of powder affects the compaction density and density distribution. The flowability of the powder is represented in terms of apparent density and tap density measured by Hall flowmeter test. The specific mass of the sample is allowed to flow through flowmeter and the time required to flow through the funnel is dependent on friction between powder particles and between the

powder and funnel wall. It also depends on the funnel geometry as well as powder shape.

A constant volume of a cylinder is completely filled with powder with the support of gravitational flow from the flowmeter placed at a certain height. Resulting mass per unit volume is recognised as apparent density. The same procedure followed for the filling the cylinder by tapping it with a frequency of 1.5-1.7 Hz with an amplitude of 3 mm against a rubber plate to estimate the tap density [74]. The variable functions that affect the packing are size distribution, mass, shape, inter particle friction and resilience of the powder.

2.4.3. Compaction

There can be two types of pressure-assisted shaping operation depending on the operating temperatures such as cold and hot. The earlier one is the most common one in the powder metallurgy industry. The process may be single axial, double axial or isostatic compaction, depending on the process utilised. The applied pressure must overcome the internal frictions to remove the bridging between the particles. The improved green compact density results maintaining product shape and density after sintering. Some of the cases lubricants are added to improve the flowability of the powder as well as to reduce die and powder interface friction and to avoid die sticking. Density distribution during the compaction process is not uniform. It depends on the pressure gradient so the density near the punch is higher in case of single axial compaction and the density near the two punches are maximum and at the centre is the least. Due to the reason the process requires a secondary treatment like forming, rolling or extrusion.

2.4.4. Sintering

If the above compaction process is not conducted at hot conditions then the green specimen needs sintering of the samples. In case of green specimen the bonding is only due to intermetallic locking caused by high compaction pressure. The green specimen has the limited strength only to handle it safely. But to form intermetallic bonding between the metallic particles, the green specimen needs to be sintered at the desired temperature. It is a process of thermally activated transportation of materials in a targeted porous compact which reduces the specific surface area by the growth of the particle contacts. The atmospheric condition during sintering is needed to be controlled for avoiding formation of oxides which reduces the strength of the component. During sintering most of the components swell, the dimensions increases and the density decreases accordingly. The

swelling effect is due to the release of stored strain energy at high pressure conditions during cold compaction process.

2.4.5. Secondary operations

In most of the cases the primary product manufactured by powder metallurgy route need the secondary treatment in order to improve the mechanical properties of the component. The process also helps in the distribution of reinforcement particles, removal of internal pores, and improved uniformity in density across the product as well as removal of oxide layers by the internal particle shearing effect. The secondary operation can give the final product a better surface finish and dimensional tolerances. For the specific cases, where there are ceramic reinforcements, secondary processes like extrusion, rolling, forging help to improve the metal-ceramic bond strength and consequently the properties of the product improves.

2.4.6. Heat treatment

It is the last treatment required depending on the requirement of the product. By suitable heat treatment process to the metal, the properties can be controlled as per the requirements. In very few of the cases surface finishing operation is also required as per the product demand.

There are number of advantages for which the powder metallurgy processing technique is adopted for the production of components. Those are as follows:

- The process has the highest raw material utilization with the lowest specific energy consumption for the production of near net shape components in a lot.
- The process has the flexibility of producing unusual mixture of both metallic and non-metallic materials with variable percentages as per the requirements.
- The products can be produced with controlled porosity which facilitates infiltration and impregnation of other material to to enhance the properties for some kind of special application.
- The homogeneous distribution of the particulates can be achieved by this technique which supports a macro scale homogeneous and isotropic properties.
- Addition of secondary treatment to the PM component adds value in the terms of mechanical properties, surface properties and dimensional accuracies.
- A self-lubricating lighter components which produces damping effect to the vibration propagation with improved dimensional precision can only be

manufactured by PM route followed by secondary treatments like rolling, forging, extrusion etc..

The product properties manufactured by ingot metallurgy can be improved up to the ultimate and afterward trials diminish the properties. Powder metallurgy is one of the best alternative techniques with the capabilities to produce high corrosive resistance, high strength, improved fatigue strength and toughness at a wide variety of working temperatures [75]. A newly emerging area, fine and ultra-fine ceramic reinforced composites are used in aeronautics and automobile sectors because of its good fracture toughness, resistance to catastrophic failure, good strength to weight ratio, high temperature and oxidation resistance [76, 77]. A number of studies have been conducted to develop the composite by reinforcing ceramic particles like SiC [78-80], Al_2O_3 [81], B_4C [82], Al_4Sr [83] etc. in different grades of aluminium series of powder matrix [84, 85]. Numerous researchers investigated and substantiated the improvement of mechanical and tribological properties owing to thermo mechanical treatments such as extrusion [78, 86], rolling and forging. As aluminium is highly reactive to atmospheric oxygen, layers of oxide formation take place in the PM specimen during sintering. During thermo-mechanical treatments the covered oxide layer breaks due to high induced shear stress, leading to a strongly bonded microstructure and improved mechanical properties which eliminate the main drawback of AMCs [87]. Mechanically milled AA6061 / Ti_3Al composite with the reinforcement percentages of 5, 10 and 15 was compacted at 300 MPa with graphite lubrication and hot extruded for the characteristics study by Adamiak et al. [88].

A very less amount of work on the glass reinforced aluminium matrix composite is there. But the scope of the composite due to the properties and availability of glass powders is very high. Aluminium based hybrid composite with the reinforcement of SiC and glass particles fabricated by powder metallurgy route technique and the properties have been investigated by Kumar et al. [89] by varying the reinforcement percentages and particle size. For the cold compaction process at 520 MPa, zinc-stearate was used as lubricant to avoid die sticking. The bond formation in between the intermetallic particles is established by sintering the green compact at 605℃. It was observed from the analysis that, increased reinforcement percentage as well as particle size tends to improve the fromability stress index and strength coefficient and strain hardening index. Better densification factor, better load transferring rate and decreased pore size are the main reason for the kind of improvements [90]. The results depict Al-4% Glass with variable

percentages of the SiC with in the investigated range is the most suitable composite for the cold analysis.

Seo and Kang [91] have investigated the improvement of extruded microstructural and mechanical properties of the SiC reinforced Al-6061 metal matrix composite. The distribution of the reinforcement has been improved which could not be achieved with only squeeze casting process. The ultimate tensile strength improves 25% to 35% after extrusion. The metallic bond strength and density improves significantly which causes the improvement of different mechanical properties.

The extruded composites show excellent distribution of the reinforcements which improves the mechanical properties manifold. Considering Al-7015 as the matrix material and 5% of reinforcements of ceramic materials of B_4C, TiB_2 and Si_3N_4 the composite has been prepared at a compaction pressure of 200 MPa for extrusion by Cambronero et al. [92]. An improvement of hardness, wear resistance and corresponding decrement of formability.was observed by Rajabi et al. [93]. Dispersed nano ZrO_2 powder in aluminium alloy were to investigate the characteristics change by changing the percentage of reinforcement in 3-15%. They obtained an optimum range of 6 percentage for the best results.

Goswami et al. [94] investigated the effect of parameters and reinforcements on the extruded product behaviour of aluminium alloy 2124/SiC_p metal matrix composite. Effect of ram speed, extrusion temperature, lubrication and extrusion ratio on the process and product surface quality have been described nicely. The higher percentage of reinforcement of SiC particle may cause improved die wear, reduced wear resistance of the extruded product with higher hardness.

Use of traditional shear faced die in extrusion causes product defects owing to the existence of higher velocity relative difference at the die exit [95, 96] along with the formation of dead metal zone. Use of mathematical contoured die (preferably zero entry and exit angle) for the MMC extrusion is highly recommendable. The inhomogeneity of the metal improves by introducing the hard metallic or ceramic reinforcements causes non uniform stress and strain distribution. The reinforced particles are also responsible for the velocity differences, surface defects central bursts and die wear. With the use of shear faced die a severe product defects can be visualised. Hence, it is suitable to utilise a mathematical die which reduced the velocity difference and supports the smooth flow of metal at die exit. The use of contoured die in the forming industries is improving due to its energy saving as well as defect free production capacity.

2.5 Summary

This chapter provides an exhaustive review on the different aspects of developments of extrusion. The progress made in the past work has been reported in detail. Following points are the directions observed from the above work in which the work can be improved.

- To find out a concrete relationship of variable parameters with respect to extrusion pressure for the simple extrusion by employing finite element analysis.
- To develop the optimal 3-dimensional die profile for a simple square bar extrusion from the round billet and experimental verification of the FEM results.
- To study the cosine profiled extrusion effect on the aluminium MMC extrusion by comparing the property change before and after extrusion.

The next chapter focouses on the objective of the work.

Chapter 3

Investigation of square bar extrusion from same shape billet using FEM Analysis

3.1 Overview

The metal forming process is preferable for manufacturing the parts of moderate complexity and greatly diversified profiles for the larger volume of productions to reduce the tooling cost. Energy saving, less scrap generation and near net shape production with better mechanical properties along with high production rate has enhanced the specific forming process, extrusion, for the production of long straight metal products [5]. During the process, a stress state of compressive nature is being developed in the billet which tends to large deformations to be accomplished. A number of internal and state variables are involved in the process which enhances the complexity of the process hence, difficult to achieve the optimum process conditions. The state variables which have the prominent effect on the process are extrusion ratio (R), operating temperature (T), ram velocity (V), friction factor (m) and die length (L) which are controllable during extrusion [97]. Hitherto there is no definite technique to predict the process, so it is hard to choose the precise considerations for economic and material saving production without anticipating any kind of failures or defects. The process is accomplished by broad working experience along with an expensive long cycle of trials, evaluations, redesign, process analysis and optimization.

Till today ascertaining the exact force required for metal deformation is unprecedented, but some analytical and numerical methods are there for estimating the approximate values [56]. Among these methods (Uniform Energy Method, Slab Analysis, Slip-line Field Analysis, Upper-Bound Method, Finite Element Analysis), Finite Element Analysis (FEA) predicts good result but a very complicated process. Hence, empirical methods were staying good with most of the industries till date. Most of the research works are going on for finding the optimum condition of parameters to improve the process efficiency [98] and product quality. For achieving uniform flow velocity at each cross-sectional zone in a plane vertical to extrusion velocity or a minimum relative

velocity difference (VRD) at die exit is the most desirable condition for a better product quality at the time of extrusion was studied by Zhang et al.[53, 58].

In this chapter, the computerized simulations of extrusion of the square section from square billet through converging die profiles were carried out by using DEFORM 3D software for Al-Mg-Si type alloy. Cosine, linear converging (LC) and shear faced die profiles were considered for the extrusion analysis. Effect of die profile on VRD was studied. Effect of few major state variables like friction, die length, ram velocity and extrusion ratio have been analysed in relation to maximum extrusion load for cold working condition by varying them in a wide range. The induced effective stress, effective strain and temperature distribution at the billet in the die during extrusion is studied.

3.2 Finite element analysis

The first attempt to develop the finite element model to solve the problems was made in 1941-1942. The technique was modified for further improvement, and a mathematical foundation to find the approximate solution of differential and integral equations was established in 1973 [36]. For a structural mechanics problem, the technique was first implemented. In the current scenario, the usage of FEM software for analysing the process has been improved significantly due to its visible improvements and prediction accuracies. Earlier practices to decide the optimum process condition by performing trial experiments were very expensive, time-consuming which accelerated the extensive use of FEM software [8]. A number of researchers have claimed a good agreement between experimental results with the simulation results conducted by different software packages like DEFORM® [14, 99-102], ABAQUS [103], Hyperxtrude [104], QForm [105], MSC SuperForm [55], ANSYS [106], DiekA [107], FORGE [108] and many more. Among all these software packages the illustrious DEFORM-3D® was used for the present investigation.

The most widely employed finite element analysis software “DEFORM” can analyse bulk metals, few non-metals and glass forming, different machining processes and heat treatment problems successfully. The software helps for improving product quality and reducing the process cost by predicting the 3-dimensional stress-strain, temperature, material flow distribution along with microstructural evolution and phase transformation. The simulations having large material deformation coupled with thermal behavior can be analysed successfully because of the capability of automatic remeshing and robust non-

linear solvers which are not under the capabilities of general purpose FEA packages. Generally, the software supports the analysis of the entire process of manufacturing from ingot to final product through forming, machining and heat treatment.

The software package consists three major steps for the complete analysis process, those are:

Pre-processor: A new problem can be generated in this step. The input conditions for the forming analysis can be established here. This step supports for positioning the objects, defining mesh, defining all thermal and mechanical boundary conditions. The pre-processer develops a database file for further processing by the simulation engine.

Run-engine: Generated database is allowed to run in this step for solving all numerical and mathematical calculations. This step takes time to resolve the problem depending on the mesh size and iteration type selected in pre-processor.

Post-processor: The results after simulation run can be canvassed in a very suitable user-friendly graphic interface. All the stress, strain, load, torque, etc. can be plotted along with its distribution at different elements of the target body. The post-processor can also be utilized for extracting graphical and numerical result for use in other applications.

3.2.1 Formulation of a new problem

Among the two typically used simple and fastest convergence material model rigid-plastic and rigid-visco-plastic, later one coupled with a heat transfer function was chosen for the investigation, as the objective is not focused on residual stress and spring-back effects. The governing equations for the rigid-viscoplastic material model for forward extrusion are as follows:

$$\text{Equilibrium equation} = \sigma_{ij.j} = 0 \tag{3.7}$$

$$\text{Compatibility condition} = \dot{\varepsilon}_{ij,j} = (\frac{1}{2})(v_{i,j} + v_{j,i}) \tag{3.8}$$

$$\text{Constitutive relation} = \sigma_{ij}^{'} = (\frac{2\bar{\sigma}}{3\dot{\bar{\varepsilon}}})\dot{\varepsilon}_{ij} \cdot \tag{3.9}$$

where $\bar{\sigma}$ = flow stress of the material, expressed as:

$$\bar{\sigma} = \sqrt{\frac{3}{2}\sigma'_{ij}\sigma'_{ij}} = \bar{\sigma}(\bar{\varepsilon}, \dot{\bar{\varepsilon}}, T) \tag{3.10}$$

and $\bar{\varepsilon}$ = strain rate expressed as $\bar{\varepsilon} = \sqrt{\frac{2}{3}\dot{\varepsilon}_{ij}\dot{\varepsilon}_{ij}}$ 3.11

$$\text{Incompressibility condition} = \dot{\bar{\varepsilon}}_{kk} = 0 \qquad 3.12$$

$$\text{Boundary conditions: } \sigma_{ij} n_j = \bar{F}_i \text{ on } S_f,\ v_i = \bar{v}_i \text{ on } S_v \qquad 3.13$$

The field equations are given above can be solved by variational principle expressed as:

$$\delta\phi = \int_v \bar{\sigma}\delta\dot{\bar{\varepsilon}}\ \mathrm{dv} + \int_v k\dot{\varepsilon}_{kk}\delta\dot{\varepsilon}_{mm}\ \mathrm{dv} + \int_{Sf} \bar{F}_i \delta v_i\ \mathrm{ds} = 0 \qquad 3.14$$

where $\dot{\varepsilon}_{ij}$, σ_{ij}, and v_i are the strain-rate , stress and velocity components of the workpiece respectively. The σ_{ij}' is deviatoric stress component, the indices i, j, k are for the three-dimensional problems and vary from 1 to 3. V indicates the volume of the workpiece, S_f is the tangential force on the surface of velocity discontinuity, S_v is the velocity surface, F_i is the frictional stress and K is a constant.

For rigid-visco-plastic material model flow stress is effective stress, effective strain-rate and temperature dependent and expressed as:

$$\bar{\sigma} = \bar{\sigma}(\bar{\varepsilon}, \dot{\bar{\varepsilon}}, T) \qquad 3.15$$

3.2.2 Thermal conditions formulation

Heat flow model in between tooling set-ups such as die, container, punch along with ambient surrounding follow the following relation:

$$(kT_{,i})_{,i} + \dot{r} - (\rho c\dot{T}) = 0 \qquad 3.16$$

where k, $\dot{r}$, T, ρ and c are the thermal conductivity, heat generation rate, temperature, specific density and specific heat respectively. The relation signifies the addition of rate of heat transfer $\{(kT_{,i})_{,i}\}$, rate of heat generation due to plastic deformation $(\dot{r})$ and internal energy $(\rho c\dot{T})$ nullify. The heat generation due to plastic deformation is represented as

$$\dot{r} = \alpha\rho\varepsilon \qquad 3.17$$

where α is the coefficient for conversion of mechanical energy to heat energy. Usually α is considered as 0.9 and the rest of energy is consumed for the formation of dislocations, changes in grain boundaries and phases. The energy balance relation for thermal equilibrium expressed in equation 3.10 can be presented by weighted residual method as :

$$\int_v kT_{,i}\delta T_{,i}\, dV + \int_v \rho c\dot{T}\delta T dV - \int_v \alpha\bar{\sigma}\dot{\bar{\varepsilon}}\delta T dV - \int_s q_n \delta T dS = 0 \qquad 3.18$$

where q_n represents heat flux normal to the tooling boundary which includes convection and radiation heat loss to the environment. It also includes frictional heat gain and external heat gain or loss. By solving these equation the temperature distribution of the profile can be obtained.

3.2.3 Boundary conditions

The interface boundary condition between tooling setup-billet is a mixed type. It could be represented as:

$$V \bullet n = 0, \quad t=0 \tag{3.19}$$

Velocity and traction vectors are abbreviated as v and t. The n is a unit perpendicular to the contact surface and $(\bullet)$ indicates the discontinuity across the contact boundary. The interface boundary condition in equation 3.19 can be expressed in the form as:

$$\int_s K_i \Delta v_n dS + \int_s t_s \delta v_s ds = 0 \tag{3.20}$$

where Δv_n is the penetrating velocity acting in normal direction, Δv_s sliding velocity acting in tangential direction and t_s the traction representing the frictional stress. The basic detail of the simulation steps are presented in Figure 3.1.

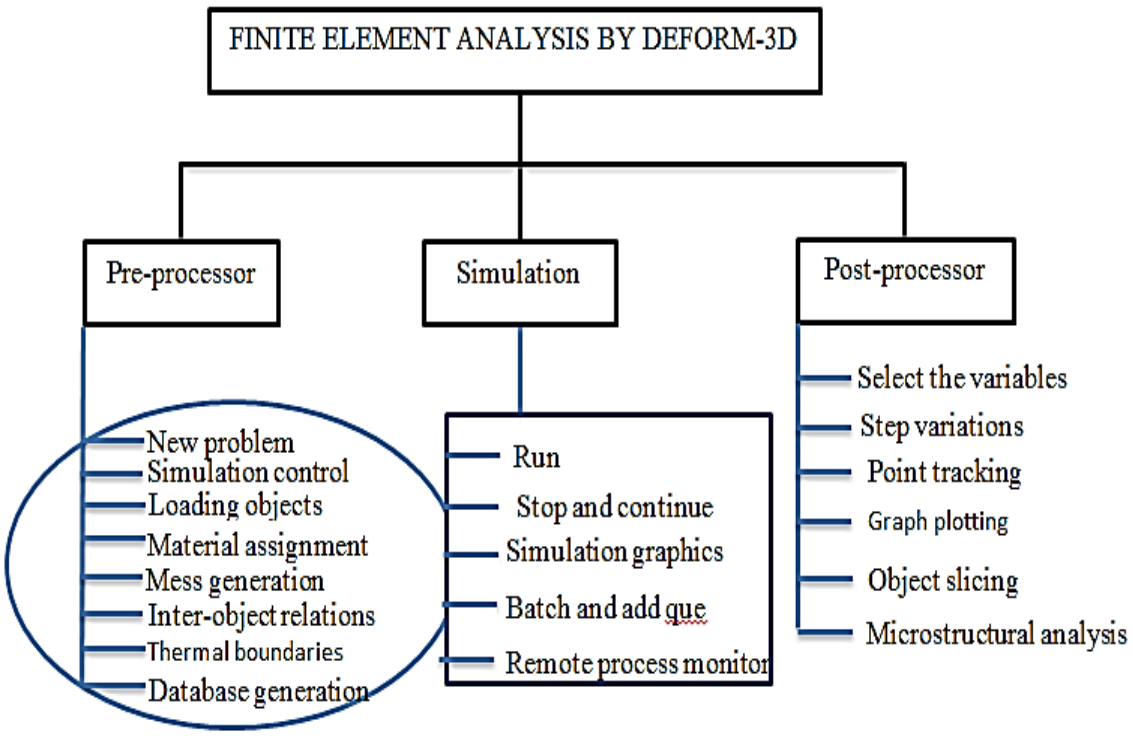

Figure 3.1: Major variable parameters of DEFORM-3D

3.2.4 Pre-processor

3.2.4.1. Simulation control

SI (International System of Units) unit convention, lagrangian incremental iteration type with deformation mode was activated for the simulation. Mechanical, thermal and phase transfer problems can be simulated by deform mode. Punch was considered as the primary die for which the stepping and stopping criteria were decided. Stepping of the primary die can be controlled by either time or displacement reference. The primary die will move the stroke length per step as specified up to the completion of the total number of steps assigned. The total travel of the primary die is the total step times primary die velocity (displacement/step). Time and total step selection is a crucial parameter. Larger time step causes inaccurate solution and convergence problem whereas smaller time step needs unnecessary extra time for the solution. Maximum displacement of a node should not exceed one-third of the edge of an element, so for a finer mesh size corresponding smaller step size should be chosen. Course meshes cause several problems like mesh degradation, problems in remeshing and excessive volume loss. Remeshing option will be triggered depending upon the time, step and stroke increment as well as penetration by the master objects. After remeshing, the data / information contained by old mesh can be interpolated to the new mesh.

3.2.4.2. Materials

If an object is defined with mesh, then it must have a material to be assigned. The material data can be allocated from selecting the material icon. The properties of most of the standard materials are available in the software database list. The software also facilitates to generate a new material model. In this case, the material model selected is an isotropic and rigid viscoplastic model.

3.2.4.3. Object definition

How the deformation will be modelled for the different objects, need to be defined here. A non-deformable body can be modelled as a rigid body and represented by the only geometric profiles (DIEGEO). This kind of objects can perform force transmission, velocity and thermal transmission, and diffusion calculations. These types are used for tooling setups. Depending on the characteristics of the material, the billet can be defined as rigid-plastic as well as rigid-viscoplastic model. After a particular value of strain-rate, the material shows plastic deformation. This material model does not consider the spring

back effects. These two material models are utilised for this investigation but other models like elastic, elasto-plastic (does not consider strain rate sensitivity), porous are also available with this software.

3.2.4.4. Inter-object relation

The master/slave relationship to define inter object relation between different objects were set. The finer mesh should be assigned to the slave or softer object. In this case, it was not necessary to define "No contact" relation. The friction value, thermal transfer property is assigned to the inter-object boundary in this step. The activated nodes indicate the contact or assignment between the node and the surface which restrict the penetration of the master object into the slave. The behaviour of the contacting object while in contact is defined here. Shear friction coefficient and conduction heat transfer coefficient between the inter-material boundary are assigned in this problem. The frictional resistance was assumed to be of shear type in this formulation and the friction factor m $(0 \le m \le 1)$ can be expressed as:

$$m = \sqrt{3}\frac{\tau}{\sigma} \qquad 3.21$$

3.2.4.5. Boundary condition

The boundary condition controls, how the boundary of an object will interact with others as well as with the environment. In most of the cases, the object boundary exchanges heat to the surrounding. The movement boundary condition of the objects is defined in such a way to satisfy the extrusion condition. The velocity of the die and container is set zero in all the directions whereas the punch is allowed to move in the extruded direction only.

3.2.5 Simulation engine

The assigned simulation or numerical work defined in pre-processor step is further processed by clicking run icon. For a faster solution with less memory consumption, the conjugate gradient solver was selected. The message window shows the execution information which also includes convergence information. The last most recent step can be visualised from the simulation graphics option while the problem is running. Different effects like effective stress, strain, temperature distribution can be visualised for that step only. The problem can be aborted by the user in case of any constraint or continued up to the message of completion.

3.2.6 Post processor

In this stage, the outcome results can be visualised, and the same can be extracted from the database. The geometry after deformation with tool movement at every step with different views can be collected. The distribution of state variables on the objects in the form of contour plots can be analysed. Contoured plots are facilitated to vary the distribution style like solid sadding distribution, line distribution, vector distribution, etc.. The graphs between any of the state variables in relation to different abscissa can be plot and extracted. Point tracking and flow net are the two most important facility to study the internal behaviour of the component at the deformation stage provided in the post processor. The graphic utility window provides the facility of manipulating the range and vision as per the analysis.

3.3 Die profile design and modelling

Die profile plays an important role for guiding the metal flow in extrusion. Metal flow in extrusion is directly influenced by the die profile and friction condition. The load requirement for deformation, by using cosine die profile is minimum at zero friction condition due to its geometrical fetcher. i.e. zero entry and exit angle [47]. But it is a traditional practice to use LC die due to the ease of manufacturing. LC and cosine die along with the container, punch and billet geometry were designed and modelled by SolidWorks® software. The die profile functions for cosine and LC die are as follows:

$$Y = f(z) = \frac{W+A}{2} + \frac{W-A}{2} \times \cos\left(\frac{\pi Z}{L}\right) \text{ [47]} \qquad 3.22$$

$$Y = A + (W - A)(L - Z) / L \qquad 3.23$$

where ‘L’ is the die length and ‘Z’ is the number of steps in between ‘0’ and ‘L’.

Die profiles for cosine die and LC die are shown in Figure 3.2 for extrusion ratio of 9.47 with different die lengths. Extrusion ratio is the ratio of the billet cross section area to the product cross section area and is abbreviated as ‘R’. In some of the cases reduction is expressed in percentages, which is 100 times of the ratio of change in cross sectional area per original cross sectional area. Percentages reduction is abbreviated as ‘r’. The variation in deformation through cosine profile in comparison to the linear converging profile can be analysed from the figure beneath. At the initial zone and final zone, the deformation is very less in cosine die whereas at the intermediate zone it is severe but in the case of linear converging die the slope is uniform. Figure 3.3 shows the cross section

view of the solid model of cosine, LC and shear faced die with the attached container. The container and die were modelled as a single unit for a simplified set-up. Solid model of dies for extrusion ratios 2.04, 3.30 and 9.47 with different die length following LC profile and cosine law have been developed referring to equation (3.22) & (3.23).

Finite element methods of computer simulations are capable of predicting the effect of all essential parameters which influence the process. Commercially available DEFORM-3D software (version-6.1) was used for the aforementioned investigation. The solid geometries were imported as .stl file and simulation of extrusion of Al-Mg-Si (AA-6063) alloy were carried out by lagrangian incremental type rigid-viscoplastic simulation with direct iteration method and conjugate-gradient solver at a normal temperature of 30℃.

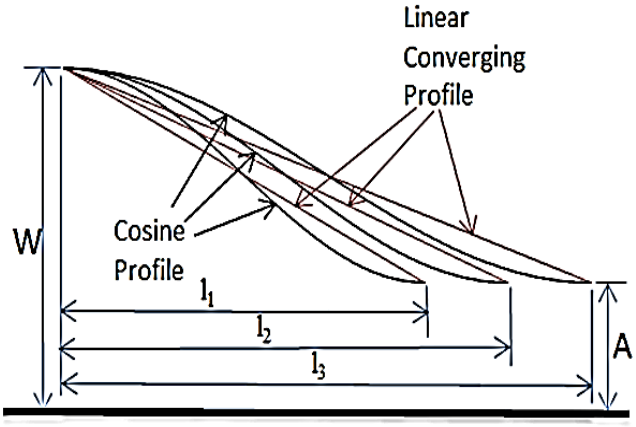

Figure 3.2: Comparative die profile curves

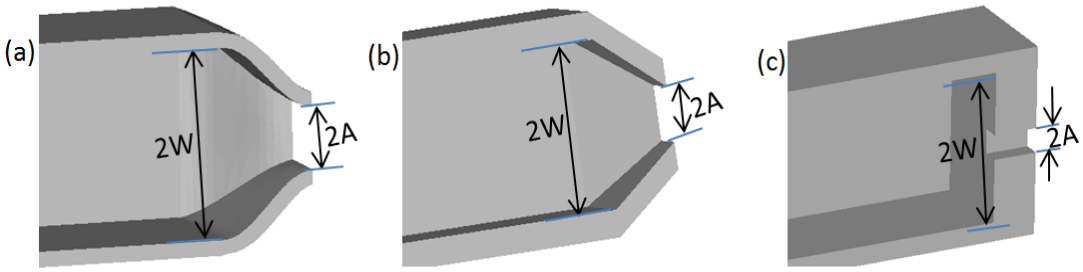

Figure 3.3: Solid model cross section view of (a) Cosine, (b) LC and (c) shear die.

Process parameters and friction factors considered for simulation are tabulated in Table 3.1. The value of friction factor, suggested by the software for cold aluminium forming has been examined for die-billet interface. The mesh density of the components has been decided by considering the three factors mentioned beneath:

- Maximum displacement of any element occurs in one step must be less than one third of the edge of the element. In the case of extrusion the maximum

displacement in a single punch step will be at the core area of die exit. It can be estimated by multiplying the ram velocity with extrusion ratio. By relating the maximum displacement to the edge of an element the ram velocity per step can be decided or the vice versa also possible.

- More the mesh size the less the volume compensation error and more accurate will be the result.
- More the mesh size the number of elements will be more. Each element consists of four nodes (for tetrahedral mesh) for which numerical calculations and iterations will be performed because of which the simulation consumes time and memory.

The billet is the representation of the collection of subdomains known as finite elements, which are bounded by the set of nodes depending the type of element selected. All the properties of the body are assigned to the nodes. It is an approximate technique to estimate the target and by increasing the elements the accuracy can be improved.

Table 3.1: Parameters considered for simulation

Process parameters	**value**
Billet length (mm)	100
Billet cross section area (mm^2)	40*40
Operating temperature (℃)	30
Extrusion ratio (R)	2.04, 3.31, 9.47
Ram velocity (V) (mm/sec)	0.1, 1, 2, 5, 10
Die length (L) (mm)	10, 15, 20, 25, 30,35,40
Friction factor at die-billet interface (m)	0.4
Friction factor at ram-container/billet interface (m)	0.1

There are wide ranges of applications of Al-Mg-Si alloys in automotive and aviation industry because of its excellent corrosion resistance, hardenability, and high strength to weight ratio [57]. Hence, AA-6063 was considered as work material for the analysis. The properties of work material selected from the software database are mentioned in Table 3.2. For the present investigation, die, container and punch were modelled as rigid bodies whereas the billet was modeled as a rigid-viscoplastic object in the tetrahedral mesh. Table 3.3 shows the strain, strain-rate sensitivity of the material selected from the database at room temperature. From the tabularized data, it is clear that AA-6063 is not the strain-rate sensitive at the cold working condition. Most of the metals

are strain-rate sensitive at hot working conditions because of recrystallization and grain growth limitations.

Table 3.2: Properties of AA-6063

Material Type	Young's Modulus (MPa)	Poison's ratio	Thermal expansion (1/℃)	Thermal Conductivity (W/m/℃)	Heat capacity (N/mm^2/℃)
AA-6063	68900	0.33	22×10^{-6}	180.2	2.43357

Table 3.3: Flow stress data for AA-6063 at different strain and strain rates

Strain	Strain Rate (mm/sec)		
	1	100	109.9
0	80	81	81
0.09	99.832	101.832	101.832
0.82	169.655	171.655	171.655
2	173	175	175
2.2	173	175	175

The important parameters in cold extrusion are extrusion ratio and die length whose effects are studied in this chapter. As ram velocity is directly linked with strain-rate, the effect is not very significant but the effect is not negligible in case of higher extrusion ratios and high production volume. Effect of ram velocity is also investigated for this kind of cold extrusion process. For investigating the effect of die length on power consumption; it was varied from 10 to 45 mm with the rise of 5 mm for R = 3.30 and 9.47 both, by keeping other variable parameters constant. The trend of the graph between maximum load required versus extrusion ratio was also checked for the die of 19 mm length by the virtual experiments. Effect of ram velocity was studied for LC and cosine profiled die by varying it as 0.1, 1, 2, 5 and 10 mm/sec each.

3.4 Results and discussion

Before adopting the simulation process of DEFORM-3D, it was verified with Zhang et al. [21] (T-shaped compression test) for the abidance of the tool. By considering the same parameters with similar tooling design the compression was performed. Results

ascertained by DEFORM-3D for load-stroke/billet diameter plot is shown in Figure 3.4. Simulated result, obtained by this technique is closely matching with the above-mentioned research paper carried out by FORGE-2005 with experimental verification.

One simulated cylinder compression test was verified with an experimental compression test at room temperature condition. For both the process the variables remained same. The simulated, as well as experimental load-stroke plot extracted from the result is shown in Figure 3.5. It clearly depicts the close agreement. As the simulation technique is confirmed by the above procedure successfully, the process was followed for the further investigation.

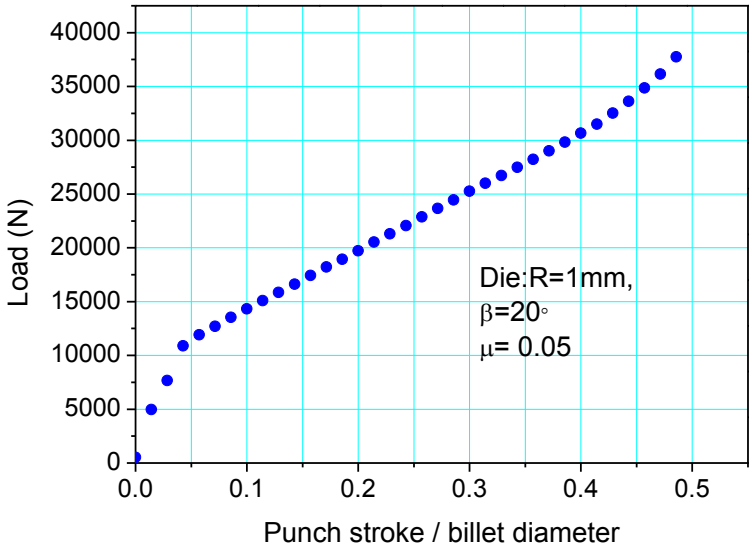

Figure 3.4: Load versus punch stroke/billet diameter for T shaped compression

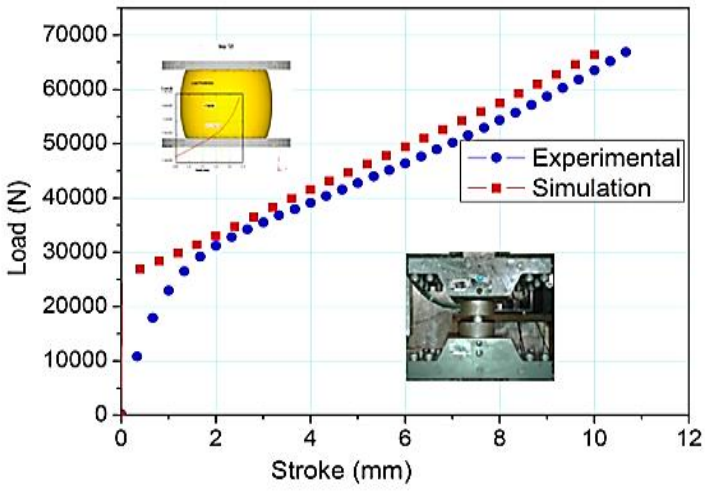

Figure 3.5: Compression test comparison.

3.4.1 Effect of die profile and die length

From the few important state variables die length is the one which controls friction losses, formation of dead metal zone and flow characteristics. An optimum die length for reducing tooling cost as well as production cost is necessary for minimizing the power consumption by internal shear deformation. Simulations were performed to investigate the effect of die length for R=9.47 through shear faced, cosine and linear converging die. The range of die length for the reduction was chosen from 10 mm (die semi-angle 53.5 degrees for R=9.47) to 45 mm (die semi-angle 16.7 degrees for R=9.47) with 5 mm of rise.

Die profile or die type is an important focus in case of extrusion as it is responsible for the formation of dead metal zone and controlling the flow characteristics. By considering the two commonly industrial practiced dies i.e LC and shear faced energy consumption for the extrusion was investigated. It was compared with the cosine profiled die. Comparative load versus stroke plot for the different dies is shown in Figure 3.6 at a constant ram velocity of 1 mm/sec. It is observed from the above figure that load required for extrusion is maximum by shear faced die, whereas it is minimum by cosine die. The area in between the plots is clearly indicating the amount of energy loss due to the redundant work. Effect of die length on the load stroke plot through cosine die is shown in Figure 3.7 and through linear converging die in Figure 3.8.

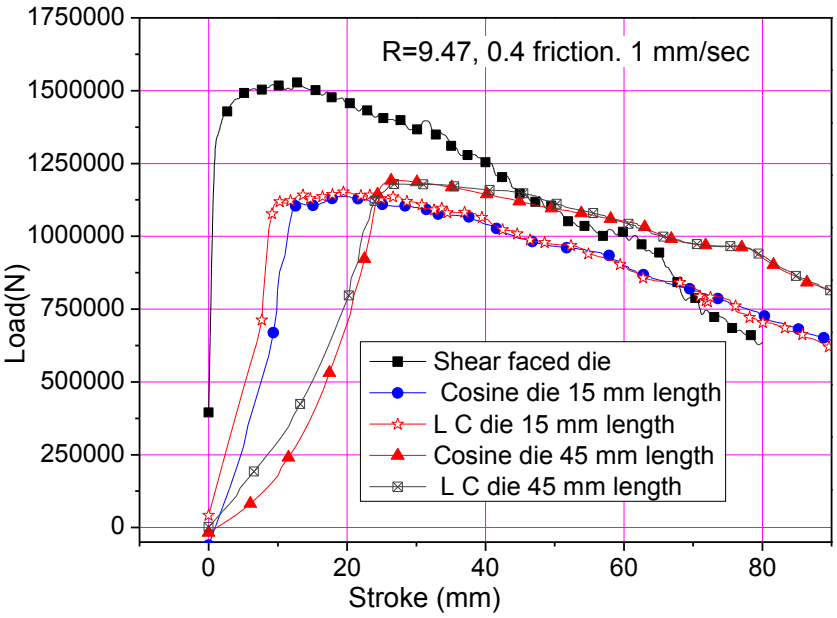

Figure 3.6: Variation of comparative load versus stroke

The increase of die length diminishes the slope of curve to achieve peak load but in shear faced die load increases suddenly with very negligible amount of stroke length,

which results in impact loading rather gradual. The load value after achieving peak condition falls downward with the increase of stroke. This slope condition is associated with the frictional work. The lesser slope is observed for the maximum die length, so there remains larger area under the curve that depicts more energy consumption. In this regard, the shear faced die results higher slope and maximum compared to other profiles. Entry and exit angle of cosine die profile is zero which causes the complete deformation in the in-between sections of die length. So load required for cosine profile extrusion is comparatively higher for larger reductions with lesser die length.

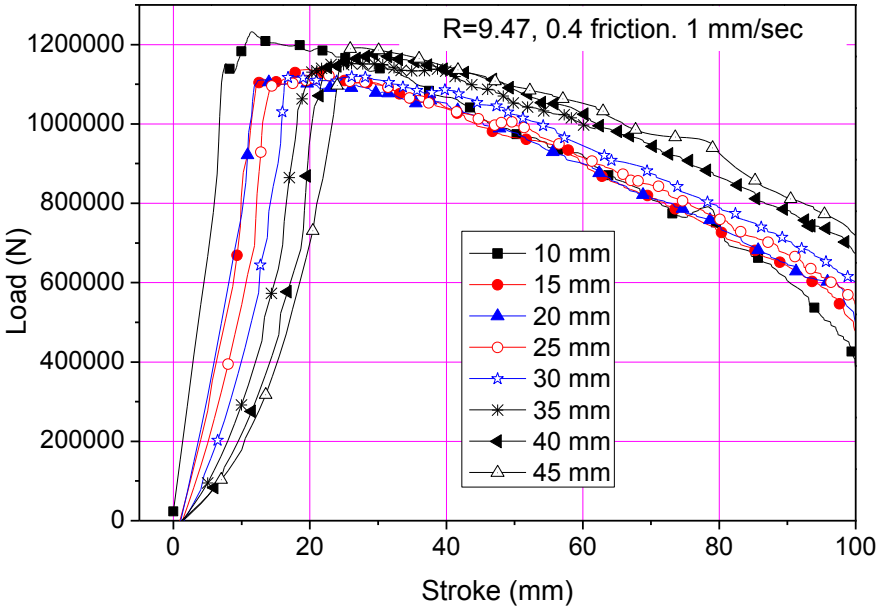

Figure 3.7: Variation of load versus stroke (cosine profiled die)

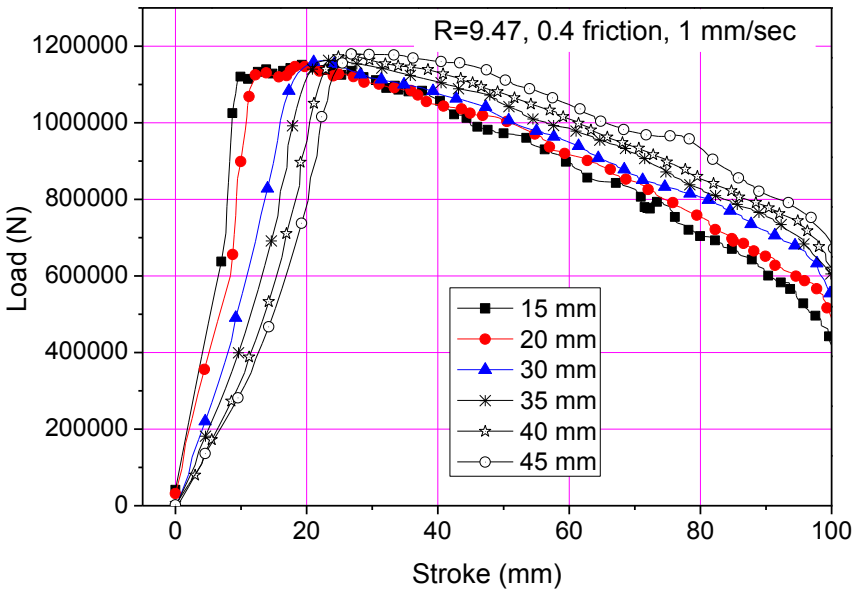

Figure 3.8: Variation of load versus stroke (linear converging die)

Effect of die length on maximum extrusion load for two different extrusion ratios 3.30 & 9.47 is clear in Figure 3.9. The optimum die length for the extrusion ratios 3.30 and 9.47 for the friction condition was found 20-25 mm and 20-30 mm respectively. This investigation is also satisfying the optimum die semi-angle i.e, 20-30 degree found for round rod extrusion by Noorani-Azad et.al [109]. At optimum die length, maximum extrusion load through cosine die is 3-5% lesser than linear converging dies. The difference in load requirement, between two different dies at optimum die length is maximum.

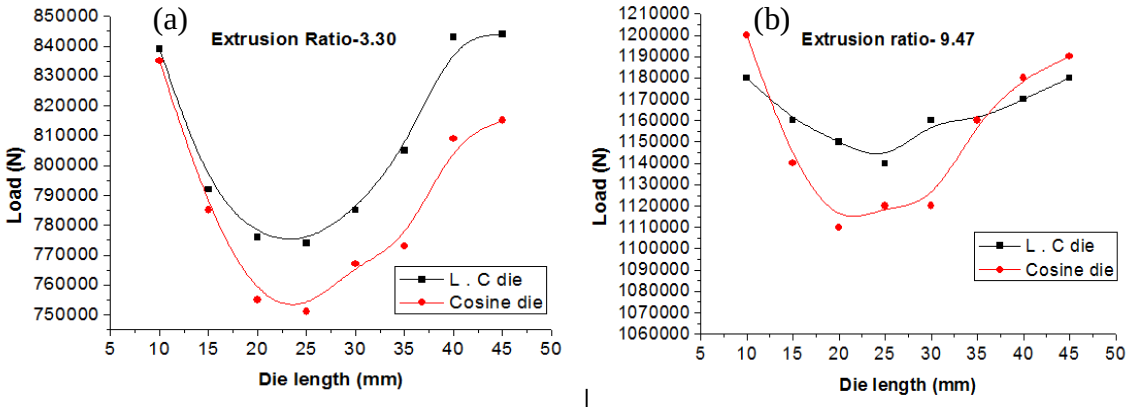

Figure 3.9: Variation of load w.r.t die length for (a) 3.30-R and (b) 9.47-R.

Effective-stress distribution with load prediction plot for extrusion ratio of 9.47 and ram velocity of 1 mm/sec is shown in Figure 3.10 for (a) cosine die (b) LC die and (c) shear faced die. The distribution for higher extrusion ratio i.e. 9.47 is shown, only because of its larger cross-sectional reduction and so the deformation zone. The distribution in a wide range is clearly visible. The distribution of different effects is more uniform for the case where there is a uniform flow. The distribution of effective stress is in increasing order from the punch side to the die exit direction. It also varies across the plane perpendicular to the extrusion direction. The uniformity of the distribution in the plane across the die (in the severe deformation zone) is necessarily required for the efficient extrusion process.

The simulation also predicts effective-strain and temperature distribution inside the billet during the process. The above-mentioned parameters for cosine and LC die are shown in Figure 3.11 and Figure 3.12 respectively. Temperature generation at die bearing area is more pronounced at higher ram velocity, and it causes the reduction of the extrusion pressure [39]. For cold extrusion, the effect is negligible because the

temperature generation may not reach the recrystallization temperature but for hot condition ram velocity is the significant factor to be considered.

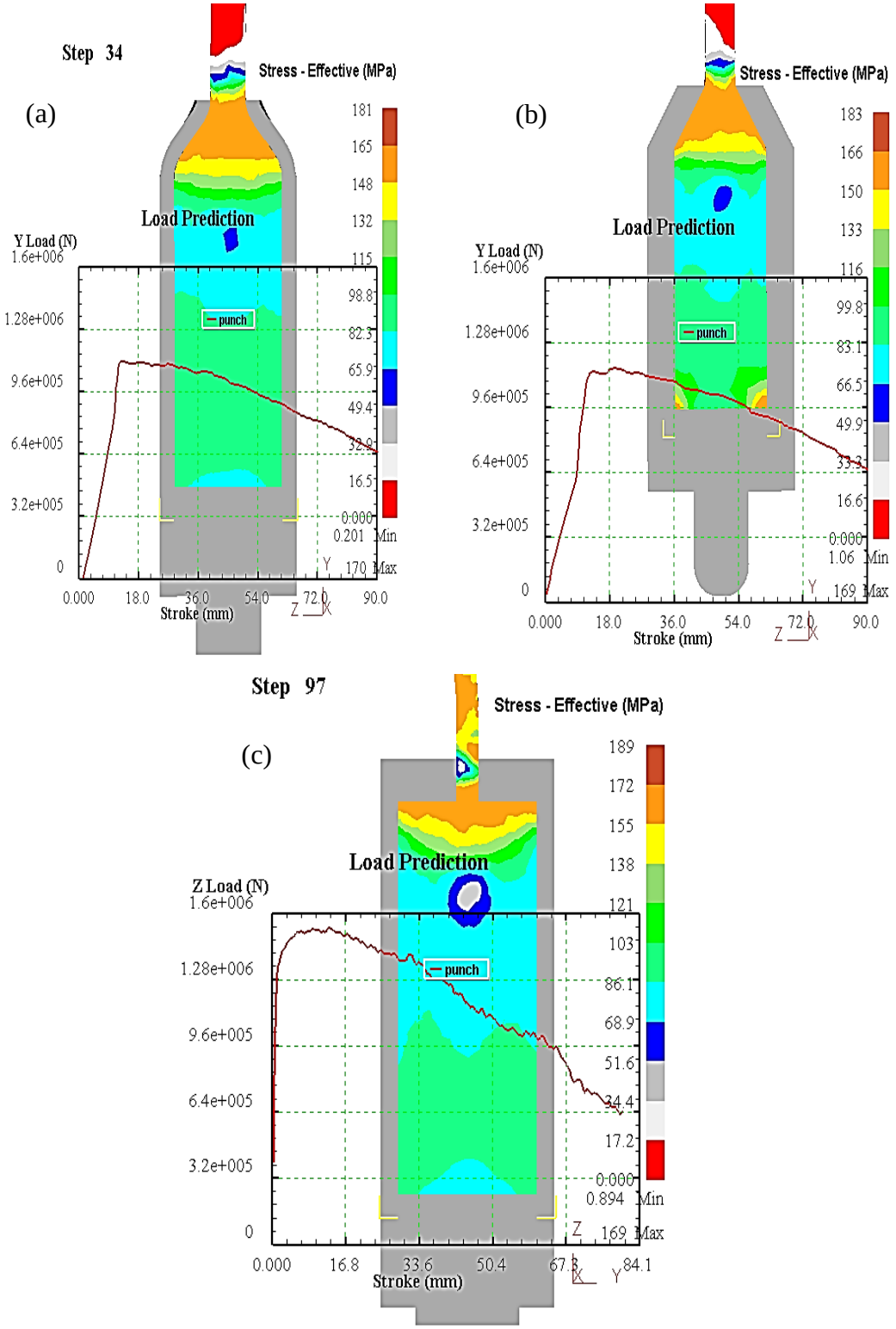

Figure 3.10: Effective stress Distribution & Load prediction graph for 9.47-R by (a) cosine (b) LC and (c) shear faced die

All the three parameters, effective stress, effective strain and temperature are larger at the corner zones in both profiles. To avoid the problem caused due to the maximum values, sharp corners should be prevented at the inside die surface by providing fillets, just up to the exit.

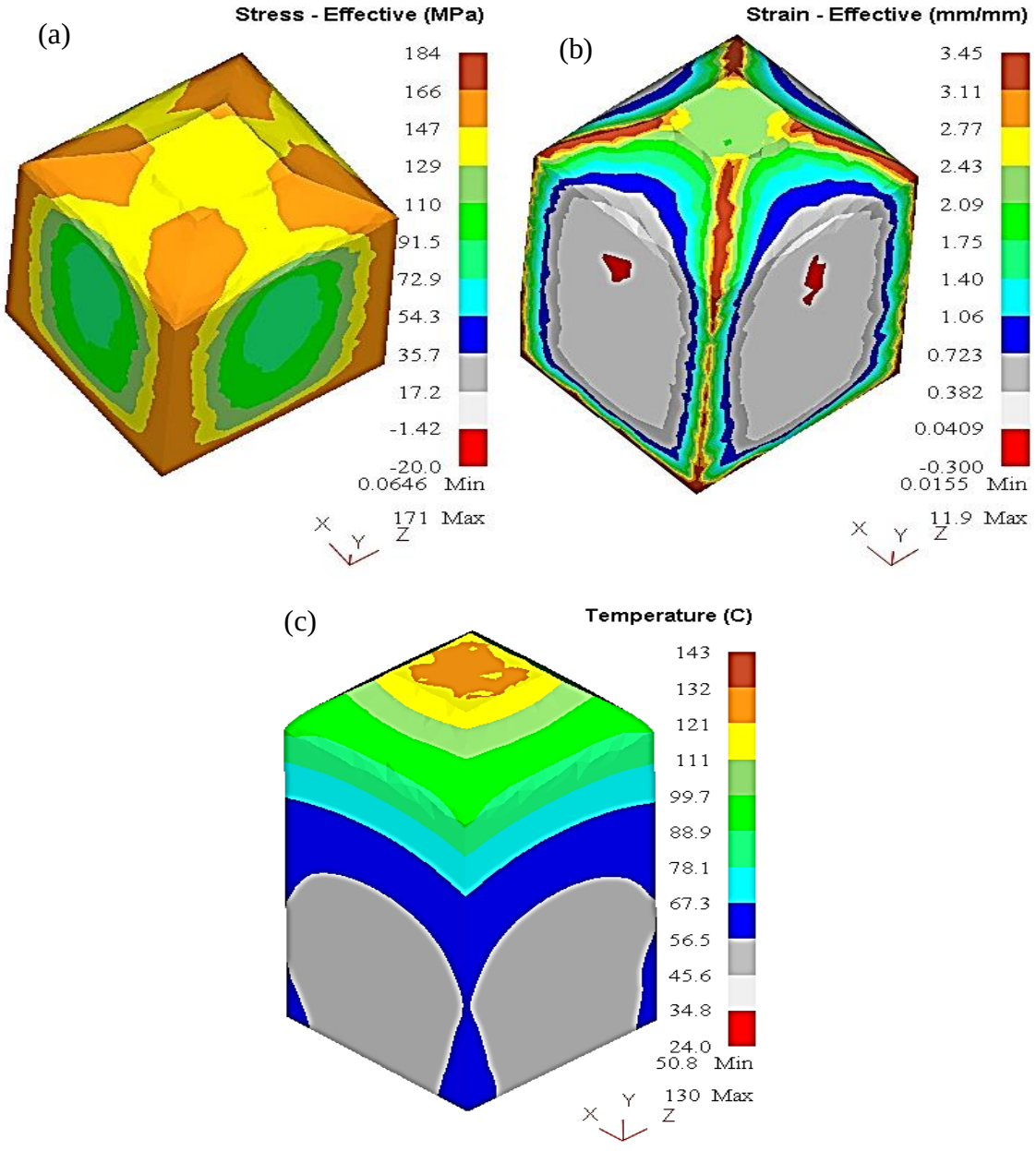

Figure 3.11: Effective (a) stress, (b) strain and (c) temperature distribution for 9.47-R by cosine die

3.4.2 Effect of ram velocity and extrusion ratio

To study the effect of ram velocity on the process, the parameter was varied from 0.1-10 mm/sec by considering other parameters constant. The variation of load with respect to stroke at different ram velocities is plotted in Figure 3.13 for shear faced die, Figure 3.14

for cosine die, Figure 3.15 for the linear converging die to examine the minimal effects on the process.

As flow stress property of the material is not strain-rate sensitive at the cold working condition, mentioned in Table 3.3, it will not influence load requirement much, but increased strain rate significantly affect heat generation. The rise of heat improves the flow property, so load-stroke graph becomes stiffer to down words with increased stroke [110]. Due to higher redundant work, heat generation in shear faced die at higher ram velocity is maximum.

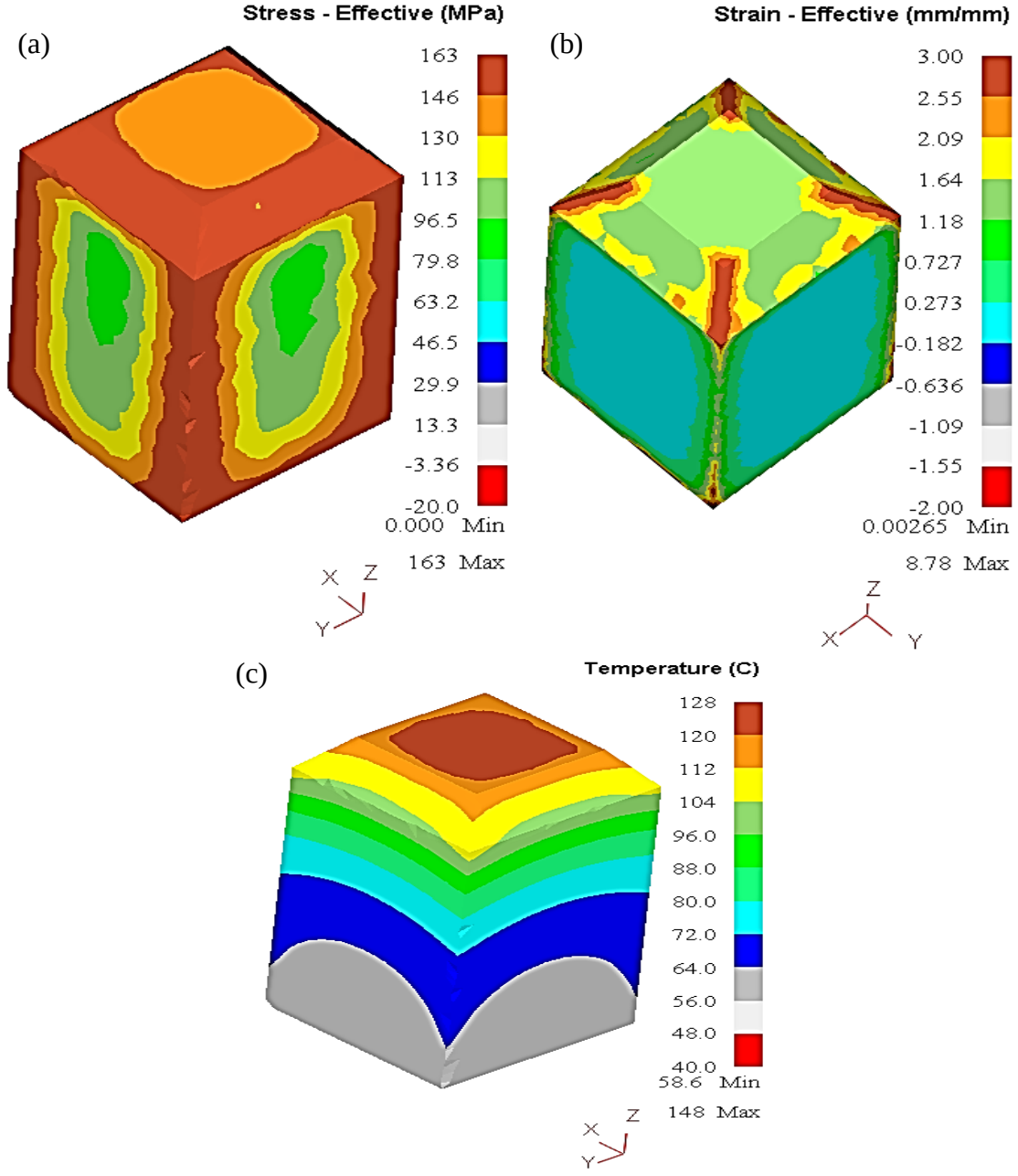

Figure 3.12: (a) Effective stress, (b) effective strain and (c) temperature distribution for 9.47-R by L.C die

The maximum heat generation ocours at the die exit which results in softening the billet and supports deformation. Hence, the plot in Figure 3.13 is much stiffer. It is evident from the above figure that, very slow ram velocity like 0.1 mm / sec, is not considerable for extrusion.

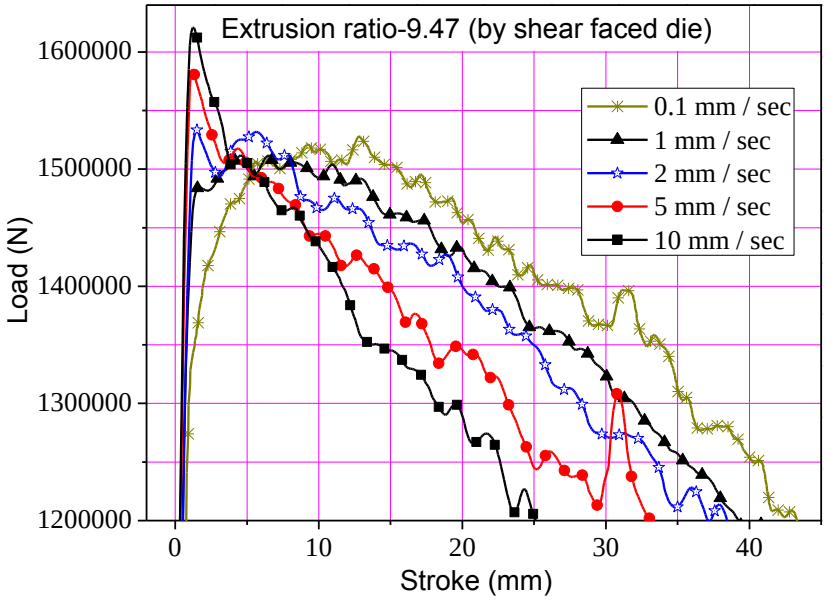

Figure 3.13: Variation of load versus stroke at different ram velocities

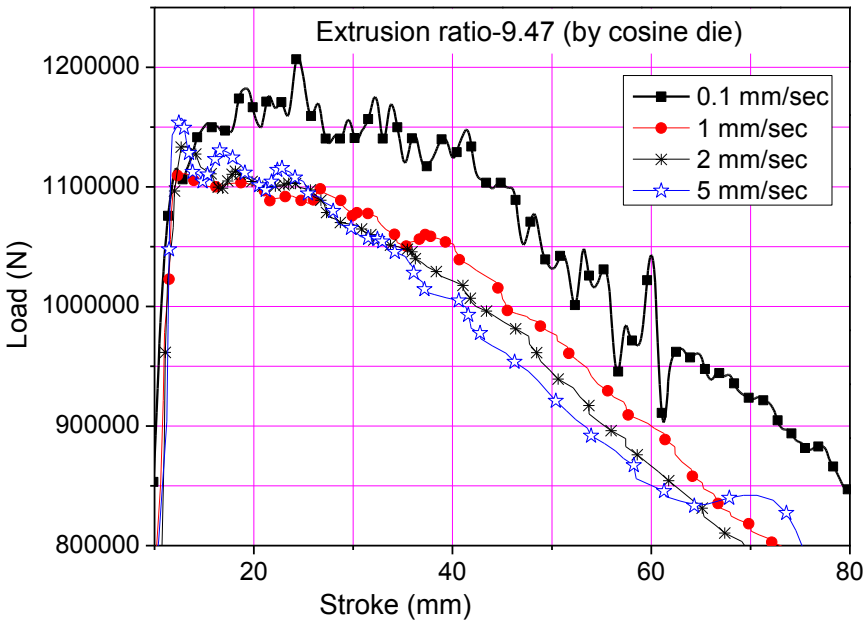

Figure 3.14: Variation of load versus stroke at different ram velocities

For a large volume of production in industries or for longer products, it is highly essential to improve greater extrusion ratios (R). Effect of extrusion ratio has the most significance on the power requirement, so the relation of maximum load with extrusion

ratio has been investigated. Simulations by varying 'R' as 2.04, 3.30, 5, 6, 7, 8 and 9.47 have been performed with constant 'L' and 'V'. From the above results the optimum range of parameters are chosen arbitrarily (die length, i.e., 19 mm and ram velocity 1 mm/sec) for estimating the load-R relation. It was depicted from the result; the load requirement for deformation increases following the logarithmic law with an increase of 'R'. Figure 3.16 shows the variation of of maximum load vs extrusion ratio. The trend line equation with five forward forecast periods is also shown in the illustration. The pattern of the plot is logarithmic for both the profiles. The trend line indicates that cosine profile is more effective at higher reductions with optimal extrusion parameters.

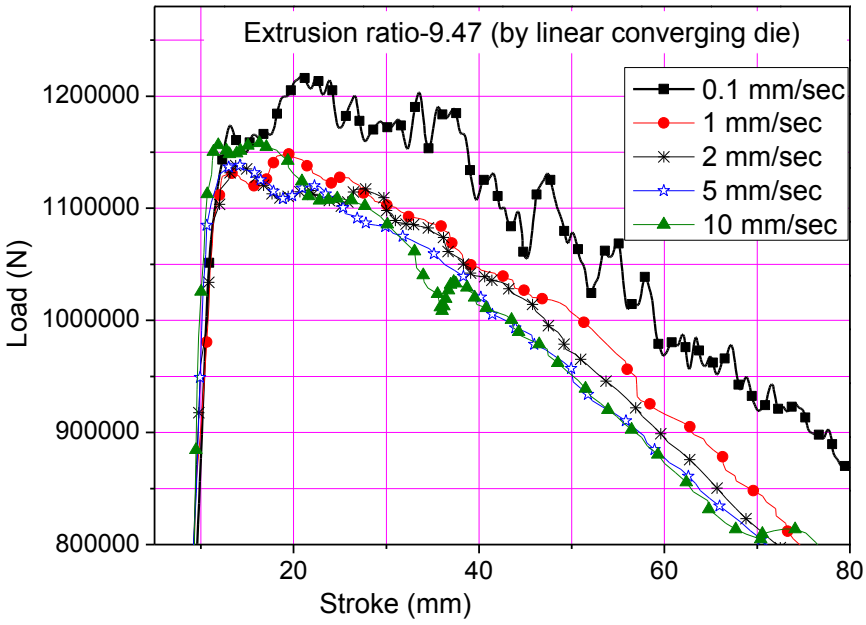

Figure 3.15: Variation of load versus stroke at different ram velocities

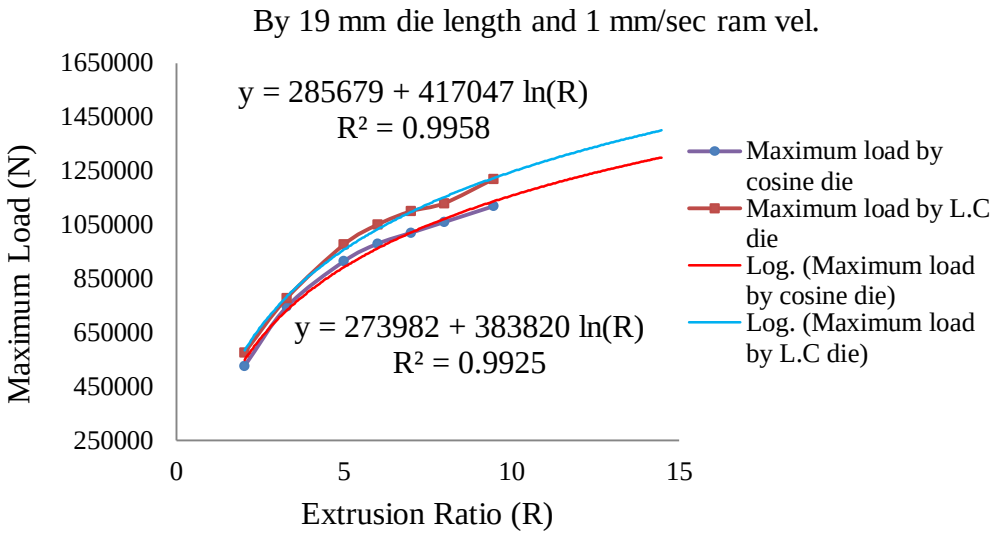

Figure 3.16: Maximum load versus extrusion ratio

3.4.3 Study of flow pattern and velocity relative difference

Flow grid pattern of the extruded billet through different die profile is investigated. Figure 3.17 shows the flow lines for extrusion ratio of 9.47, with ram velocity of 0.1 mm/sec and die length of 19 mm for (a) shear die, (b) cosine die and (c) linear converging die profile. It is depicted from the figure that dead metal zone exists with shear die and the flow of metal follows nearly cosine path at the boundary of dead metal and flow region. For linear converging die, die angle is constant from entry to exit, so metal approaches an abrupt change to flow direction at entry zone that creates a distortion zone at the entry corner, also a thick sticking layer exists at the inner periphery. In cosine die flow of material is smooth with very less sticking zone at the inner profile of the die hence a very less redundant work.

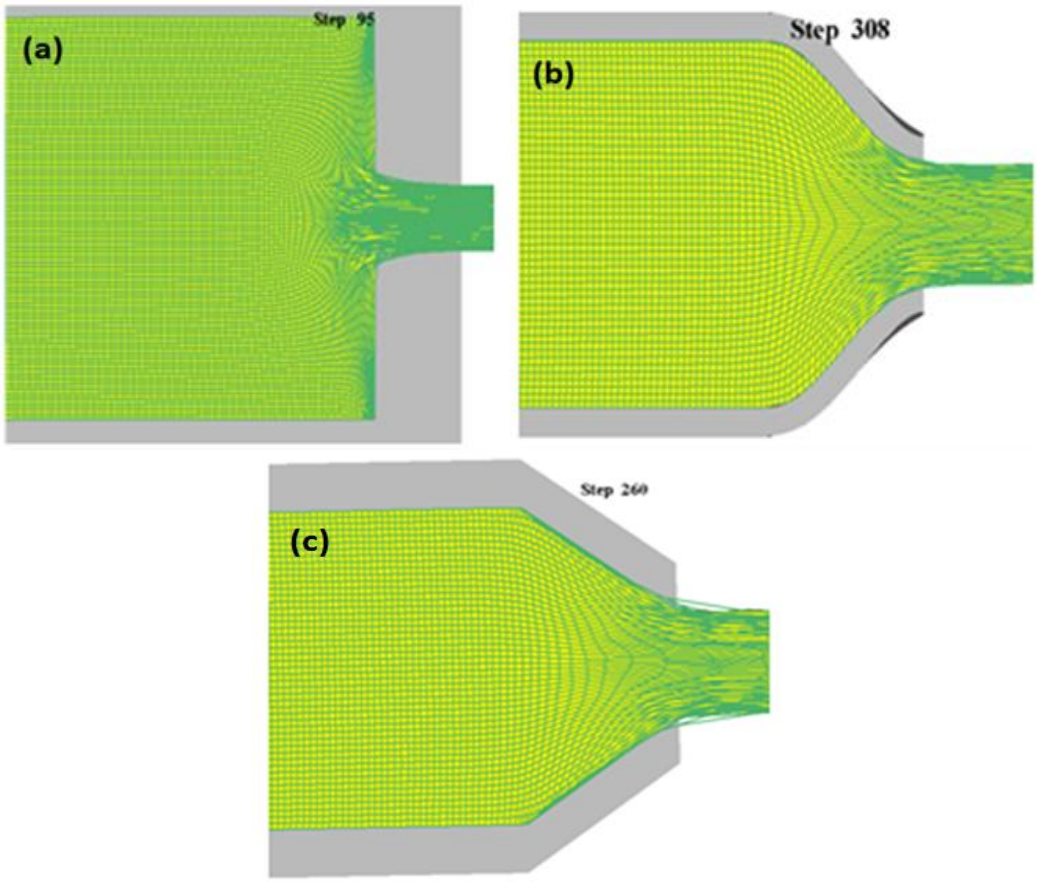

Figure 3.17: Flow pattern study of (a) shear faced (b) cosine profile and (c) linear converging die profile.

The relative difference of velocities of different points at the cross section of die exit is calculated by following the expression mentioned below:

$$VRD\ (\%) = \frac{\sum_{i=1}^{n} \left| \frac{v_i - v_a}{v_a} \right|}{n} \times 100 \quad [53] \qquad 3.24$$

where v_i is the velocity of an individual component, v_a is the average velocity of the selected components and n is the number of elements selected for the appraisal.

Figure 3.18 shows the relation between velocity relative difference with extrusion ratio for cosine as well as linear converging profile for 13mm and 19 mm die length. For both of the cases, cosine die profile gives lesser VRD (%) as there is no deformation at the exit end because of zero exit angle of the die. At the optimum die length, the VRD also remains less.

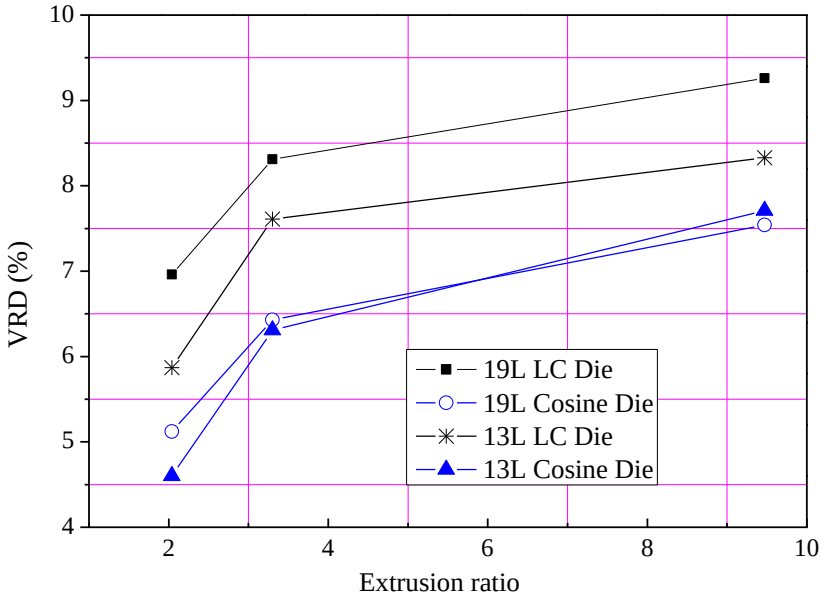

Figure 3.18: VRD (%) versus Extrusion ratio for cosine as well as LC dies

3.5 Conclusions

In the present investigation finite element modelling and simulation of square shape reduction from a square billet has been performed by DEFORM-3D software after its validation. Effects of different variable parameters on the process have been analysed and concluded as follows:

- Cosine die require lesser load for the extrusion operation of AA-6063 at room temperature condition compared to linear converging and shear faced die. At an optimum die length, maximum load required for extrusion by cosine die is 3-5% less than linear converging die.

- Load requirement improves with the increase of extrusion ratio logarithmically. At higher extrusion ratios, cosine die with optimum die length is more reliable than the linear converging profile.
- Effect of ram velocity in case of cold extrusion is very less, but it is not negligible. In case of shear faced die due to higher ram velocity, the temperature generation becomes maximum compared to other dies and puts significant effect.
- Heat generated, effective stress and effective strain at the corner zones are comparably higher than another zone in case of square bar extrusion.
- Velocity relative difference of metal flow is minimum for cosine die than linear converging (LC) and shear die, which can give a better surface finish and defect free product

Chapter 4

Extrusion Analysis of Al-6XXX through Linear Converging Die

4.1 Overview

In the field of automobile, architecture, aerospace and construction, use of heat treatable aluminum alloy is highly appreciable because of its attractive properties like excellent strength to weight ratio, high corrosion resistance, good formability and weldability [57]. Alloying of a number of additives (Cr, V, Zr, Ti, SiC etc.) with various series of aluminum alloy and processing by secondary manufacturing system forming, increases its mechanical properties manifold [111-113]. Extrusion is the only economical way in the sector of manufacturing for producing long, straight and complex cross-sectional products. Among a number of internal variables and state variables, few variables such as chemical composition, metallurgical structure, extrusion ratio (R), operating temperature and friction factor have the most significant effect on the process. For selecting an optimum combination of parameters and die shape, commercially available analogous simulation approaches based on either finite element method or finite volume method are extensively utilised these days to avoid a number of trial experiments of complex extrusions. A substantial amount of work has already been done to study the influence of variable factors on extrusion of aluminium alloy. During all the simulated investigation, friction factor is employed as a constant input variable. But in practical approach the friction condition is not constant; it varies with temperature, pressure and sliding velocity. Selection of a suitable lubricant for metal extrusion process is quite complicated. In the case of aluminium alloy a great probability of lubricant or impurity pickup from the die surface, so for unlubricated extrusion is the most preferable.

The design of a tooling setup must fulfil the uniform and stable metal flow at its die exit to avoid warped deformation and bending of the product. Zhang et al. [53] optimized the process parameters by considering 32 combinations of parameters for a hollow and complex cross-section of AA-6063 to get a minimum velocity relative difference (VRD) at die exit. Extrusion ratio, friction condition and ram speed have the greatest influence on the VRD. Effect of ram speed on several variables along with VRD has been investigated to find the optimum range [58, 64]. Not only die profile but also

punch shape influence the flow characteristics of the metal. Effect of inner cone punch for avoiding dead metal zone is established by numerical simulations and verified by experimentation [10]. The analysis was performed for the extrusion through shear faced die.

In this chapter, both flow stress and frictional coefficient with the die material at a constant strain rate are determined at different temperatures. A computerised simulation approach was applied to find the influence of friction on the extrusion load. The interrelation between redundant work and frictional force with respect to variation of die length was analysed. The numerical simulation results were validated through experimental hot extrusion from round to square bar through linear converging die. The effect of friction on required load as well as VRD has also been investigated. In addition, the effect of punch type on flow property as well as the load-stroke plot has been studied in detail.

4.2 Determination of flow stress and friction factor

Determination of flow stress of work material is indeed a crucial prerequisite for a metal worker to estimate the power requirement to accomplish an experiment. Flow stress is essentially temperature (T), strain ($\bar{\varepsilon}$) and strain rate ($\dot{\bar{\varepsilon}}$) dependent i.e. $\sigma = f(T, \bar{\varepsilon}, \dot{\bar{\varepsilon}})$ [38, 57]. At cold working condition there is no significant effect of strain rate, but in case of hot working the effect of strain rate is more sensitive because of dynamic recrystallization within the deformation zone. Flow stress of the work material 'Al-6XXX' containing major chemical compositions such as mass fraction of 0.520 Mg - 0.530 Si - 0.031Mn - 0.199 Fe - 0.056 Cu - 0.020 Zn - 0.029 Ti - 0.015 Cr and rest Al has been investigated at a constant strain rate of 0.1 s^{-1}. The test has been conducted in an isothermal environment at four disntict temperatures viz. 300℃, 400℃, 500℃ and 550℃. Aspect ratio (height/diameter) of billet for cylinder compression test was considered as 1.5 : 1 = 30 : 20 mm as shown in Figure 4.1. Before compression, the setup was arranged in a temperature controlled furnace as shown in Figure 4.2. The requisite operating temperature was set with a rate of temperature rise of 6℃/min and a dwell of 30 minutes was maintained.

A flat ring shape specimen was compressed to a known reduction for determining the shear friction factor (m), as the changes in dimension is very much friction sensitive [56]. Ring compression test was conducted under the same condition as cylinder compression, to determine friction factor for the specimen with an aspect ratio (outer

diameter : inner diameter : height) 6 : 3 : 2 = 30 : 15 :10 (Figure 4.3) at 300℃, 400℃, 500℃. Commercially available high-temperature lubricant molybdenum disulfide (Molykote-1000) [114] was applied for both the tests. It is a lead and nickel free high temperature stable lubricant.

Figure 4.1: Pre-tested specimen along with the tested specimen

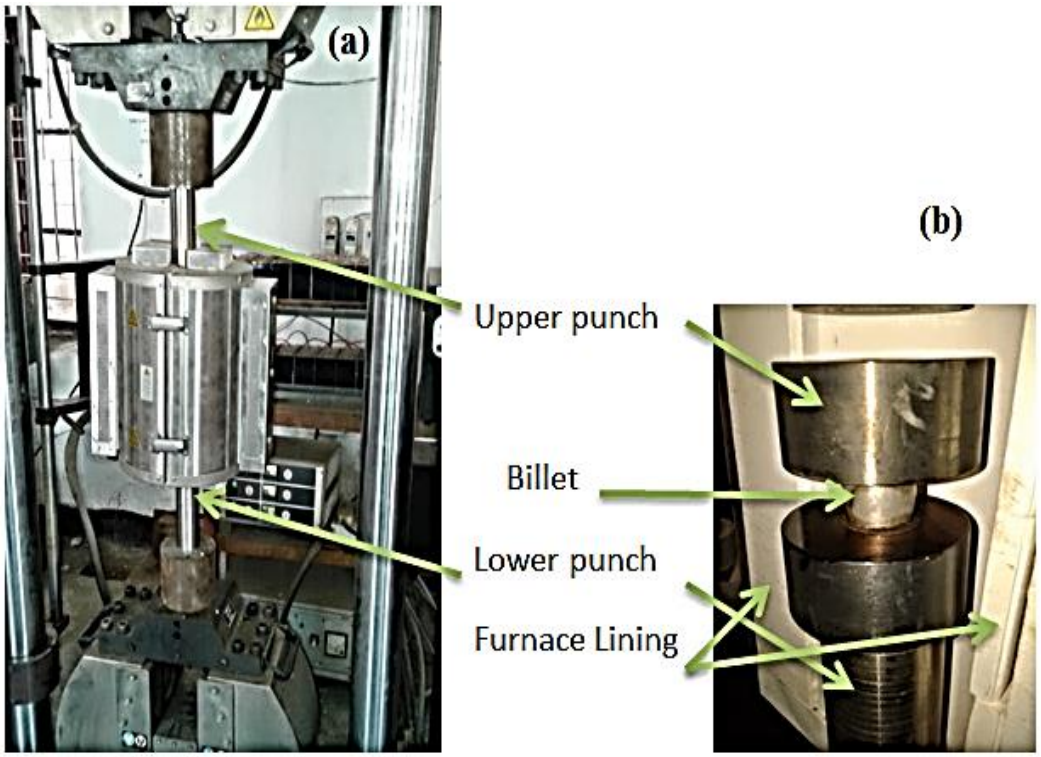

Figure 4.2: (a) The hot compression set up during operation (b) Inside view of the furnace

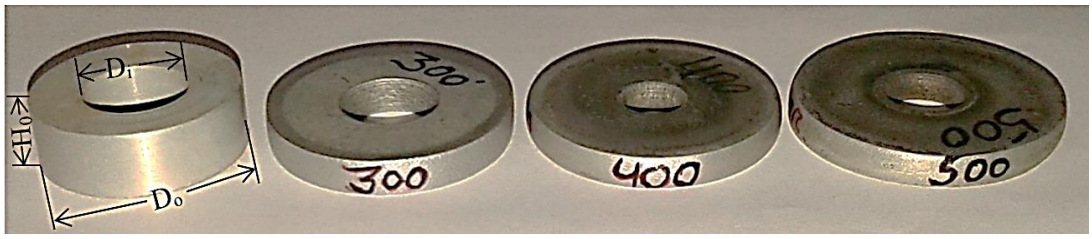

Figure 4.3: Initial ring specimen along with the tested specimen

4.3 Modelling of extrusion

Commercially available DEFORM-3D^{TM} simulation system was conceived for the investigation. The tooling geometries were imported as .stl file and simulation were carried out at different friction conditions for different extrusion ratios at various temperatures. The detail description of the software procedure is described in Chapter-3. Effect of friction coefficient, die length and punch shape of the process with respect to power consumption has been investigated. The modelling parameters considered for the analysis are presented in Table 4.1.

AA-6063, in tetrahedral mesh has been considered as work material for the extrusion modelling. The properties of the work material selected from the database are presented in Table 4.2. Flow stress of the considered metal for simulation is effective strain, effective strain-rate and temperature dependent. Yielding of the material follows the Von-Mises yield criterion.

Table 4.1: Parameters considered for simulation

Process parameters	**Values**
Billet length (mm)	30
Billet diameter (mm)	20
Operating temperature (°C)	30, 500
Extrusion ratio (R)	2.0, 3.33, 10
Ram velocity (V) (mm/sec)	1
Interface Friction factor (m)	0.1, 0.2, 0.3, 0.4, 0.5, 0.6, 0.7

Table 4.2: Properties of AA-6063

Material	Young's Modulus (MPa)	Poison's ratio	Thermal expansion (1/°C)	Thermal Conductivity (W/m/°C)	Heat capacity (N/mm^2/°C)
AA-6063	68900	0.33	22×10^{-6}	180.2	2.43357

4.4 Results and discussion

4.4.1 Flow stress and friction condition

Typical true stress versus true strain plot obtained during the hot compression test of a cylindrical specimen is shown in Figure 4.4 at a constant strain rate of 0.1 s^{-1}. It is revealed from the figure that the temperature is directly related to flowability. Because of dynamic precipitation and dynamic recrystallization, at higher temperatures true stress

value increases up to a strain of 0.25 and then marginally decreases. At lower temperatures recrystallization and precipitation process is not significant within the short time period. On the other way, strain hardening effect persists in the billet so true stress value increases with the increase of true strain.

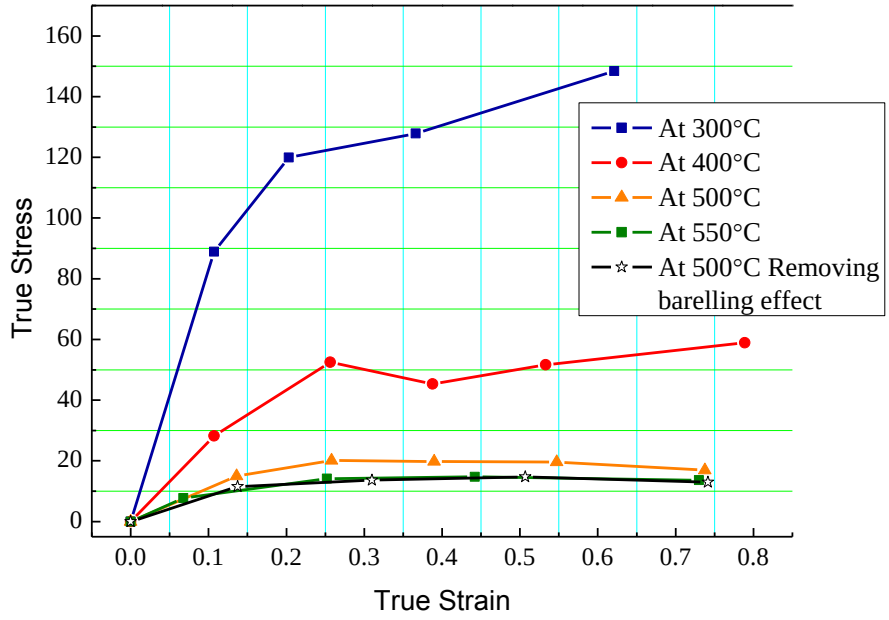

Figure 4.4: True stress versus true strain at a strain rate of 0.1 s^{-1}

Ludwik's power law $\sigma = k \times \varepsilon^{n}$ to express the flow stress at different temperatures for the investigated material, neglecting the strain rate dependence is noted beneath. Here the strength coefficient and the strain hardening coefficient are abbreviated as 'k' and 'n'. The power laws to express flow stress at different temperatures and a constant strain rate are as follows:

$$\text{(at 300°C)} \quad \sigma = 190.73 \times \varepsilon^{0.351} \qquad 4.25$$

$$\text{(at 400°C)} \quad \sigma = 108.95 \times \varepsilon^{0.614} \qquad 4.26$$

$$\text{(at 500°C)} \quad \sigma = 92.52 \times \varepsilon^{0.543} \qquad 4.27$$

$$\text{(at 550°C)} \quad \sigma = 24.46 \times \varepsilon^{0.42} \qquad 4.28$$

In metal forming industries ring compression test is a very common technique to determine the interface friction condition between two metallic bodies. When a flat ring specimen of the standard dimension is pressed under zero friction condition, the radial expansion of the material occurs as if it were a solid cylinder. Expansion of the inner and outer diameter of the ring at the expense of specimen height is the indication of low friction condition. At a critical friction condition, the inner periphery remains stable and

with increased friction condition inside material flows towards the center and the internal diameter decreases. In the present investigation three sets of compression were conducted for a sample at a constant temperature and after each reduction the dimensional changes have been measured. The accounted points were fitted in a standard calibration plot of height reduction versus internal diameter reduction for 6:3:2 specimen dimension as shown in Figure 4.5. The increase in temperature leads to improved friction condition as revealed from the analysis [115]. The range of shear friction coefficient (m) lies between 0.4 - 0.7 within the temperature range of 300 – 500 ℃. Due to the temperature change the thermal property, visco-elastic property along with some other physical property changes significantly which directly influence interface friction behaviour.

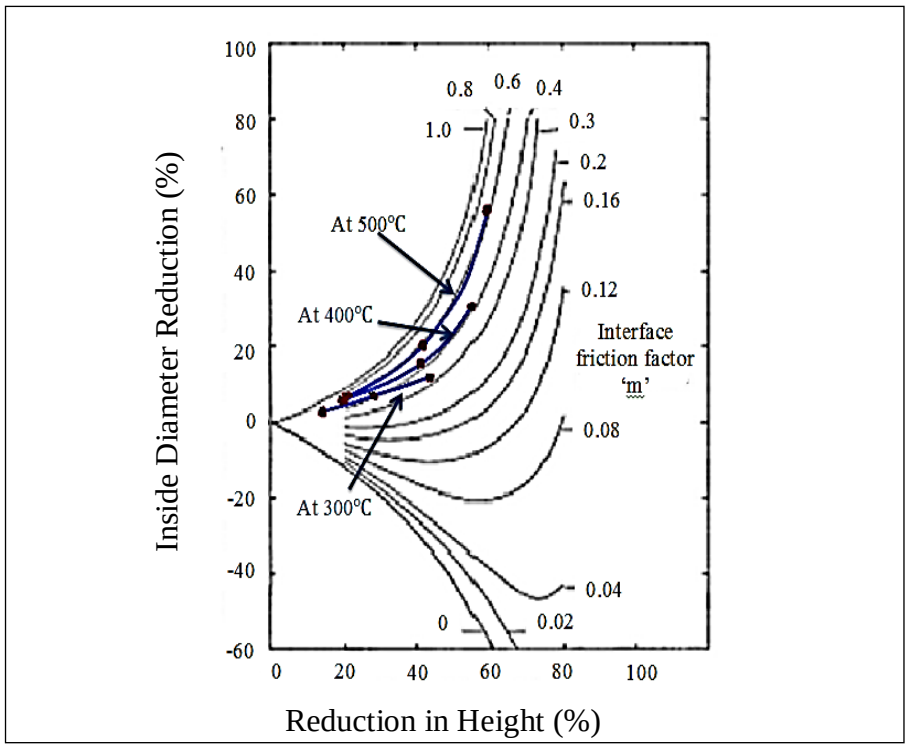

Figure 4.5: Standard calibration curve for ring specimen of 6:3:2 dimension

The performance of the lubricant decreases with the increase in temperature. The billet compressed at 300℃ is having very negligible amount of barrelling because of good lubrication effect. But the specimens compressed at higher temperatures have visible amount of radius of curvature (Figure 4.1) indicating the decrease of lubricant performance.

4.4.2 FEM analysis

FE analysis in the field of metal forming has revolutionised the art of investigation during the last decades due to its easy, cheap and user-friendly computer technology. The

extrusion process is affected by a number of variables; these estimations during experimental operation are unprecedented. So in this investigation effect of friction, die length and punch shape on the process has been analysed in order to minimize power consumption and to improve product quality by means of an illustrious finite element modelling software.

4.4.2.1 Effect of friction

The total energy necessary for accomplishing extrusion is the area under load-stroke plot. Most of the energy is spent for homogeneous deformation as well as to overcome friction in the process. The frictional energy consumption depends on the billet length, working environment like temperature and lubrication as well as material type. The friction coefficient at every place of the die-billet interface is not remain constant; it varies depending upon temperature, pressure and sliding velocity, but in the FEM analysis the friction condition is assumed constant throughout the process. Load versus stroke plot for 'R' = 2, 3.33 and 10 is shown in Figure 4.6, Figure 4.7 and Figure 4.8 respectively for different friction conditions. It is elucidated from the figures that as the shear friction coefficient (m) increases between billet and die/container interface, the pressure required to accomplish the process significantly increases. For every 'R' maximum load requirement for extrusion at the frictional condition of 0.7, is more than double of 0.1 friction state. At the same time with the increase in friction coefficient, relative velocity of the metal across the cross section increases, this requires more energy for internal deformation: improved redundant work.

The plot between maximum pressure required (P_{max}) for extrusion and shear friction coefficient is shown in Figure 4.9 for the aforementioned extrusion ratios. The figure revealed that P_{max} increases with the increase in friction condition. The graph fit with fourth and fifth order polynomial curve with the very negligible amount of residual errors. The regression equations were also generated for prediction of maximum pressure required for extrusion in relation with frictional coefficient by keeping other variable parameters constant. Effect of friction is more significant in higher extrusion ratios, which is apparent from the higher slope of the curve. As the extrusion ratio increases, the temperature generation, deformation rate and internal pressure increases which are directly supports the raising of friction condition. To overcome all the redundant work, the force require is higher so the slope of the plot at higher extrusion is higher.

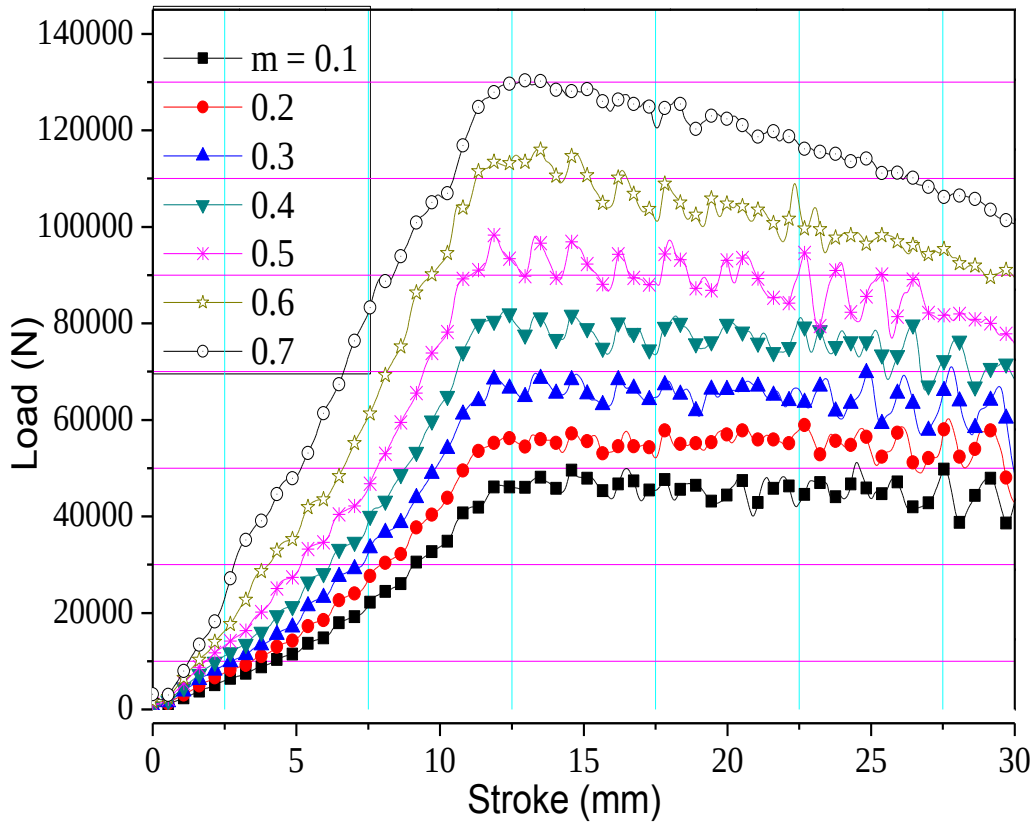

Figure 4.6: Variation of load versus stroke for extrusion ratio-2

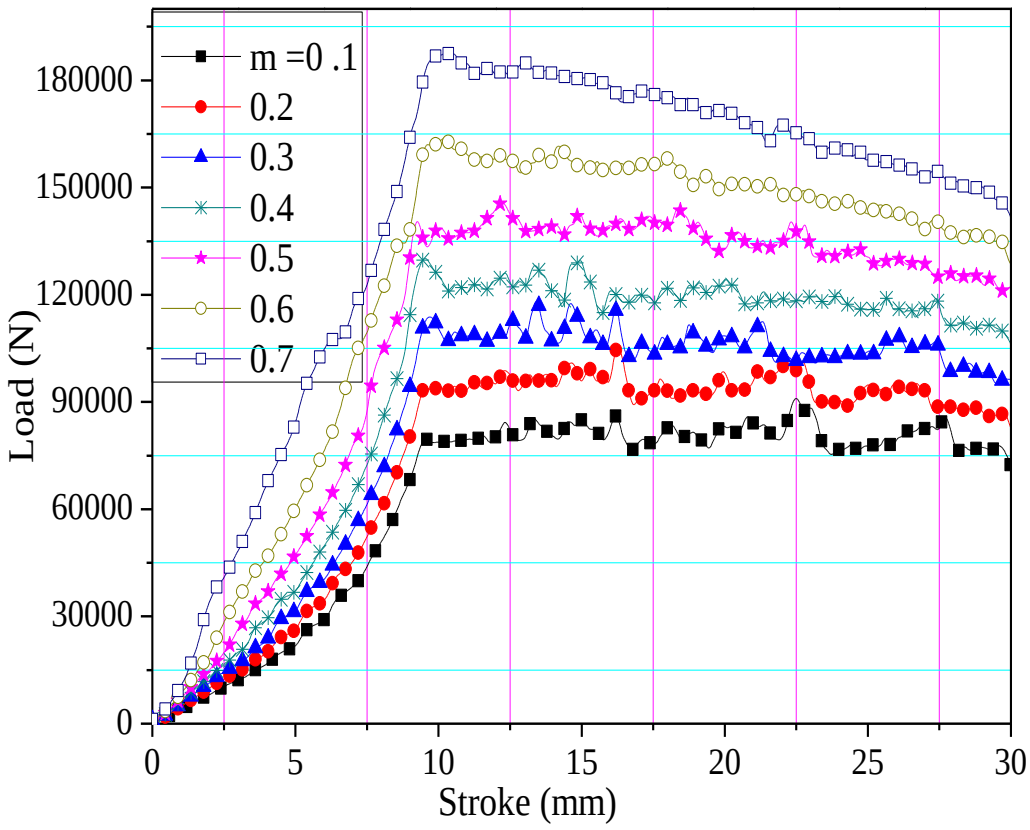

Figure 4.7: Variation of load versus stroke for extrusion ratio-3.33

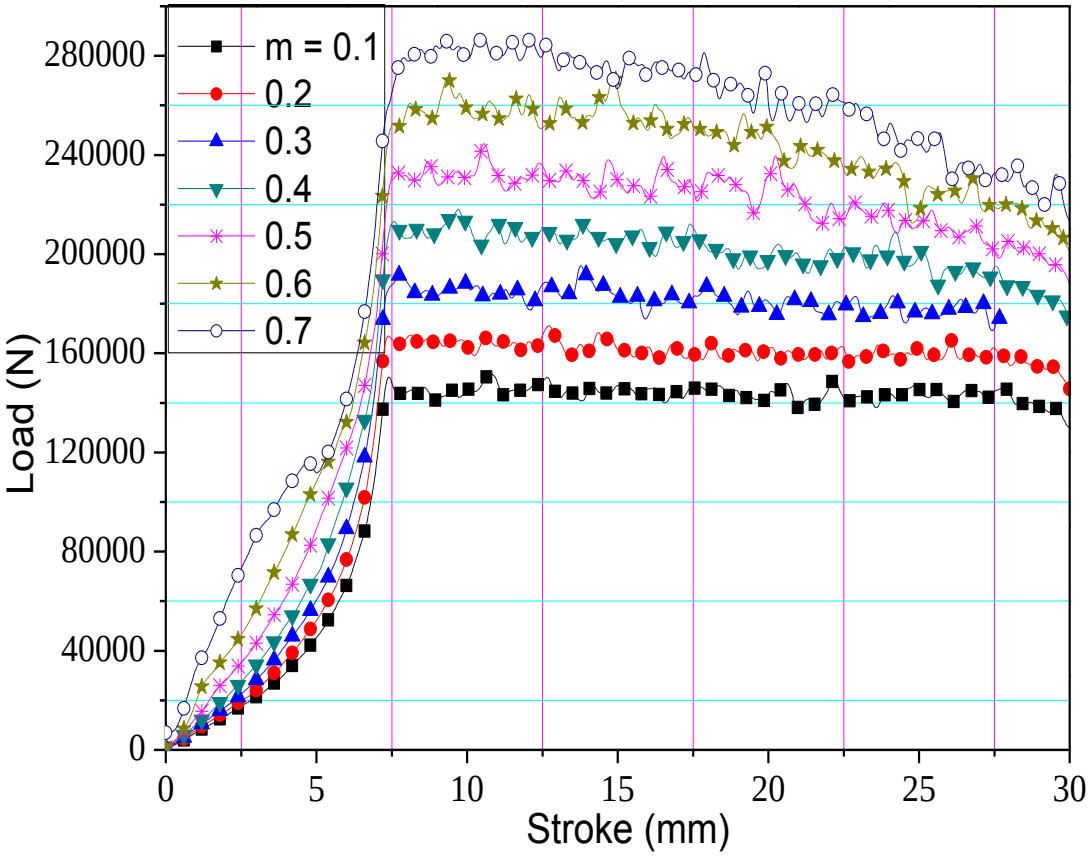

Figure 4.8: Variation of load versus stroke for extrusion ratio-10

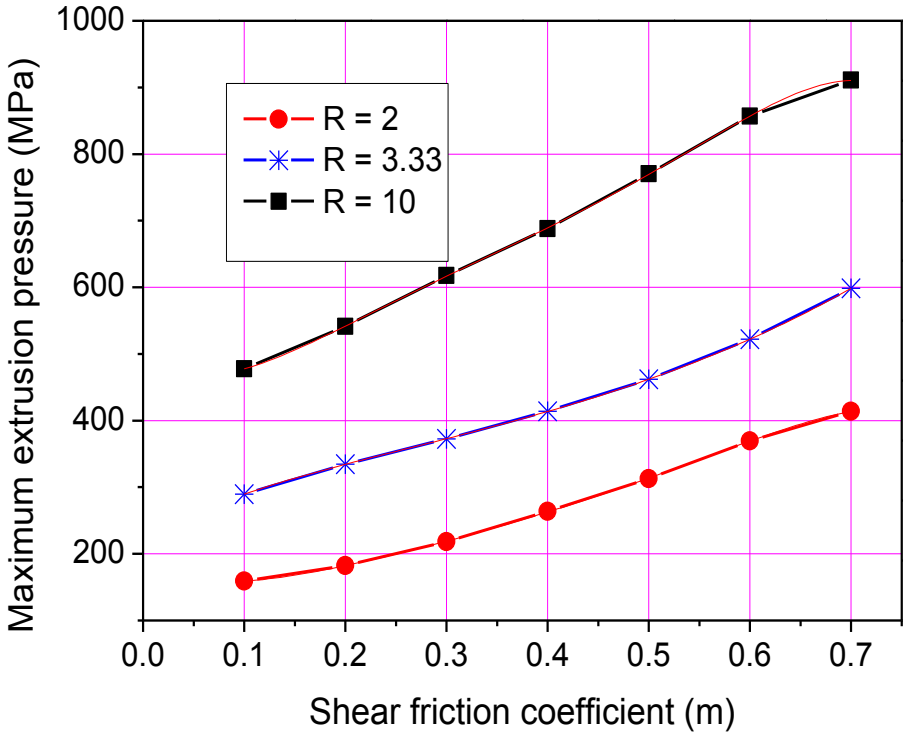

Figure 4.9: Variation of maximum extrusion pressure w.r.t frictional co-efficient

The regression equations with their residuals for three extrusion ratios are mentioned below:

$$P_{max}\ (R=2) = -1170.1x^4 + 1138x^3 + 126.06x^2 + 144.51x + 141.99 \quad (4.29)$$

$R^2 = 0.9999$ (Coefficient of determination)

$$P_{max}\ (R=3.33) = 884.64x^3 - 724.14x^2 + 589.8x + 237.49 \quad (4.30)$$

$R^2 = 1$ (Coefficient of determination)

$$P_{max}\ (R=10) = -3980.9x^4 + 5396.3x^3 - 2242.6x^2 + 1034.9x + 390.81 \quad (4.31)$$

$R^2 = 0.9997$ (Coefficient of determination)

4.4.2.2 Effect of die length

The load required for complete extrusion is the aggregate of load necessary to overcome friction (at die and container interface), load required for homogeneous deformation or ideal work and some amount of redundant work. As die length increases, die angle decreases and work required to overcome friction increases whereas, redundant work increases with the decrease of die length. Two factors here (friction and redundant work) are antagonizing each other with the variation of die length. To investigate the effect of die length extrusion of aluminium alloy by varying the die length from 5-30 mm with the rise of 5 mm was performed by simulations considering other parameters constant.

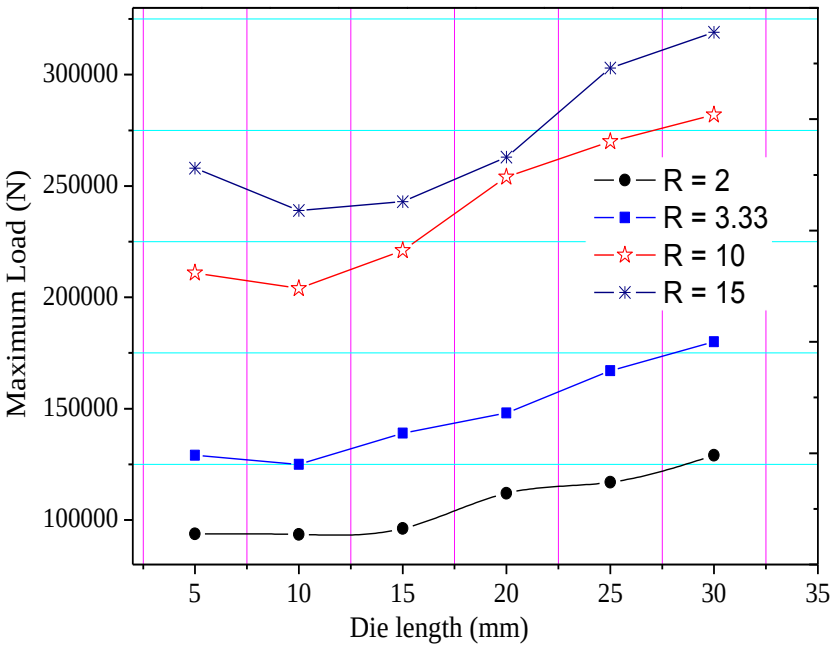

Figure 4.10: Variation of maximum load w.r.t die length

The shear friction coefficient, ram velocity, temperature are considered are 0.5, 1mm/sec, and 500℃ respectively. The value of friction factor here is high (m = 0.5,

depending on the temperature condition). So it has the more ascendance over redundant work, that is because maximum load requirement increases with the increase in die length (shown in Figure 4.10). optimal die length also increases with the increase in extrusion ratio and friction condition [116].

4.4.2.3 Velocity relative difference (VRD)

In all extrusion cases, the product quality is significantly influenced by the uniformity in flow velocity at the die exit plane. It is inconceivable to get the same velocity at every point at the cross section of the product. The velocity at the boundary layer of the billet, which is in contact with the inner periphery wall of the container and die, is restricted to move freely due to frictional effect. The die profile which guides the flow path has also the influence on VRD. So there exists a relative difference in velocities between different layers of extrudate in a plane perpendicular to the extrusion direction at the die exit. Earlier review shows that the VRD increases with the increases of the frictional coefficient that is directly affecting the amount of work done and surface properties [58]. By using linear converging die with considering the optimum die length i.e., 10 mm at 500℃ and ram velocity of 1 mm/sec relative velocity difference for different reductions at different friction conditions were determined.

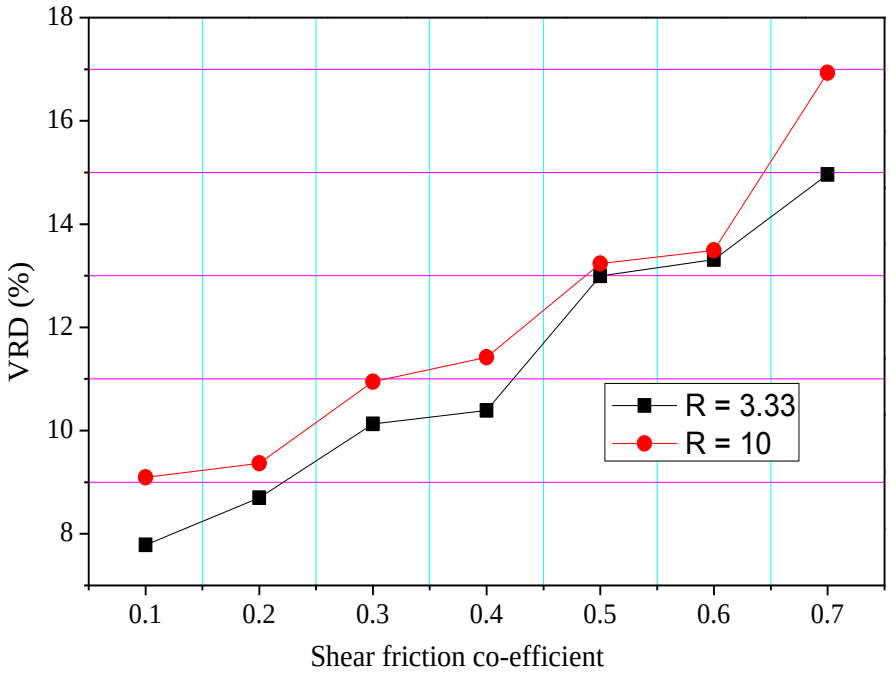

Figure 4.11: VRD versus shear friction coefficient

VRD to represent metal flow uniformity in percentages is expressed as follows:

$$VRD(\%) = \frac{\sum_{i=1}^{n} \frac{|v_i - v_a|}{v_a}}{n} \times 100 \qquad 4.32$$

where n is number of considered nodes, v_i is the instant velocity of the node i at die exit and v_a is the average velocity of considered nodes. Number of nodes in different zone at die exit has been selected for calculating VRD.

The smaller the value of VRD the better will be the product quality. For low 'R' the effect of VRD is negligible. So it was checked for R= 3.33 and 10. Figure 4.11 shows the curve that presents VRD in terms friction factor for two different reductions. As discussed earlier relative velocities induced in the metal due to the effect of die shape and friction factor that causes internal shear deformation. For these unwanted shear deformation, consumption of power decreases process efficiency. Maximum pressure for extrusion is also increasing exponentially with relation to VRD revealed from Figure 4.12. The velocity difference caused during extrusion through shear faced die is very high, because of this reason, the process through shear faced die is inefficient as well as gives bad product quality.

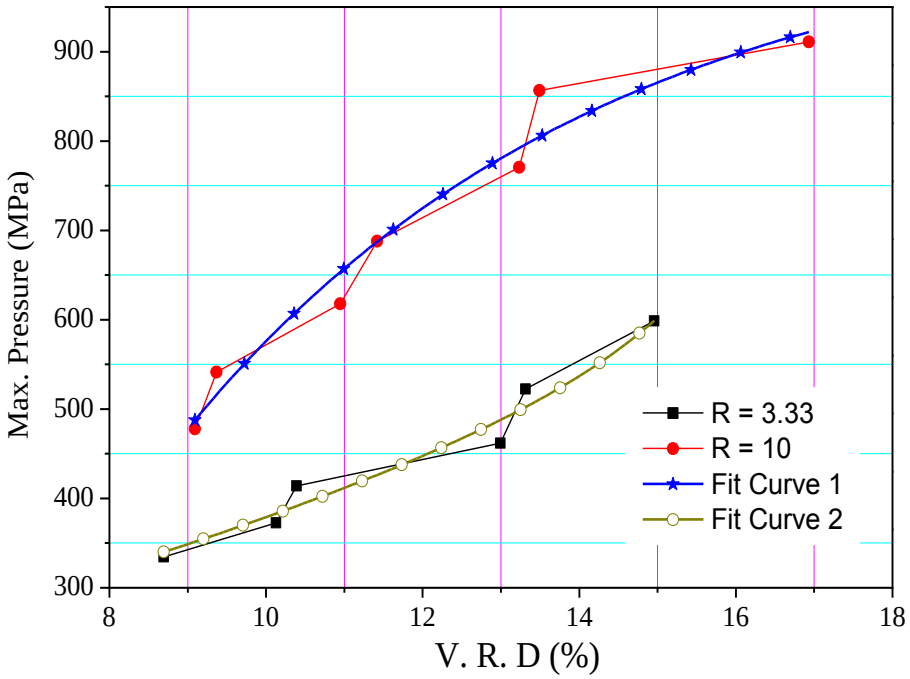

Figure 4.12: Variation of max pressure w.r.t VRD

4.4.2.4 Effect of punch shape

Velocity difference inside the container across a plane perpendicular to extrusion direction exists due to the frictional effect. The highest velocity at the core along the extrusion

direction and the lowest velocity at the boundary causes product defects. By using different types of punch, the flow of the metal gets affected in case of extrusion through shear faced die. In this case, various kinds of punch are used to analyse its effect on flow characteristics. The process is examined with the inner cone as well as conical punch with semi-angle of 45°, 60° and also with a flat punch as shown in Figure 4.13 (a). The simulations with the same database by changing only the punch type were performed. To investigate the flow characteristics, grid pattern analysis at a plane along the extrusion direction has been performed. Figure 4.13 (b) shows the corresponding flow line grid pattern caused by different types of punch. Of course there exists a visible amount of change in flow line grid pattern in side the container. In the case of two conical punches, the metal at the back end flows from center to the extreme corners where it counteracts the reverse relative movement of the metal from the shear boundary zone. These types of punch are useful to create extra pressure at the boundary layer to flow forward against the frictional force.

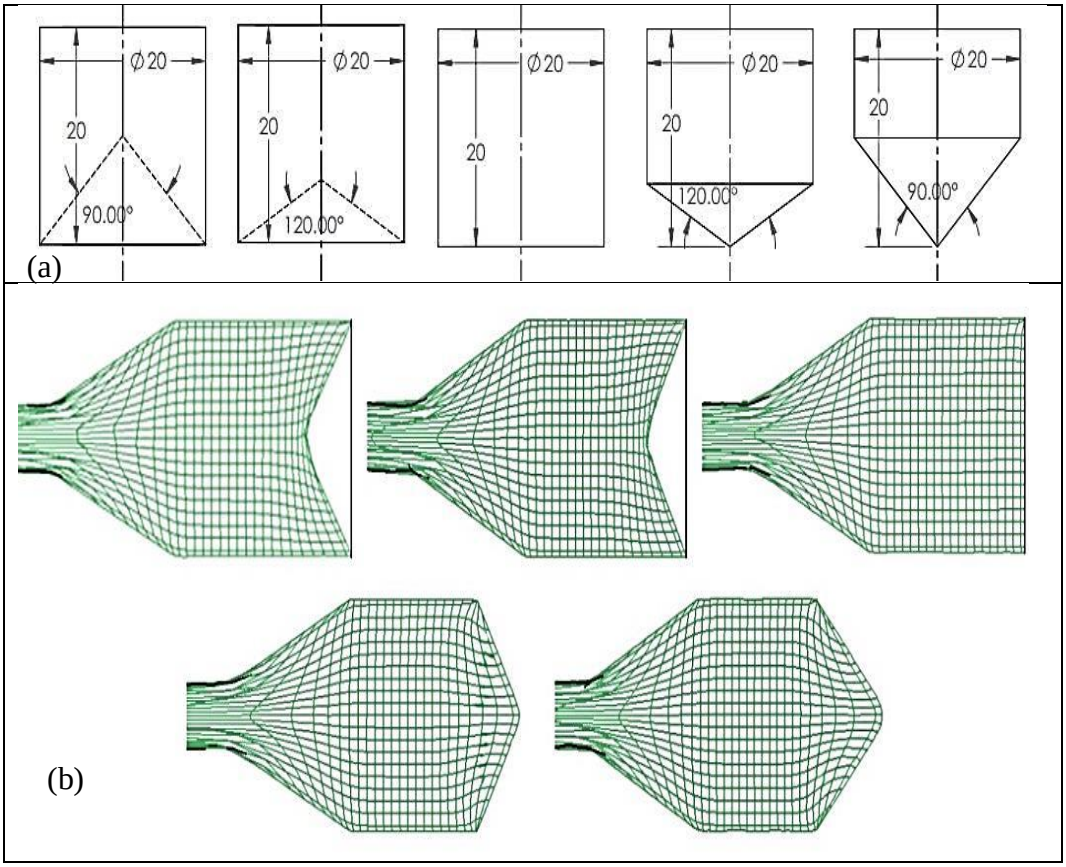

Figure 4.13: (a) 2D drafting of punch shapes and (b) flow grid pattern

The use of inner cone punch acts reverse to the conical punch. In this case, the metal at the back end tries to flow from the periphery to the centre end and forward along

the ram direction. Use of this punch creates pressure along the core line to move forward and the boundary layer of material faces lesser frictional registances.

There is no clear indication of any significant difference in the flow pattern due to the variation of punch shape across the die. Use of converging die helps to avoid dead metal zone, so the role of punch shape is not significant for the flow characteristics and to prevent dead metal zone. Use of inner cone punch only affects the flow pattern and prevents dead metal zone significantly where there is the use of shear faced die [10].

Load-Stroke curve by using different types of punch is shown in Figure 4.14 for 'R' = 3.33 and in Figure 4.15 for 'R' = 10. Maximum pressure required for deformation for each type punch is more or less similar but in case of inner cone punch the energy consumption is comparatively less as the flow in boundary zone does not counter acts the frictional force. The slope to achieve peak defers in the graph as it depends on the volume of metal deformed per stroke length up to the initiation of metal flow at the die exit. Experimentally use of inner cone punch with semi-angle 80° - 85° helps to carry the lubricant for the smooth operation.

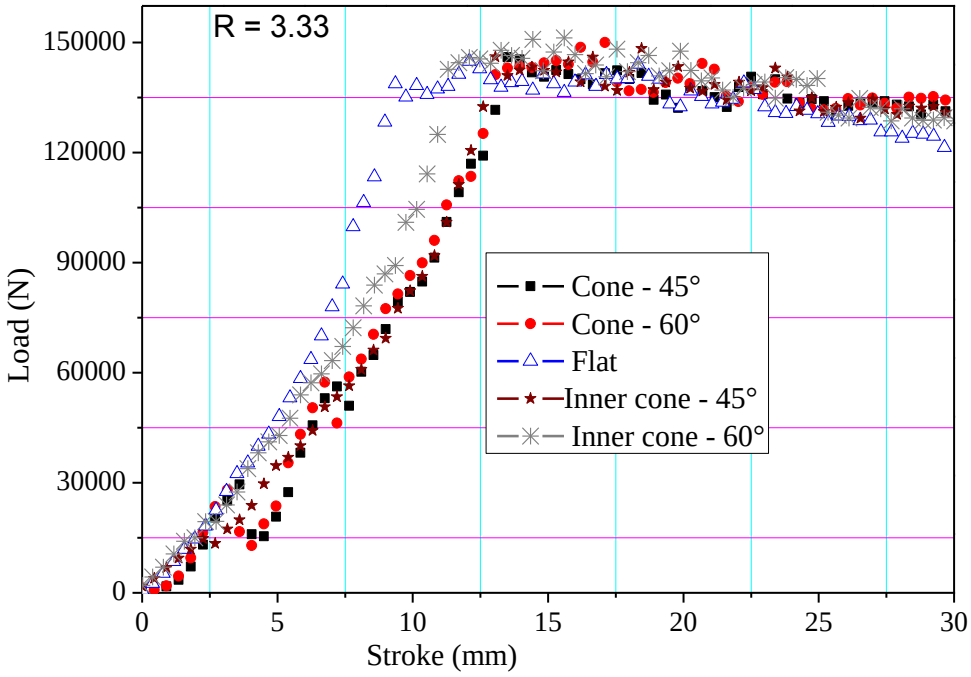

Figure 4.14: Variation of Load w.r.t stroke by different punch shape

4.4.3 Experimental investigation

To validate the FEM results and to study the changes in microstructural properties Al-6XXX series round bar of 20 mm diameter was extruded to a square section with 50% reduction. For the experimentation the tooling setup is manufactured indigenously. The

list of the components is presented in Table 4.3. The setup and materials are designed and decided for the hot extrusion process. The solid models are designed and generated by the help of SolidWorks® software and the components are manufactured by following the desired procedures. The billet length was maintained 35 mm to avoid unnecessary frictional work caused between container billet interfaces. The diameter of the billet is maintained a bit smaller than the internal diameter of the container by considering the thermal expansion into account.

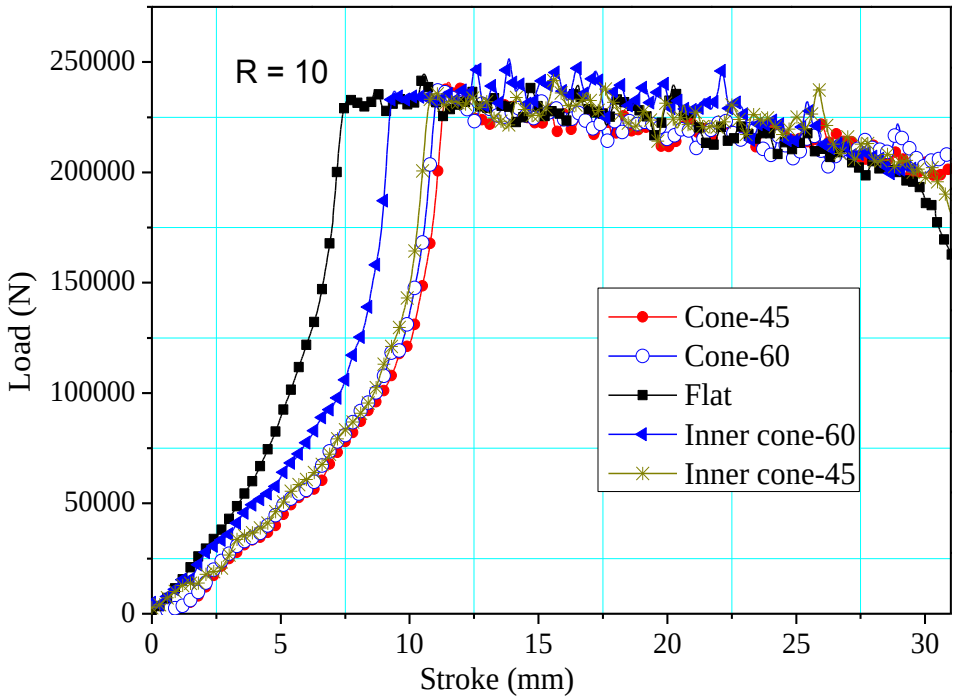

Figure 4.15: Variation of load versus stroke by different punch shape

Figure 4.16 shows the two-dimensional cross-sectional drafting of the tooling setup for extrusion. The experimental setup has been manufactured indigenously. The complete assembly with glass wool wounded around (for insulation), at the time of operation is clear in the figure beneath. The lower jaw of the hydraulic press is stable and the upper jaw is provided a constant ram velocity.

4.4.3.1. The test rig

The experimental setup utilised for this investigation as shown in Figure 4.16 is the assembly of punch holder, punch, container, die, die holder and support plate. The detail list of the components is presented in Table 4.3. The 2-D drawing with dimensions along with the manufactured component for all seven elements are shown individually.

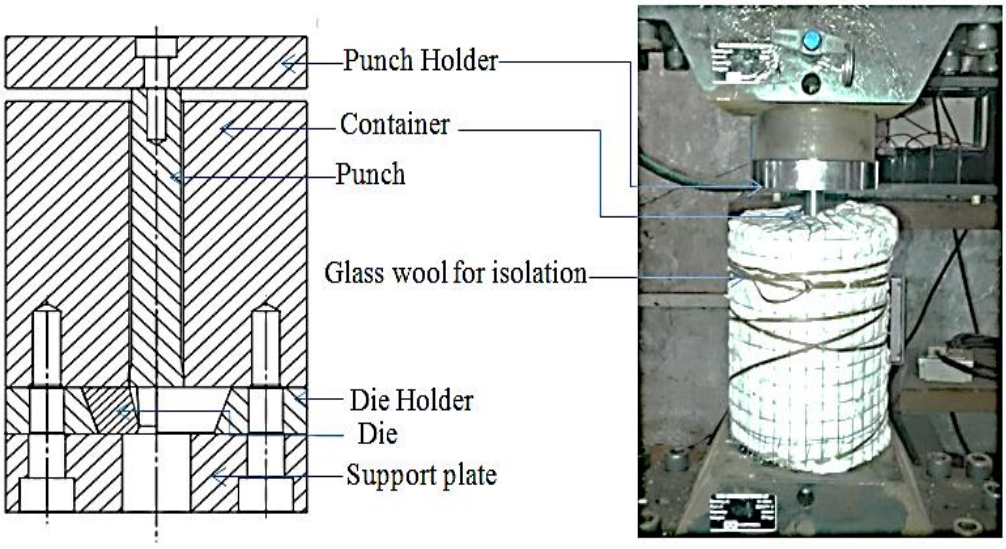

Figure 4.16: 2-D drafting as well as the setup during experimentation

Table 4.3: List of individual tooling components

Sl. No	Name of the part	Material	Remarks	Manufacturing processes
1	Punch holder	EN31	HRc 52-56	Turning, drilling, polishing
2	Punch	D2	HRc 52-56	CNC Turning, polishing, drilling, tapping
3	Container	D2	HRc 56-60	Turning, drilling, polishing
4	Die	H13	HRc 42-46	CNC milling, polishing, taper turning
5	Die holder	D2	HRc 52-56	Tapper turning, drilling, polishing
6	Support plate	EN31	HRc 42-46	Turning, drilling, polishing
7	Allen screw	STD		As available in the market

The load from the upper jaw of INSTRON, hydraulic universal testing machine is applied directly on the Punch holder (Figure 4.17). Punch holder transfers the load to the aluminium alloy billet through punch (Figure 4.18). The punch is provided with two

alignment rings at the body which confirms the alignment as well as supports to carry the lubricant.

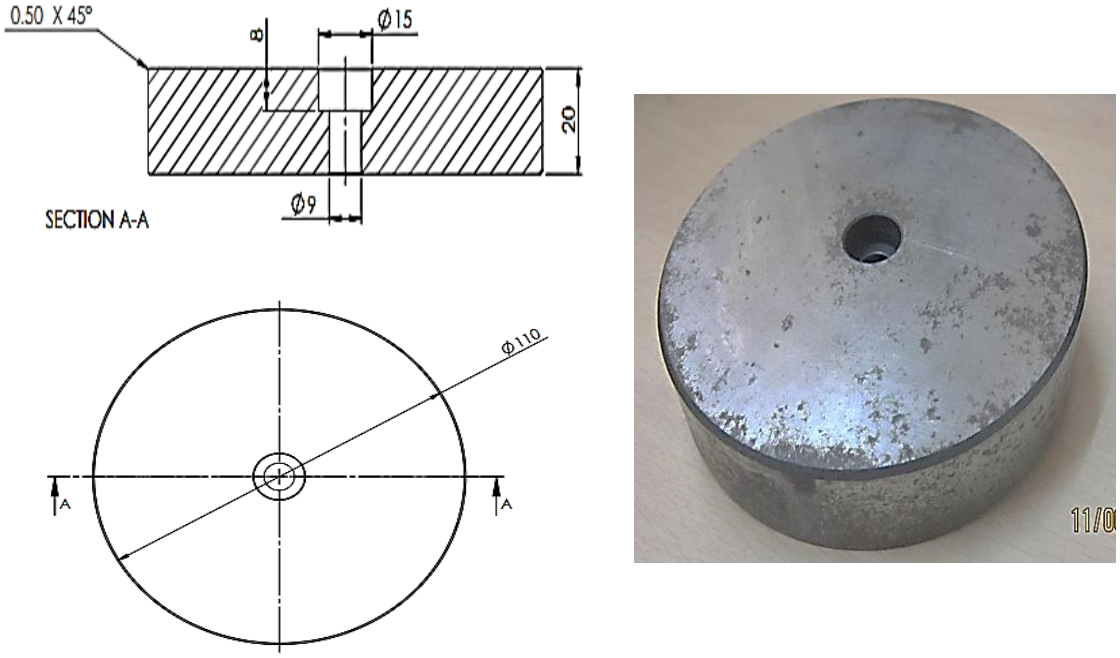

Figure 4.17: Punch holder

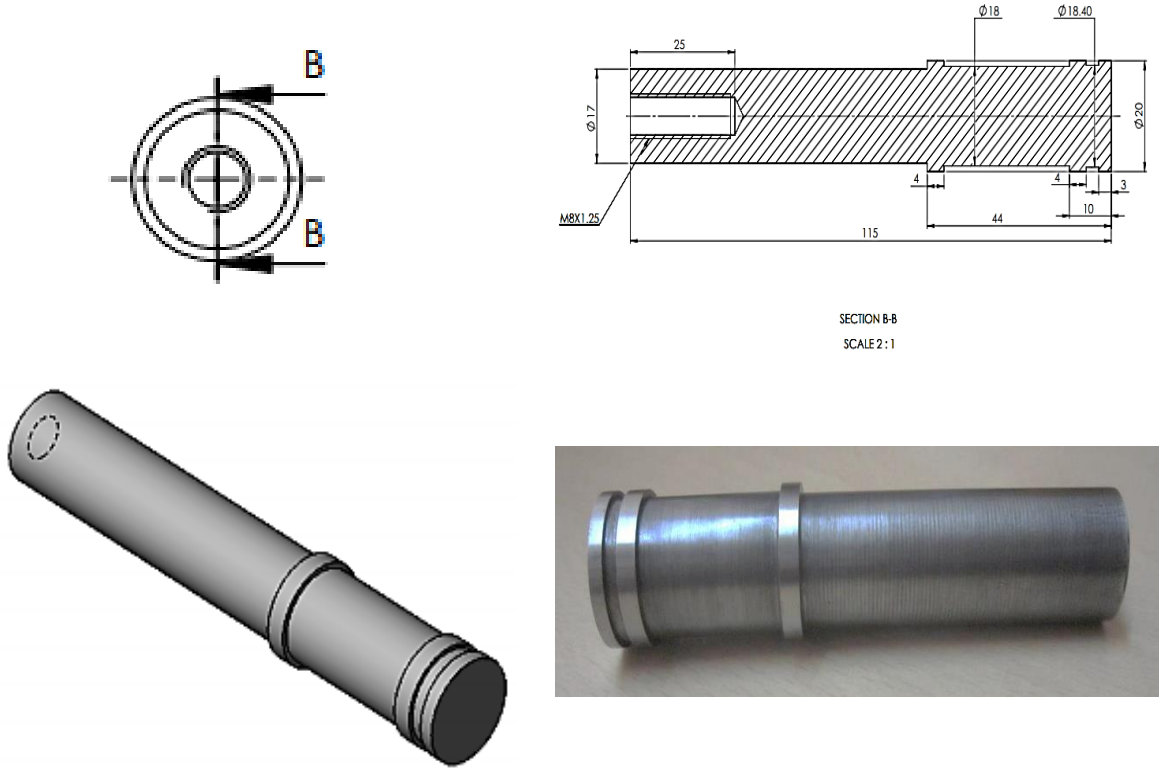

Figure 4.18: Punch

The billet is bounded by the inside surface of the container (Figure 4.19) chamber and allowed to flow through the linear converging die (Figure 4.20) which forms the circular cross section to 50% reduced square shape. The dimensional changes of the die

from round section to square section are achieved by the area interpolation technique. The die is held by the die holder (Figure 4.21). The contact surface between die and die holder is provided a slope of 20° to improve the contact surface area and for partial resolution of forces. All the assembly is mounted on the support plate (Figure 4.22). The support plate, die holder and container is tightened by the allen screw and the split die is placed in side with a tight alignment. Punch and punch holder is also tightened by the allen screw separately.

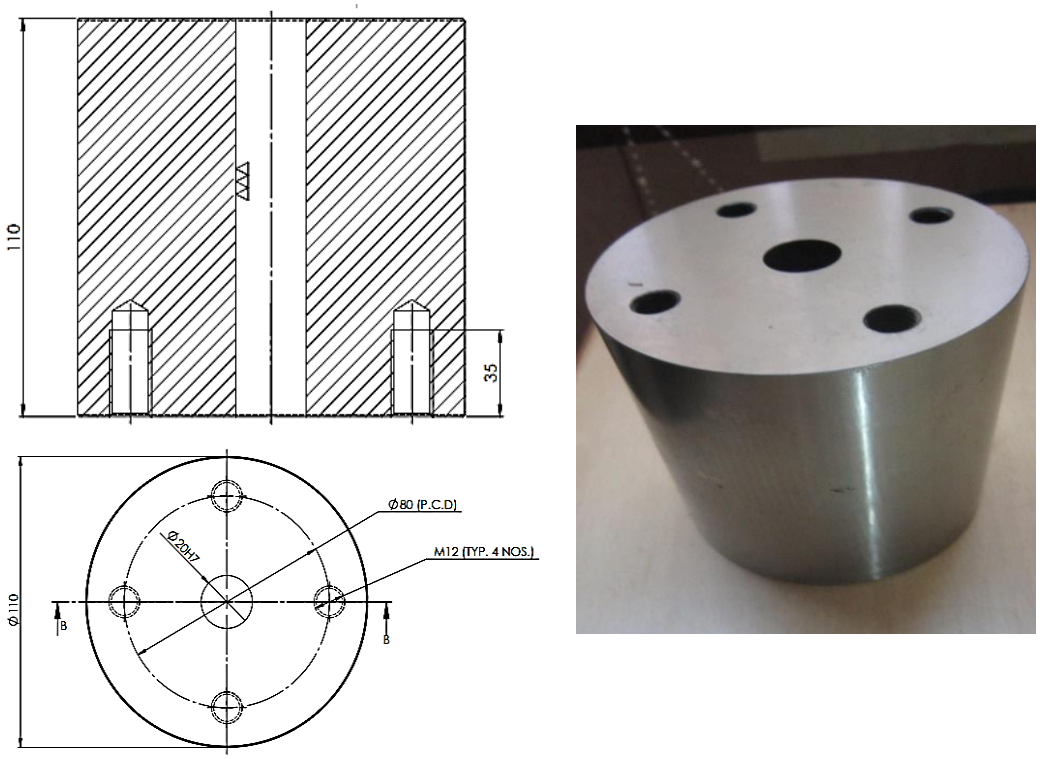

Figure 4.19: Container

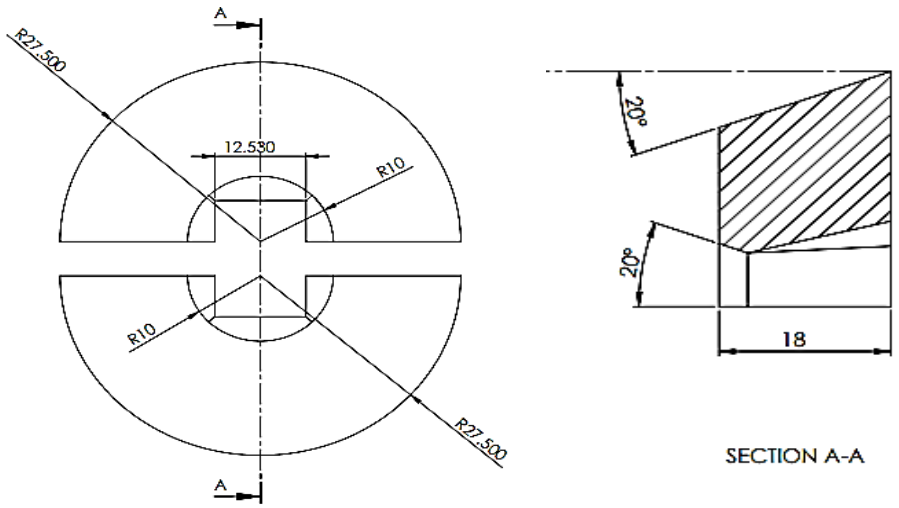

Figure 4.20: Linear converging round to square split die

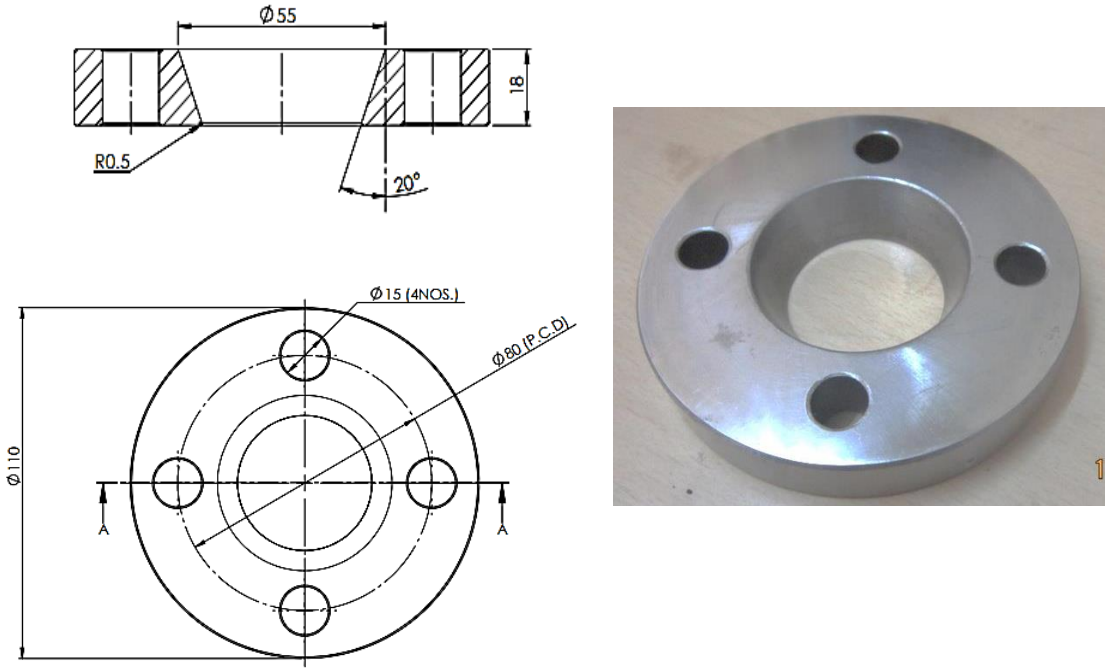

Figure 4.21: Die holder

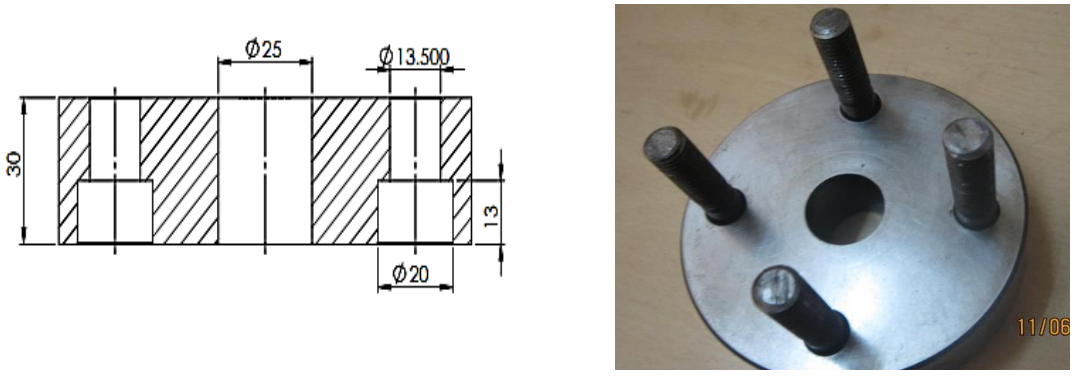

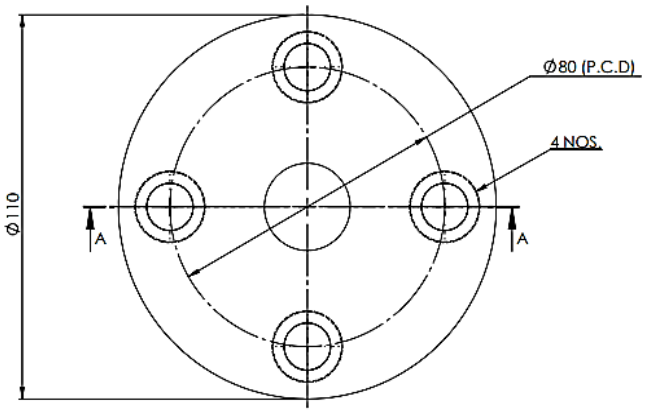

Figure 4.22: Support plate

Before preheating the metal for extrusion, the billet was homogenized at 600℃ for four hours with furnace cooling. Homogenized Al-6063 has been extruded by using dry graphite powder and commercially available Molykote as lubricant at an operating temperature range of 400-500℃. The hot extrusion without lubricant and with dry graphite powder as lubricant and by considering other parameters same were also compared. Ram speed was maintained at 1 mm/min.

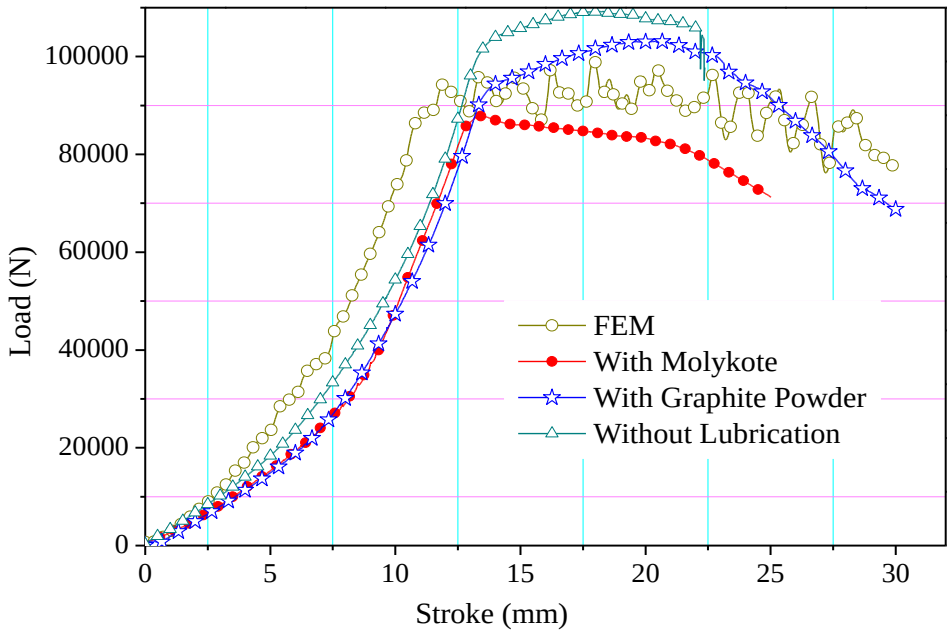

Figure 4.23: Variation of load w.r.t stroke

In Figure 4.23 load-stroke graph of experimental trials for extrusion of Al-6063 is plotted along with simulated results at a temperature of 500℃. Experimental load-stroke plot by using commercially available lubricant Molykote-1000, without lubrication and using dry graphite powder is compared with the simulation conducted at friction factor of

0.5 at 500℃. Underneath Figure 4.24 shows the extruded Al-6063 alloy at various lubrication conditions. Energy consumption for extrusion by using Molykote-1000 is less in comparison to all experimental results. The lubricant is suitable for hot working condition specifically used for forming operation within the temperature of 500℃. It is observed that the FEM output is closely matching with experimental results.

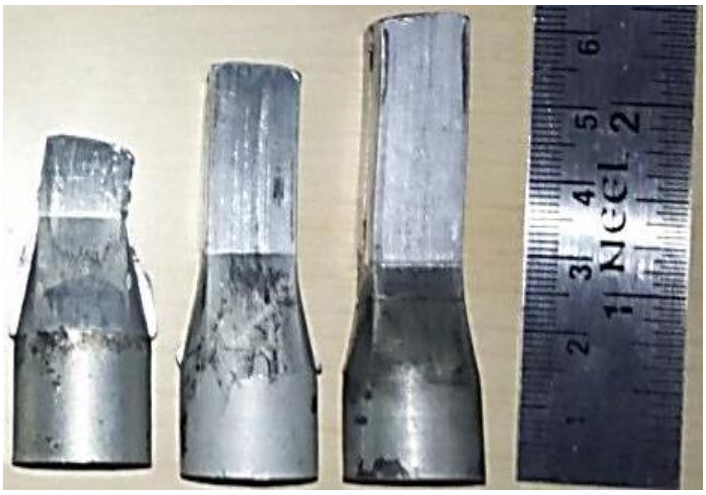

Figure 4.24: Experimented samples

4.4.3.2. Study of microstructural effect and microhardness

Microstructural changes in the deformation zone were studied. The grain sizes, orientation at the zone before deformation and after deformation have been examined by the photomicrograph. Specimen surface was prepared by standard surface finishing techniques and etched by Keller's reagent (190 ml H_2O, 5 ml HNO_3, 3 ml HCL and 2 ml HF). Randomly oriented coarse grains of the billet get deformed and change its shape and orientation to get elongated and unidirectional after passing through the die which is revealed from the Figure 4.25.

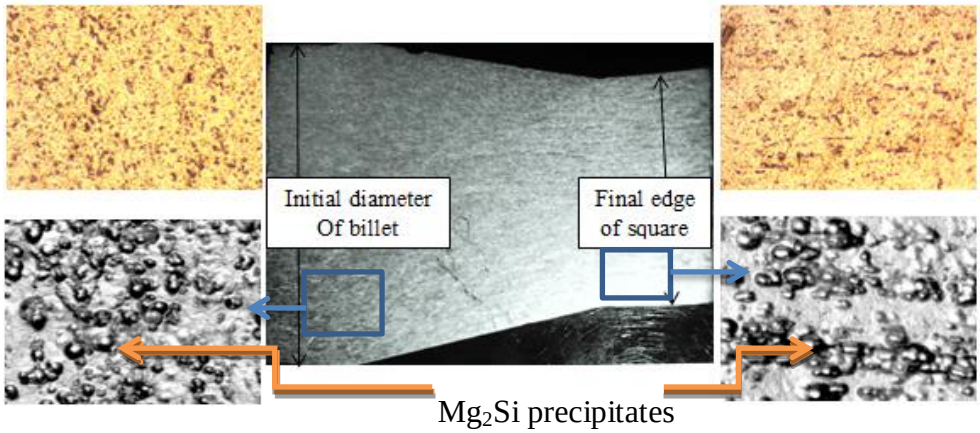

Figure 4.25: Microstructural effect

Uniformly distributed aluminium silicide particles in α-Al also changed its orientations, and got agglomerated, so its size increased and distributed in an axial direction after deformation. Effect of thermo-mechanical action on the hardness of the metal was investigated by means of microhardness testing. Effect of microstructural changes and induced residual stresses is there on microhardness of extrudate throughout the die length as well as across the product. The extruded product was sectioned in two ways: first in a plane perpendicular to the extrusion direction and second along the extrusion direction across the deformation zone.

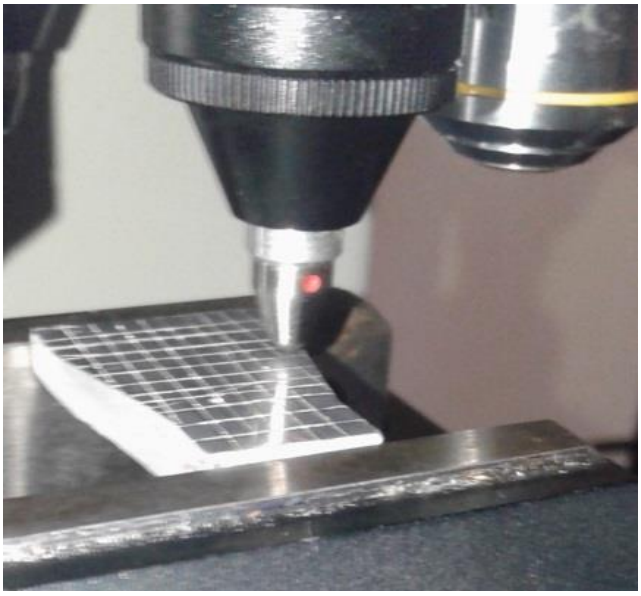

Figure 4.26: Micro-hardness testing

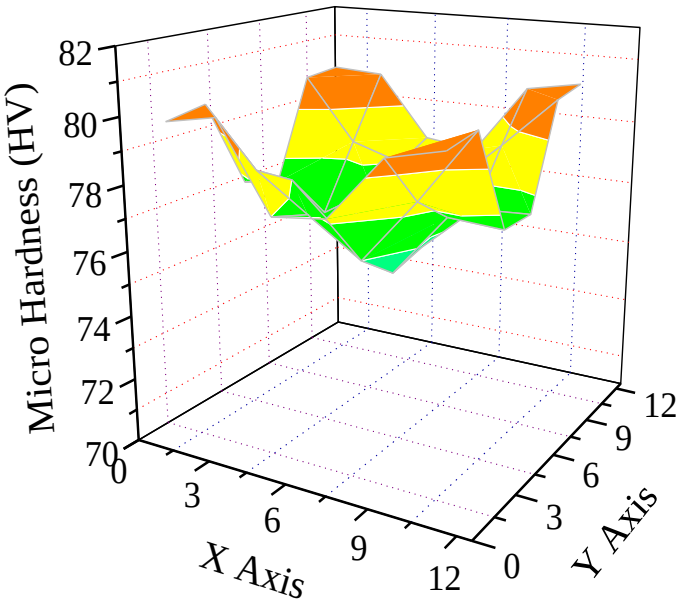

Figure 4.27: Hardness of the product across the extrusion direction

Figure 4.26 clearly shows the way how the sample is divided by the parallel and transverse scribes to indicate small squares. The hardness at every small square is measured by applying 50 gms of the load with a dwell period of 15 seconds to avoid spring back effects. Figure 4.27 shows the variation of microhardness at the surface (12.5×12.5) mm^2 of the extrudate perpendicular to the extrusion direction and Figure 4.28 shows the variation on a surface along the extrusion direction across the die length.

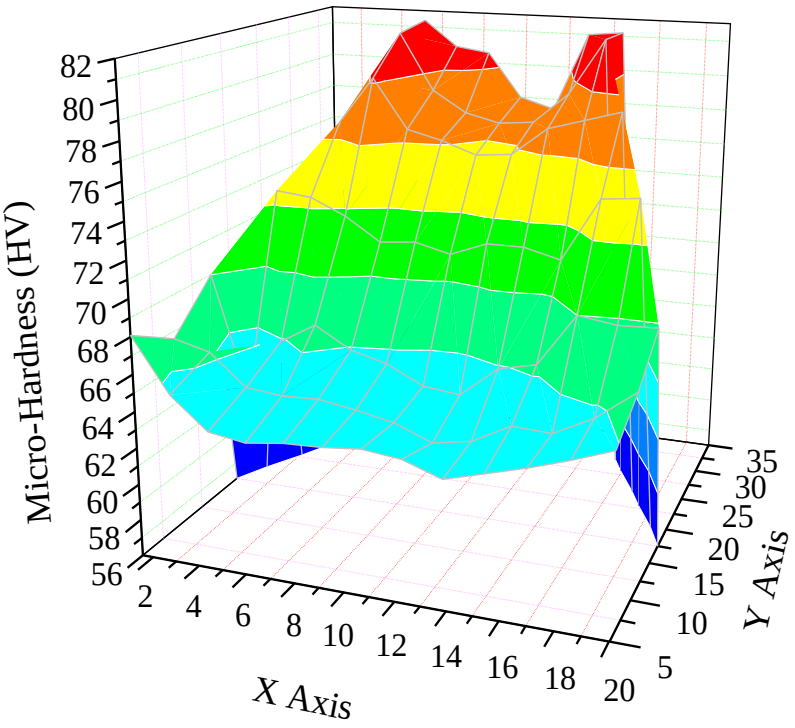

Figure 4.28: Hardness of the product along the extrusion direction

The plots show, the hardness at the boundary is comparably higher and it is also increasing along the extrusion direction. Shear deformation at the boundary of the billet is much higher than core areas so the fibers formed at higher deformation zone is thin and short (due to dynamic recrystallization). So the hardness at these zones is higher and at the core it shows the lower value.

4.5 Conclusions

Primary analysis of the extrusion of simple bar of the square section was performed for Al-6063 type alloy through linear converging die. The major outcomes of this study can be summarized as follows

- The simulation results attended by DEFORM-3D are in good agreement with experimental findings. So it can be accepted as a good predictor before experimentation.
- The second most power consumption in extrusion is due to frictional effects. So proper die length and appropriate lubrication must be optimised before production.
- Friction value has a great role over velocity relative difference at die exit, so maximum pressure requirement for complete extrusion is increasing significantly with an increase of friction value. However, this is limited to the studied range of process parameters.
- There is a significant effect of punch shape on the flow behaviour of metal inside the container. The conical and inner cone punch creates two different types of flow characteristics inside the container chamber which counteracts and favours frictional effect respectively.
- The slope to achieve the peak load varies by using various types of punch. This is because the volume of metal deformed per stroke varies up to the commencement of extrusion.
- Microhardness of the product at various points in a plane perpendicular to the extrusion direction and in a plane along the direction varies due to non-uniform grain structure and orientation. It needs further heat treatment.

Chapter 5

Round to Square Extrusion through Converging Die

5.1 Overview

The flow of metal through a designed die orifice featuring the shape for desired product dimensions at the die exit with the application of suitable pressure and temperature condition is cognized as metal extrusion. The primary practical limitation of the conventional shear faced die is the dead metal zone which leads to redundant work. To achieve a better product quality with minimal power consumption, it is necessary to have a profound knowledge about the flow characteristics of metal through the die [117].

Extensive research has been conducted for developing a well-designed streamlined die to get a uniform velocity of the extrudate at the die exit. Suitable die profile and / or die angle plays a pivotal role in diminishing redundant work resulting the lesser load requirement as well as improvement in surface properties of an extrudate. Expensive traditional empirical practices have stimulated the growth of computerized simulations for predicting the optimum combination of process parameters as well as investigating the product defects these days. A number of commercial finite element codes such as FORGE, HyperXtrude [5, 6], LS-DYNA, SUPER-FORGE^{TM}, ABAQUS^{TM} [7], DEFORM^{TM} [8-10], Q-FORM^{TM} are being utilized for the metal forming analysis. Numerous metal forming investigations have been performed successfully by the application of the code in different fields. Rigid-viscoplastic FEM analysis, as well as the experimental investigation, has been carried out to study the stress profile and strain rate distribution by Lin et. al. [118]. Prediction of different parameters like stress, strain, temperature and velocity distribution of aluminium alloy extrusion process can be made by DEFORM-3D using updated Lagrangian approach [100, 101].

In this chapter a new method of designing round to square die profiles following cosine, linear converging, elliptic, hyperbolic and 3rd order polynomial laws have been proposed. Simulations have been carried out to analyse the effect of die shape on the flow characteristics. From the comparative analysis, the most favourable die profile is manufactured indigenously. Simulation results were validated with experimental trials using designed cosine profiled die.

5.2 Development of mathematically contoured die profiles

5.2.1 Cosine die profile

Same shape reduction from a round bar through cosine die requires minimum power consumption, which was numerically proved by Narayanasamy et al. [60]. But in practical approach for a complex cross section extrusion, most of the profiles are not symmetric around one axis.

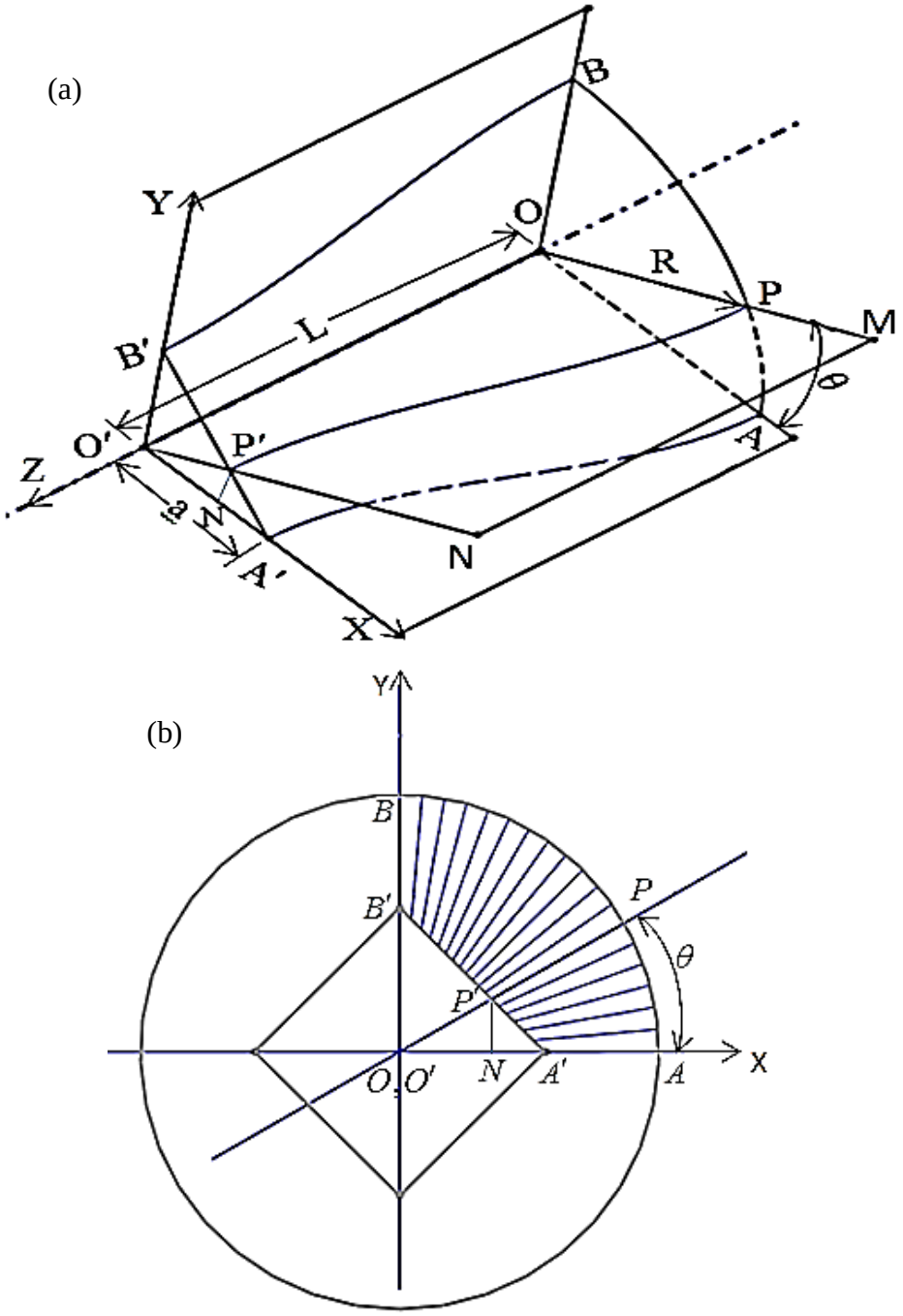

Figure 5.1: Round to square line diagram of cosine profiled die (a) isometric view in one quadrant and (b) front view with 18 divisions, 10 degrees each.

For the simplest one i.e. round to square die has been investigated here. The line diagram of an isometric and front view of the round to square profile in one quadrant is shown in Figure 5.1. The 'R' is the billet radius and $\sqrt{2}a$ is the side of the square section and 'L' is the length of the die in 'Z' direction. A plane ($OMNO'$) is passing through the die axis and makes angle 'θ' to the XZ plane as shown in figure. The plane passes through the initial billet radius at point P (x, y) and touches the square edge of the extruded product at P′ (x_1, y_1). From the simple geometry, the point P (x, y) can be presented as

$x = R\cos\theta$ and $y = R\sin\theta$

O′A′ = O′B′ (as it is a square section)

$\Rightarrow \angle O'A'B' = \angle O'B'A' = 45°$. So $\angle$O′P′A′ will be $135° - \theta$.

From the sine law (applied for the triangle O′P′A′)

$$\frac{O'P'}{\sin\angle O'A'P'} = \frac{O'A'}{\sin\angle O'P'A'}, \Rightarrow O'P' = \frac{O'A'\sin\angle O'A'P'}{\sin\angle O'P'A'} = \frac{O'A'\sin 45°}{\sin\angle O'P'A'}$$

$$\text{So } x_1 = \frac{O'A'\sin 45°}{\sin\angle O'P'A'}\cos\theta = \frac{a\times\sin 45°}{\sin\angle O'P'A'}\cos\theta$$

$$\text{And } y_1 = \frac{O'A'\sin 45°}{\sin\angle O'P'A'}\sin\theta = \frac{a\times\sin 45°}{\sin\angle O'P'A'}\sin\theta$$

Considering the above two endpoints (x,y) and (x_1,y_1) the coordinates of the die profile following cosine law and can be written as:

$$X = (R\cos\theta + \frac{a\times\sin 45°}{\sin\angle O'P'A'}\cos\theta)/2 + (R\cos\theta - \frac{a\times\sin 45°}{\sin\angle O'P'A'}\cos\theta)/2 * \cos\frac{\pi Z}{L} \quad 5.1$$

$$Y = (R\sin\theta + \frac{a\times\sin 45°}{\sin\angle O'P'A'}\sin\theta)/2 + (R\sin\theta - \frac{a\times\sin 45°}{\sin\angle O'P'A'}\sin\theta)/2 * \cos\frac{\pi Z}{L} \quad 5.2$$

By varying the value of 'θ' in between 0-90° and 'Z' in between 0-L, the coordinates of the profile has been generated from equation 5.1 and 5.2. Figure 5.2 shows the MATLAB generated cosine profile by plotting the coordinates (X,Y,Z).

5.2.2 Linear converging die profile

This profile is trending its demand because of easy design and manufacturing compared to other mathematical contoured dies. The similar process which is applied for developing

the cosine profile is applied for developing the linear converging three-dimensional co-ordinates. The X and Y coordinates for each Z value are mentioned as follows:

$$X = \{a\sin 45°*\cos\theta / \sin(135° - \theta)\} + [R\cos\theta - \{a\sin 45°*\cos\theta / \sin(135° - \theta)\}]*(L - Z)/L \quad 5.3$$

$$Y = \{a\sin 45°*\sin\theta / \sin(135° - \theta)\} + [R\sin\theta - \{a\sin 45°*\sin\theta / \sin(135° - \theta)\}]*(L - Z)/L \quad 5.4$$

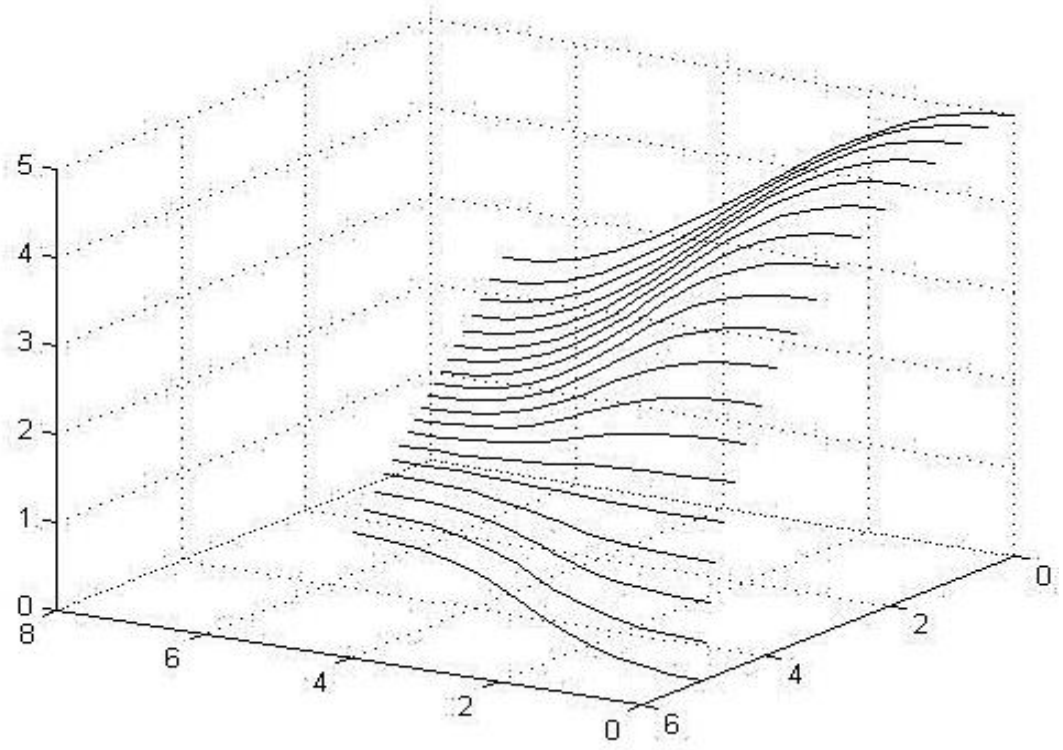

Figure 5.2: Three-dimensional coordinates of the cosine die profiles in one quadrant.

By varying the value of 'θ' in between 0-90° and 'Z' in between 0-L in equation 5.3 and 5.4 the coordinates of linear converging round to square die profile has been generated. Figure 5.3 shows the MATLAB generated linear converging profile by plotting the coordinates (X,Y,Z).

5.2.3 Hyperbolic die profile

From the same two dead / fixed end points (x,y) and (x_1,y_1) (which was clearly illustrated in 5.2.1) three-dimensional coordinates for the die profile can be generated by following the hyperbolic law. The relation to find out X and Y are as follows:

$$X = \sqrt{\{a\sin 45°*\cos\theta / \sin(135° - \theta)\}^2 + [(R\cos\theta)^2 - \{a\sin 45°*\cos\theta / \sin(135° - \theta)\}^2]*(Z/L)^2} \quad 5.5$$

$$Y = \sqrt{\begin{matrix}\{a\sin 45°*\sin\theta/\sin(135°-\theta)\}^2 + \\ [(R\sin\theta)^2 - \{a\sin 45°*\sin\theta/\sin(135°-\theta)\}^2]*(Z/L)^2\end{matrix}} \quad 5.6$$

By varying the value of 'θ' in between 0-90° and 'Z' in between 0-L in equation 5.5 and 5.6 the coordinates of the hyperbolic round to square die profile has been generated. Figure 5.4 shows the MATLAB generated hyperbolic profile by plotting the coordinates (X, Y, Z).

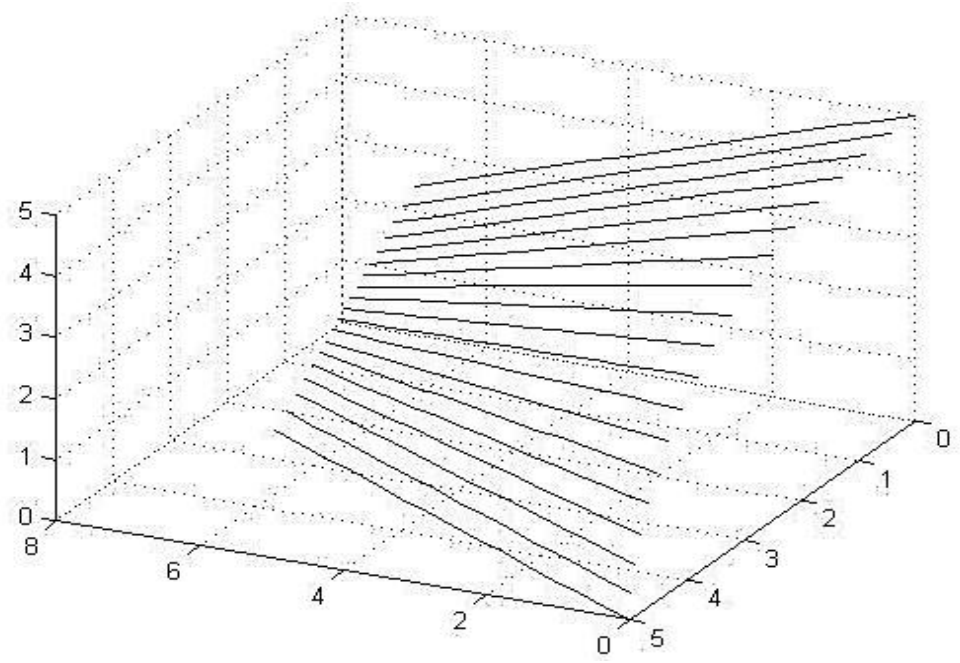

Figure 5.3: Three-dimensional coordinates of the linear converging die profiles in one quadrant.

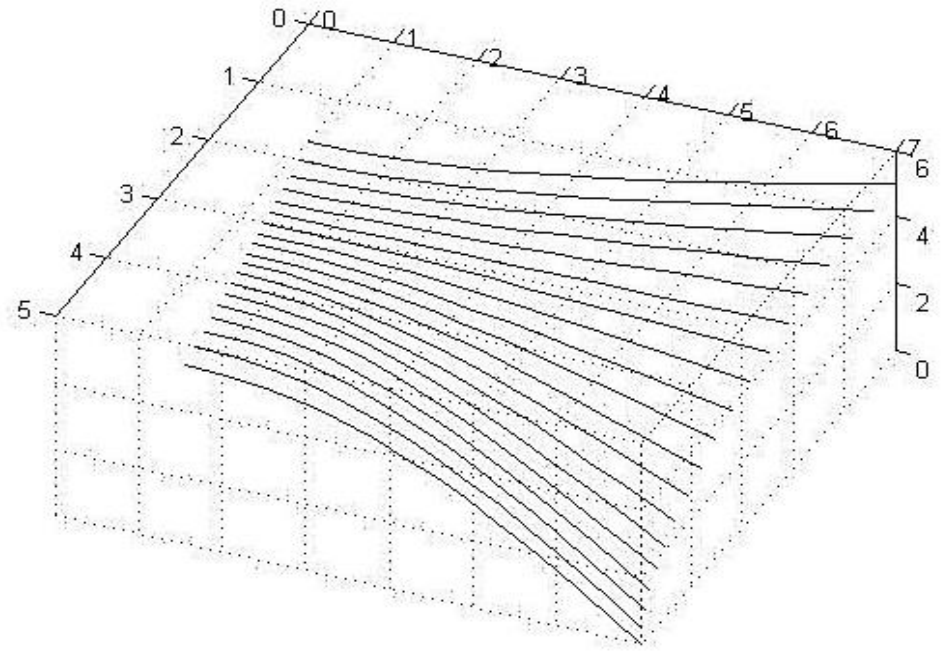

Figure 5.4: Three-dimensional coordinates of the hyperbolic die profiles in one quadrant.

5.2.4 Elliptic die profile

From the aforementioned two dead / fixed ends points (x,y) and (x_1,y_1) (which was clearly illustrated in 5.2.1) 3-dimensional coordinates for the die profile has been generated by following elliptic equations. The relation for X and Y for every 'Z' value are mentioned as follows:

$$X = \sqrt{(R\cos\theta)^2 - [(R\cos\theta)^2 - \{a\sin 45° * \cos\theta / \sin(135° - \theta)\}^2] * (Z / L)^2} \quad 5.7$$

$$Y = \sqrt{(R\sin\theta)^2 - [(R\sin\theta)^2 - \{a\sin 45° * \sin\theta / \sin(135° - \theta)\}^2] * (Z / L)^2} \quad 5.8$$

By varying the value of 'θ' in between 0-90° and 'Z' in between 0-L in equation 5.7 and 5.8 the coordinates of the profile has been generated. Figure 5.5 shows the MATLAB generated elliptic profile by plotting the coordinates (X,Y,Z).

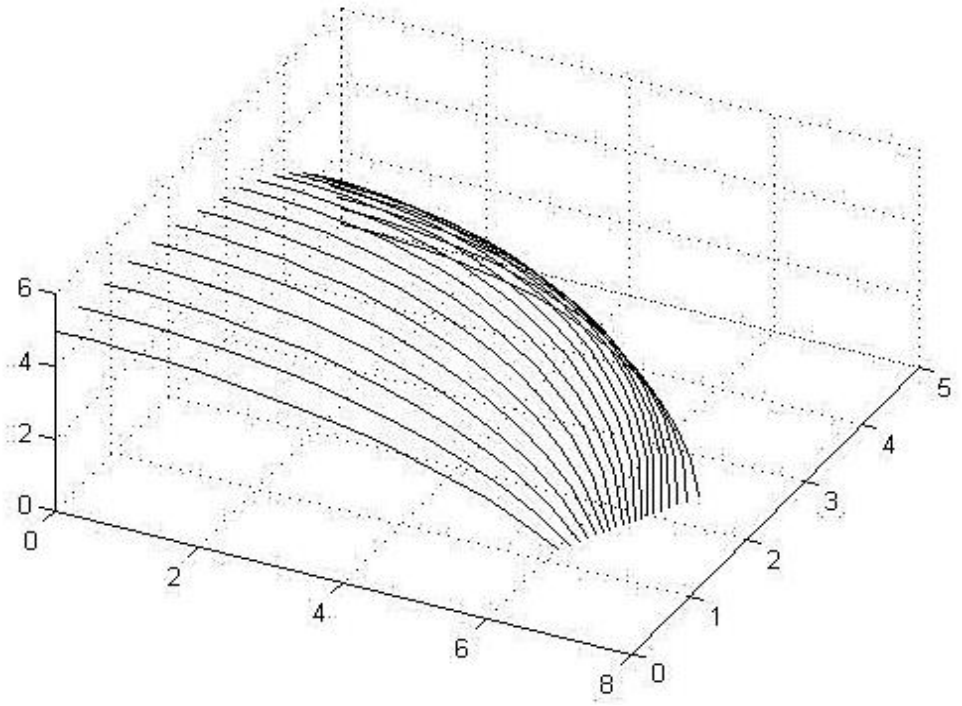

Figure 5.5: Three-dimensional coordinates of the elliptic die profiles in one quadrant.

5.2.5 3rd order polynomial die profile

By following 3rd order polynomial equations, the 3-dimenisonal coordinates are generated for developing round to square extrusion die profile. The X and Y coordinates are generated by the equations mentioned as follows:

$$X = (R\cos\theta) + [(R\cos\theta) - \{a\sin 45° \times \cos\theta / \sin(135° - \theta)\}] \times [2\frac{Z^3}{L^3} - 3\frac{Z^2}{L^2}] \quad 5.9$$

$$Y = (R\sin\theta) + [(R\sin\theta) - \{a\sin 45° \times \sin\theta / \sin(135° - \theta)\}] \times [2\frac{Z^3}{L^3} - 3\frac{Z^2}{L^2}] \qquad 5.10$$

By varying the value of 'θ' in between 0-90° and 'Z' in between 0-L in equation 5.9 and 5.10 the coordinates of the profile can be generated. Figure 5.6 shows the MATLAB generated 3rd order polynomial profile by plotting the coordinates (X,Y,Z).

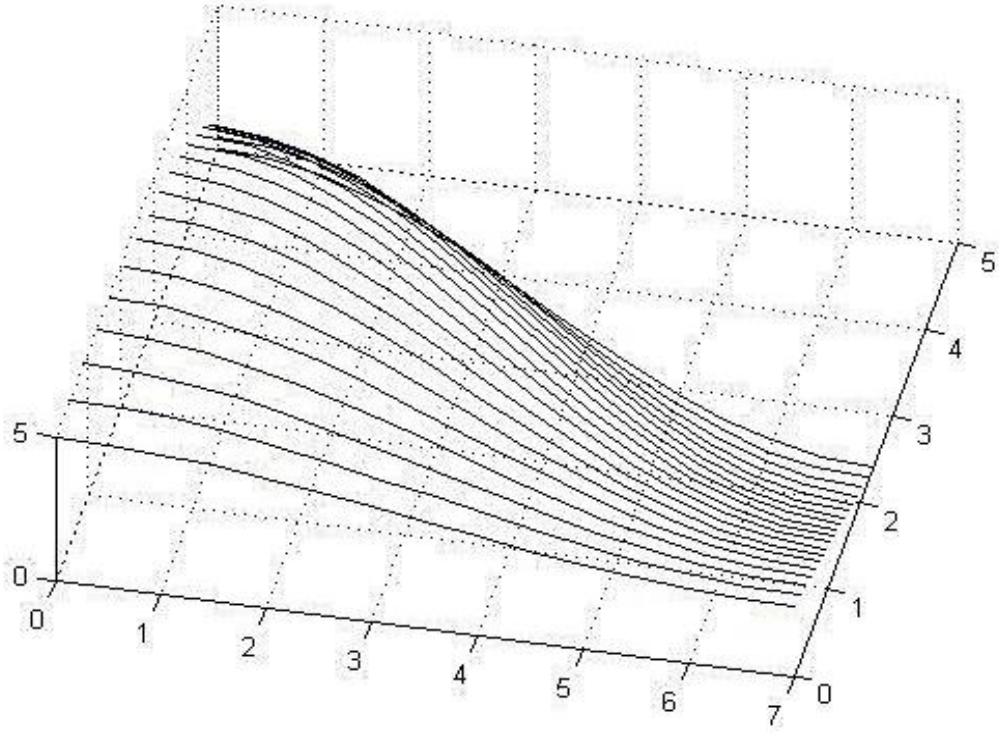

Figure 5.6: Three-dimensional coordinates of the 3rd order polynomial die profiles in one quadrant.

5.3 Finite element modelling

Commercial DEFORM-3D FE code was used to analyse the influence of die profile on the process as well as to study its effects on metal flow characteristics. The detailed procedure along with fundamental equations (equilibrium equation, compatibility and incompressibility equation) is mentioned in Chapter 3. A rigid-viscoplastic material model (as elastic deformations are neglected in the bulk plastic deformation process) was considered for the investigation of hot extrusion. Load-stroke plot and grid pattern analysis of the billet was studied from the FE analysis to investigate the power efficiency and flow characteristics.

By considering the three-dimensional coordinates, the solid dies of above profiles along with billet and punch were generated by SolidWorks® software. These parts were imported to DEFORM-3D window in the form of .stl file for the database generation.The

The $\phi 10 \times 30$ mm Al-6063 billet meshed into 74589 elements with the facility of specific mesh box for higher mesh density at the severe deformation zone coupled with global remeshing was considered for numerical analysis, by lagrangian incremental type direct iteration. Punch velocity was set as same with the experiment, i.e. 3 mm/min. Interfacial shear friction constant (m) and heat transfer coefficient (conduction) for the modelling are considered as 0.5 (from the ring compression test at higher temperature range) and 11 (N/sec/mm/C) (suggested by the software manual). Figure 5.7 shows the simulated extrusion process with all the setup (die-container, punch, billet) by DEFORM-3D software through cosine profiled die.

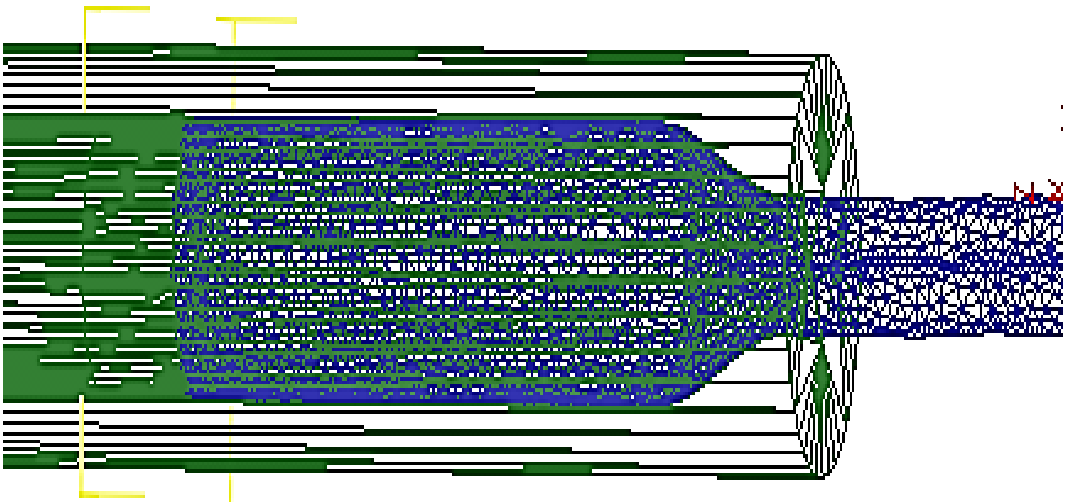

Figure 5.7: Simulated extrusion of the alloy by DEFORM-3D.

5.4 Results and discussion

Three-dimensional analysis of round to square extrusion through different converging profiles utilizing DEFORM-3D FEM package is intended to present the results here. Effective strain, strain-rate, velocity, temperature and stress distribution of the extruded product at any position can be checked by the proposed formulation. The effective strain-rate and effective strain distribution across all the type of die was determined by the simulation programme. The effective strain rate, an important deformation parameter, which signifies the momentary deformation per time at the instance across the die and it depicts the accumulated strain value. The computed effective strain rate distribution inside the material across die is shown in Figure 5.8. The amount of deformation distributed throughout the volume of the extruded specimen in terms of strain across the die at the same stage is shown in Figure 5.9. The variation in the effective strain-rate and effective strain value of the extrusion ratio of 6.66 is observed across the die profile. The predicted

value of maximum effective strain-rate by the simulation tool at the exit corner zones for cosine, linear-converging, hyperbolic, elliptic and 3rd order polynomial die profile are 0.150, 0.193, 0.128, 0.290 and 0.210 ((mm/mm)/sec).

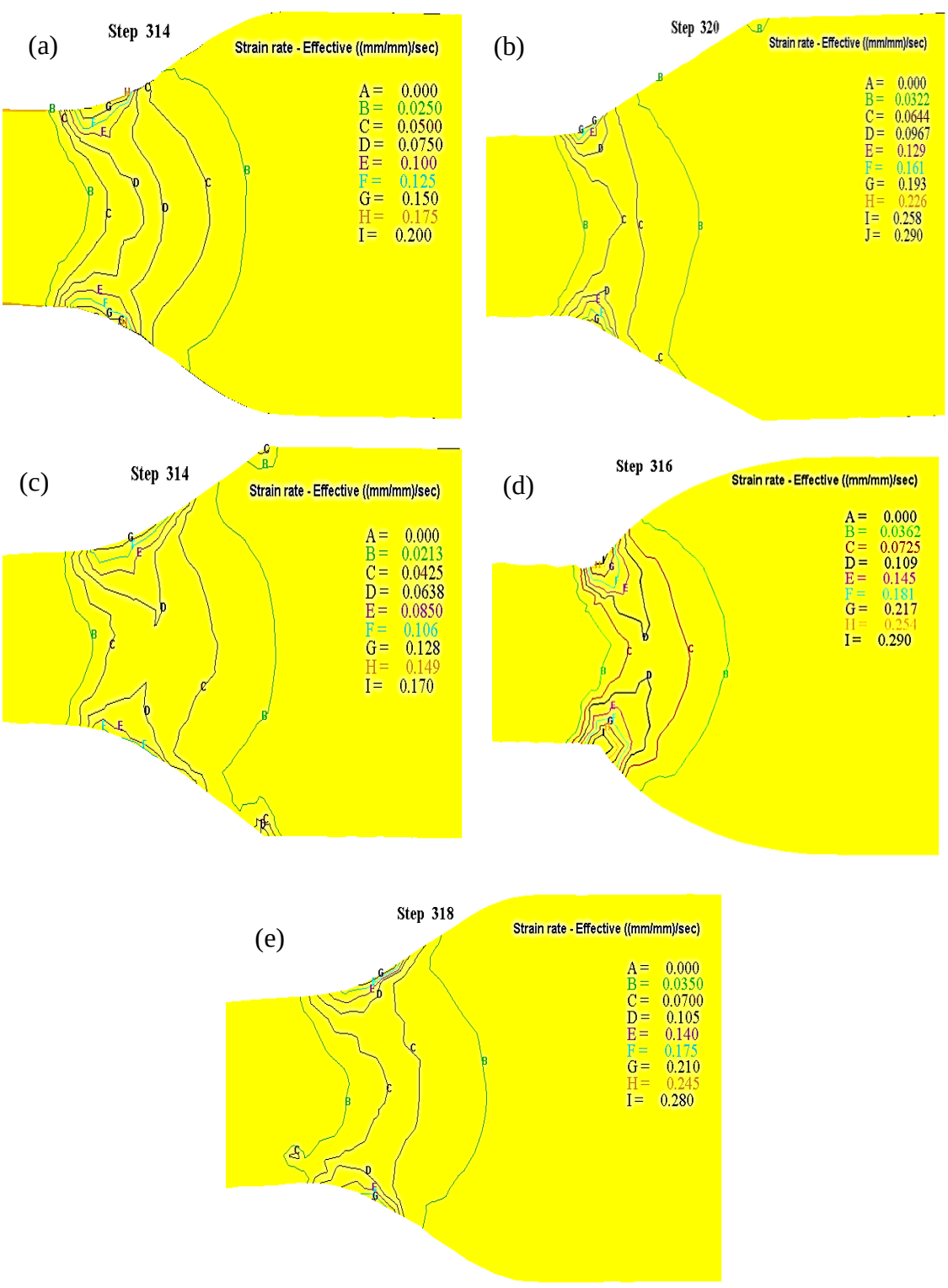

Figure 5.8: Strain-rate distribution across the billet through (a) cosine (b) linear converging (c) hyperbolic (d) elliptic (e) 3rd order polynomial die profile.

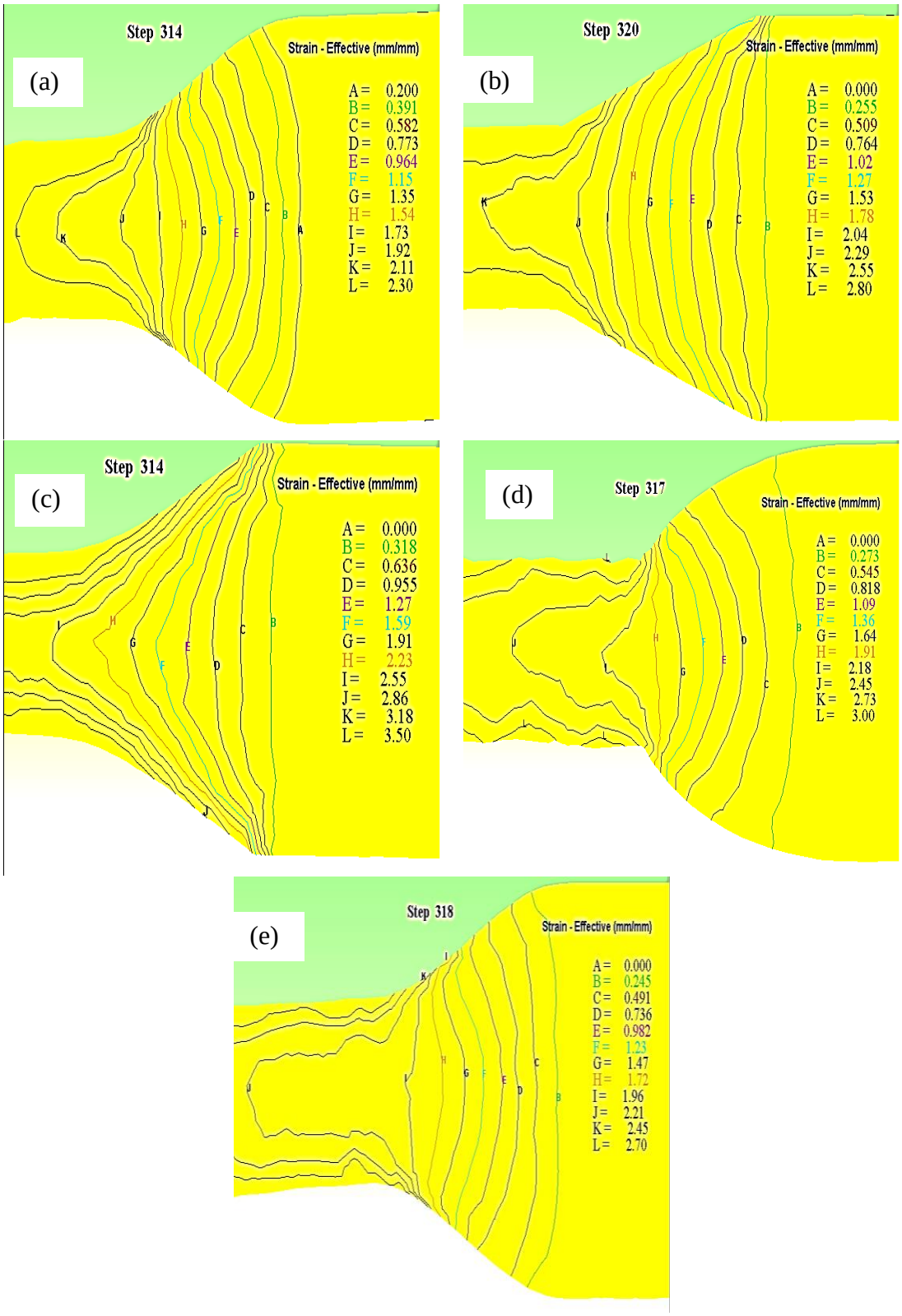

Figure 5.9: Effective-strain distribution across the billet through (a) cosine (b) linear converging (c) hyperbolic (d) elliptic (e) 3rd order polynomial die profile.

The minimum value is achieved across hyperbolic die, but as the entry angle of the die is non-zero, visible amount of strain-rate distribution (0.0638) is observed at the entry corners. The increasing strain-rate leads to improve the energy absorbing ability and can

be co-related to the pressure requirement for the process [17]. The distribution of deformation inside the billet in terms of effective strain distribution at the die exit of the extrusion is clear in Figure 5.9. The core of the billet is strained less than the outer surface during forward extrusion. The non-uniformity of the strain and strain rate causes unnecessary internal shear deformation leading to redundant work.

Load versus stroke curve of extrusion through different die profile for 6.63 extrusion ratio is shown in Figure 5.10. Though elliptic and 3rd order polynomial die profile causes lesser power consumption in the process, the higher relative velocity distribution of the product at the die exit (evident from the strain-rate and strain distribution) may lead to product defects. In the case of higher extrusion ratios, the trend may cause severe defects and massive power consumption for the complete process. Hence, the cosine profile having zero entry and exit angle for the extrusion process may be considered suitable.

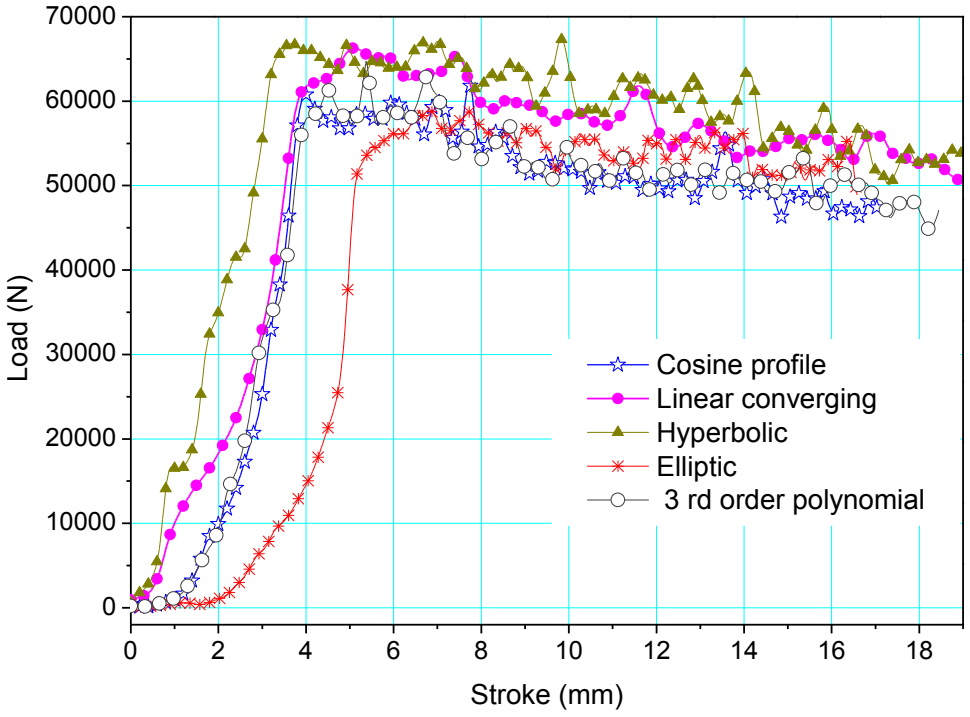

Figure 5.10: Load versus stroke for extrusion through different die profile.

5.5 Experimental investigation

In computational and numerical analysis a number of assumptions are made for the process invariably the nature of deformation and material properties. Hence, the theoretical and numerical outcomes must be compared to experimental results to know the percentage variation of the matching. A number of research has been performed to

develop the die profile to improve the flow of metal across die [59, 109, 118, 119]. Most of them are based on numerical analysis or computational simulations but to manufacture a mathematically contoured die profile for the experimental investigation and validation with FEM results were carried out in this chapter.

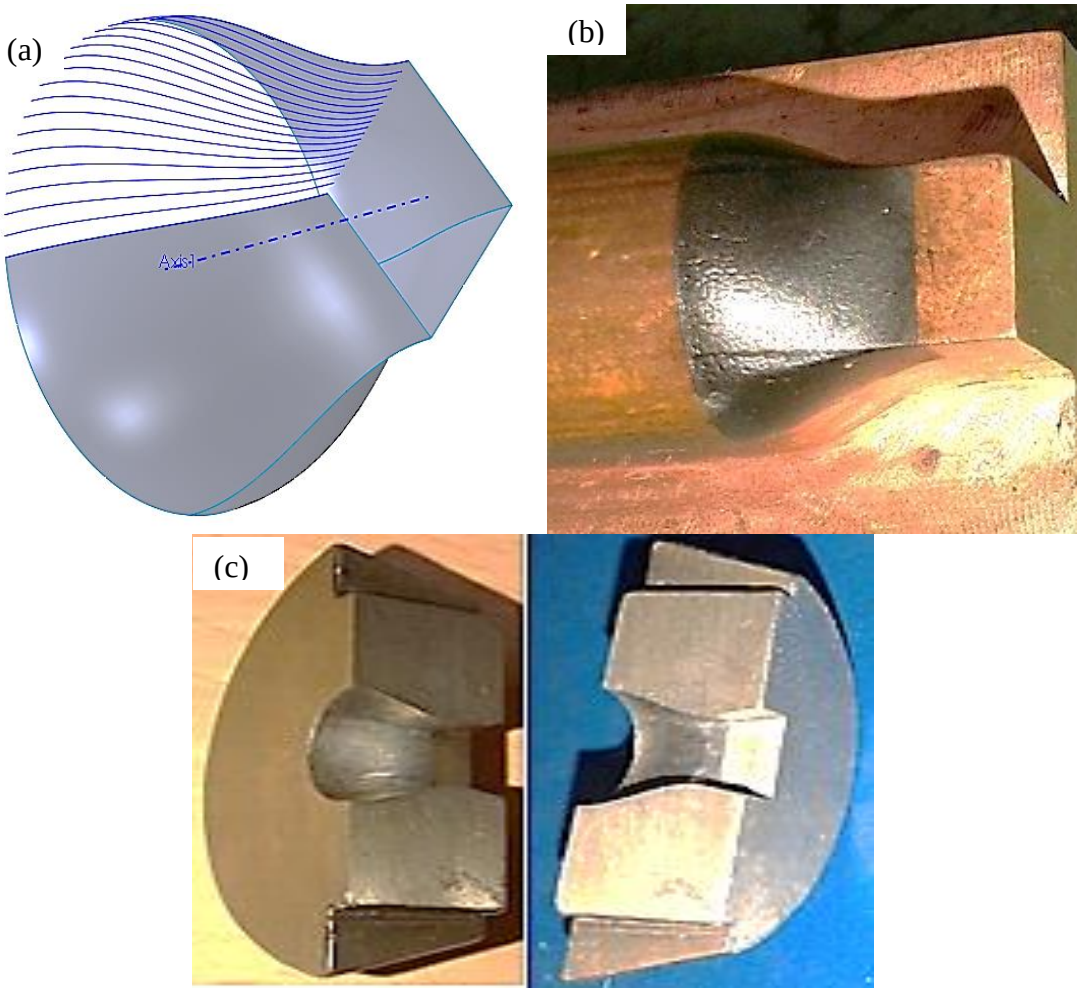

Figure 5.11: Sequences of die making process (a) SolidWork's model (b) copper tool (c) Split cosine die.

The solid geometry of the die profile was built with the help of SolidWorks® software from the generated coordinates. The inside surface of the solid die has been replicated to a copper metal as shown in Figure 5.11 (b) with the help of CNC milling. The copper body having the patterned die profile acted as a tool for machining cosine profiled dies by the electro-discharge machining process. Figure shows the sequential process for manufacturing the die (a) the surface geometry of the profile (b) copper tool (c) split cosine die. Experimentation has been carried out for round to square simple bar extrusion at a temperature range of 400-450℃ for an extrusion ratio of 2.504. At a punch velocity of 3 mm/min, the square section has been extruded through cosine profiled die.

Experiments were performed on a Universal testing machine (INSTRON®600KN) from round to square section extrusion through split cosine die. The tooling setup for the laboratory experimentation is designed and fabricated indigenously.

5.5.1 The test rig

The tooling setup arrangement sequence (2-D drafting) utilised for the present experimental investigation is shown in Figure 5.12. The setup primarily consists of seven parts, namely punch holder to hold the punch of 10 mm of maximum diameter, extrusion punch to transfer the applied pressure to the billet, the container having 10 mm diameter chamber, split cosine die to allow the metal to flow through a defined contour, die holder to hold the die rigidly, support plate to hold the die holder by four allen screw. The detailed description is presented in Table 5.1. Figure 4.13 depicts the experimental setup after the assembly of the components. The individual components punch holder (Figure 5.14), punch (Figure 5.15), container (Figure 5.16), die (Figure 5.17), die holder (Figure 5.18) and support plate (Figure 5.19) with the detailed dimensions are presented.

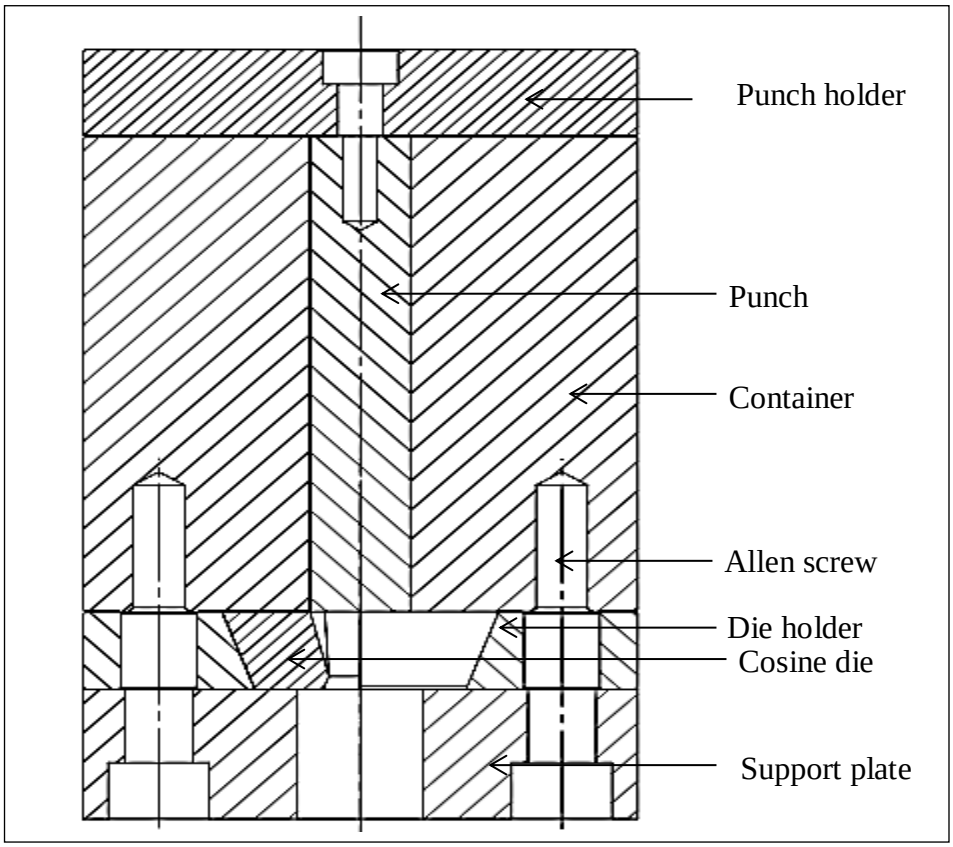

Figure 5.12: 2 D drafting of the tooling setup.

Table 5.1: List of individual components.

Sl. No	Name of the part	Material	Remarks	Manufacturing processes
1	Punch holder	EN31	HRc 45-48	Turning, drilling, polishing
2	Punch	D2	HRc 50-55	CNC Turning, polishing, drilling, tapping
3	Container	D2	HRc 50-55	Turning, drilling, polishing
4	Die	H13	HRc 51-53	CNC milling, EDM, polishing, taper turning
5	Die holder	EN31	HRc 45-48	Tapper turning, drilling, polishing
6	Support plate	EN31	HRc 45-48	Turning, drilling, polishing
7	Allen screw	STD		As available in the market

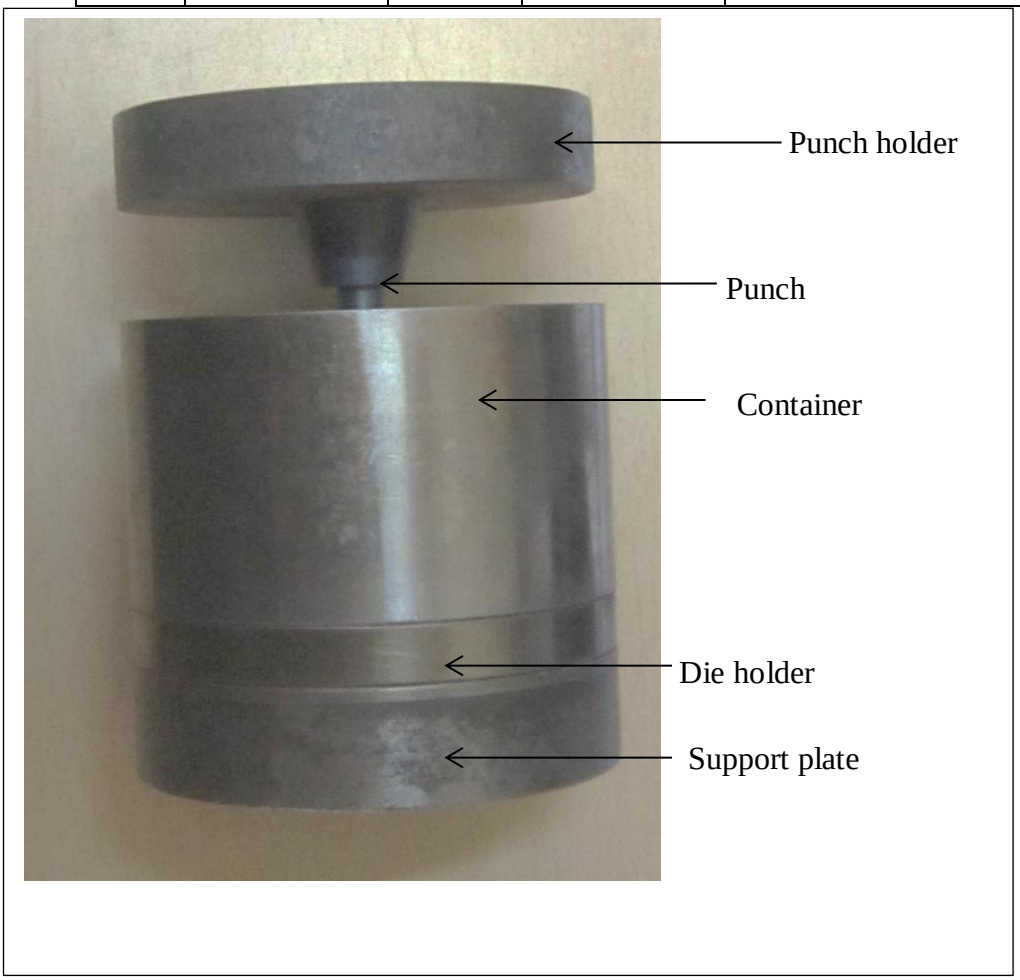

Figure 5.13: The assembled tooling setup

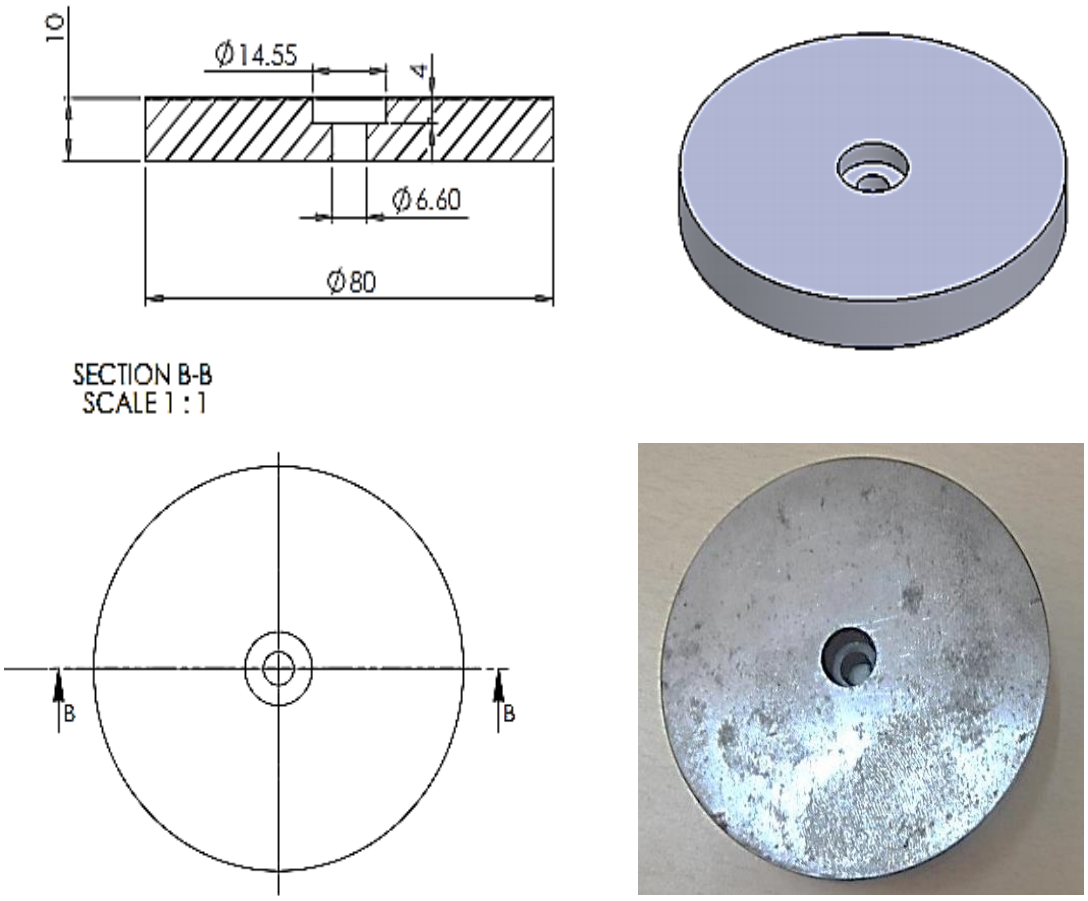

Figure 5.14: Punch holder

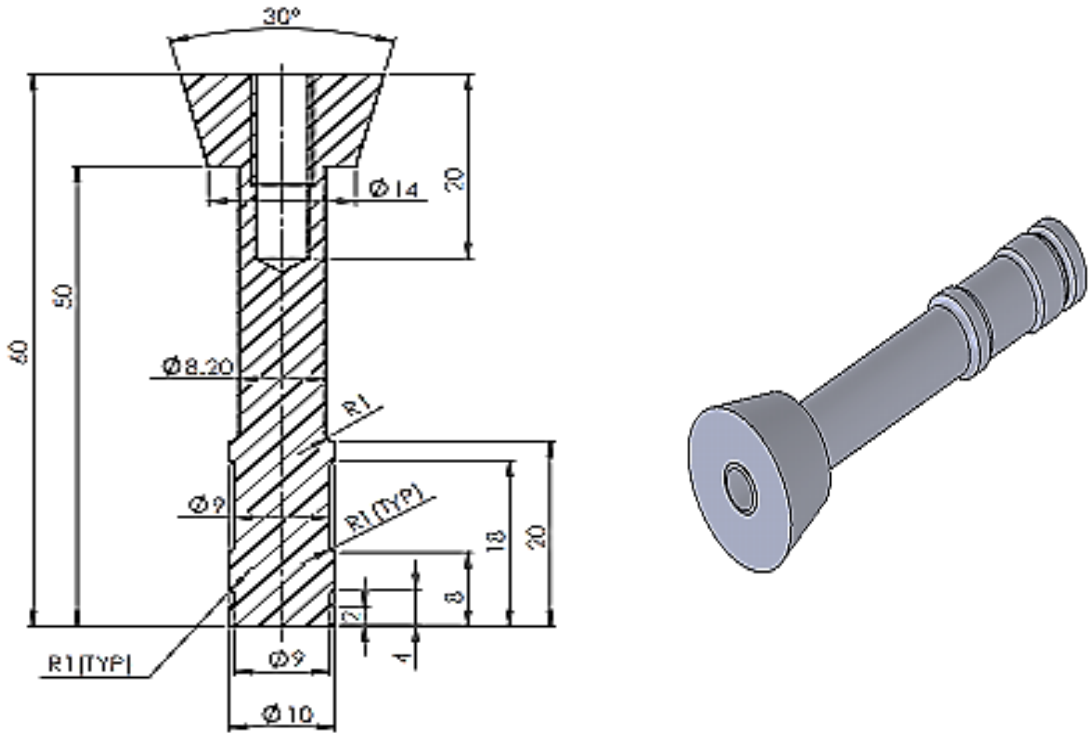

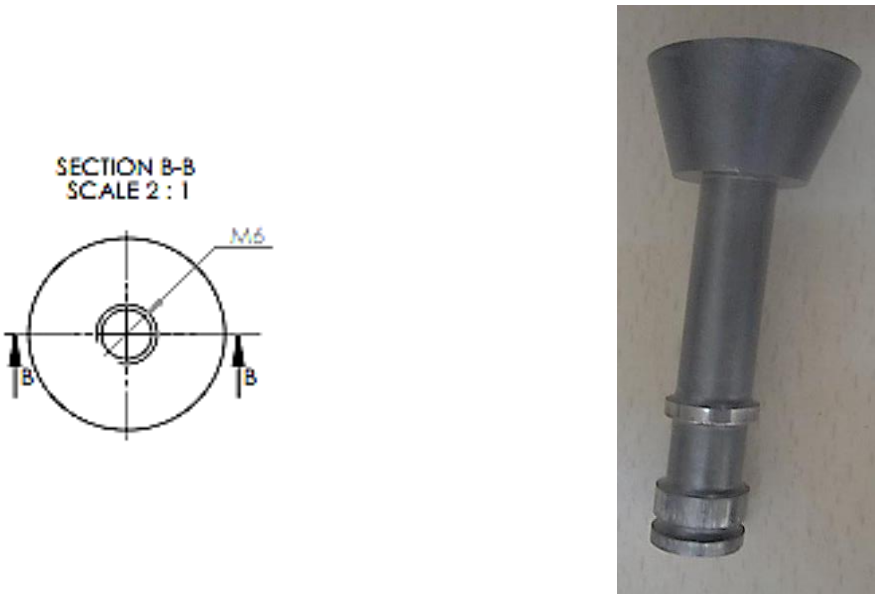

Figure 5.15: Punch

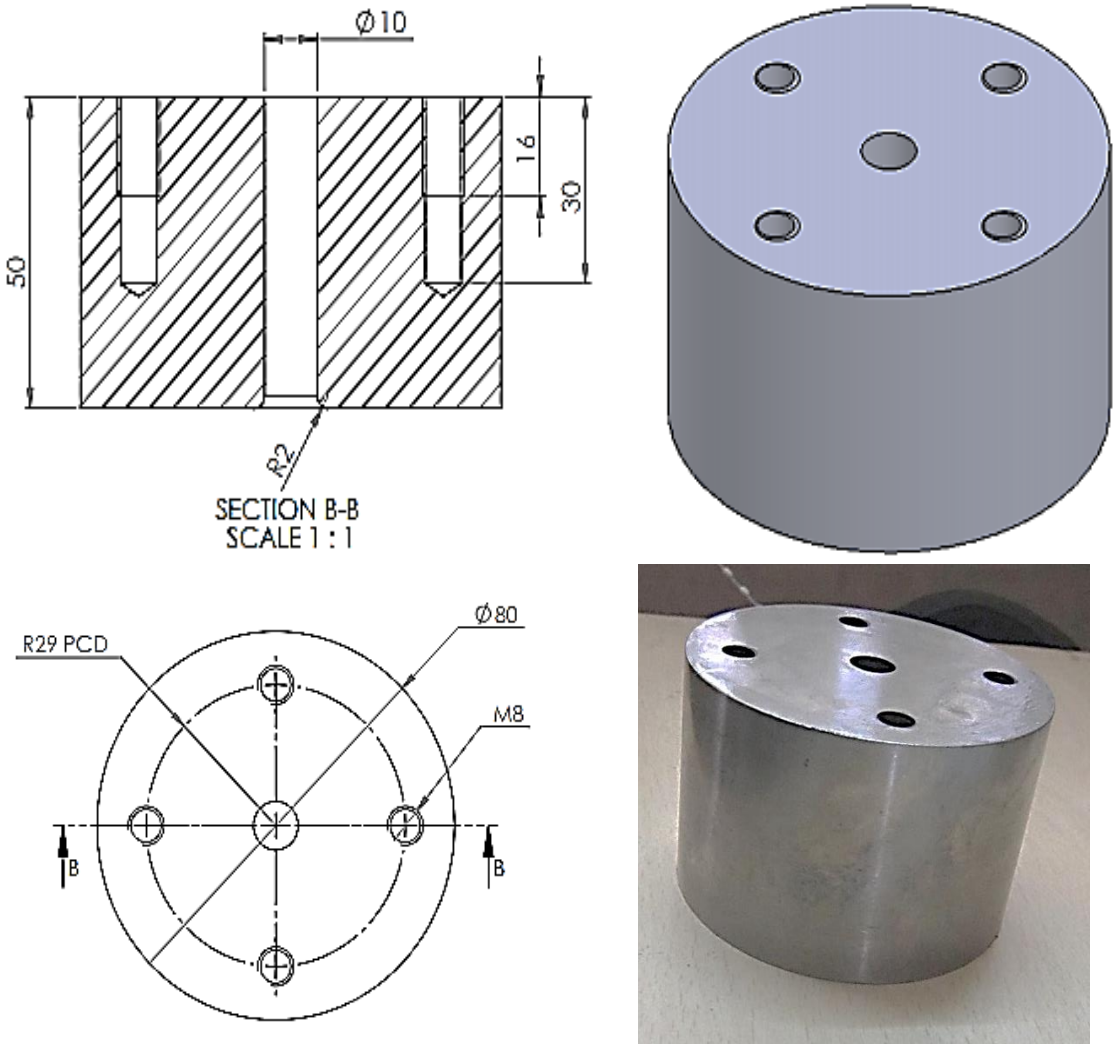

Figure 5.16: Container

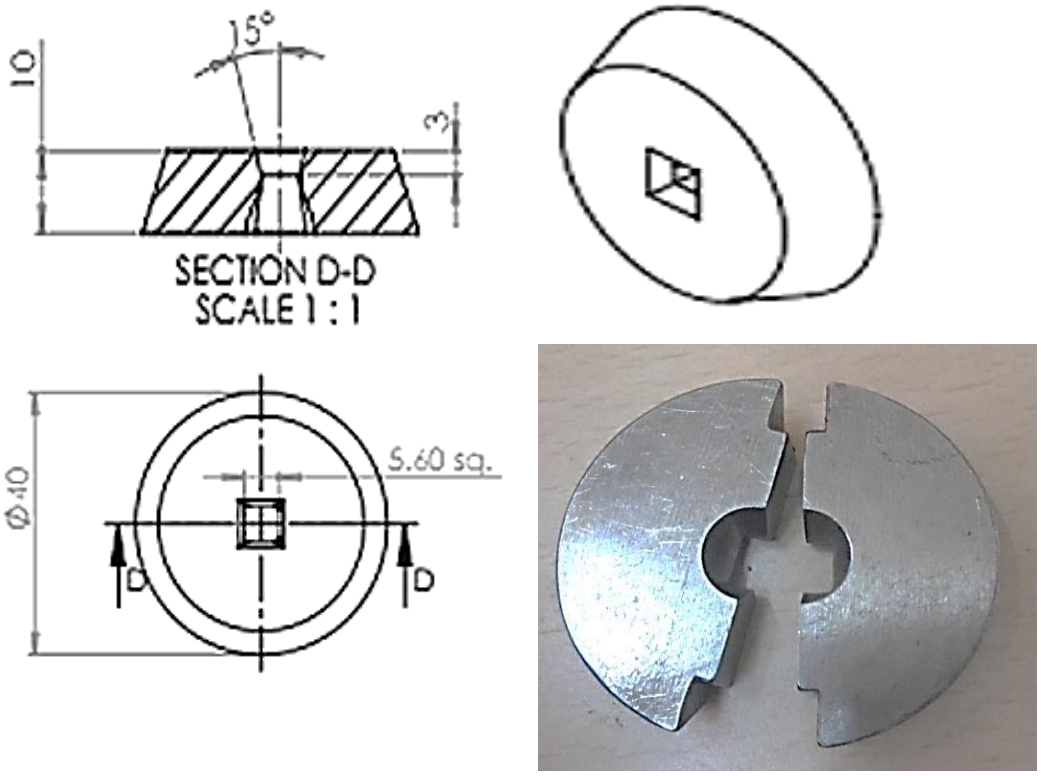

Figure 5.17: Cosine profiled split die

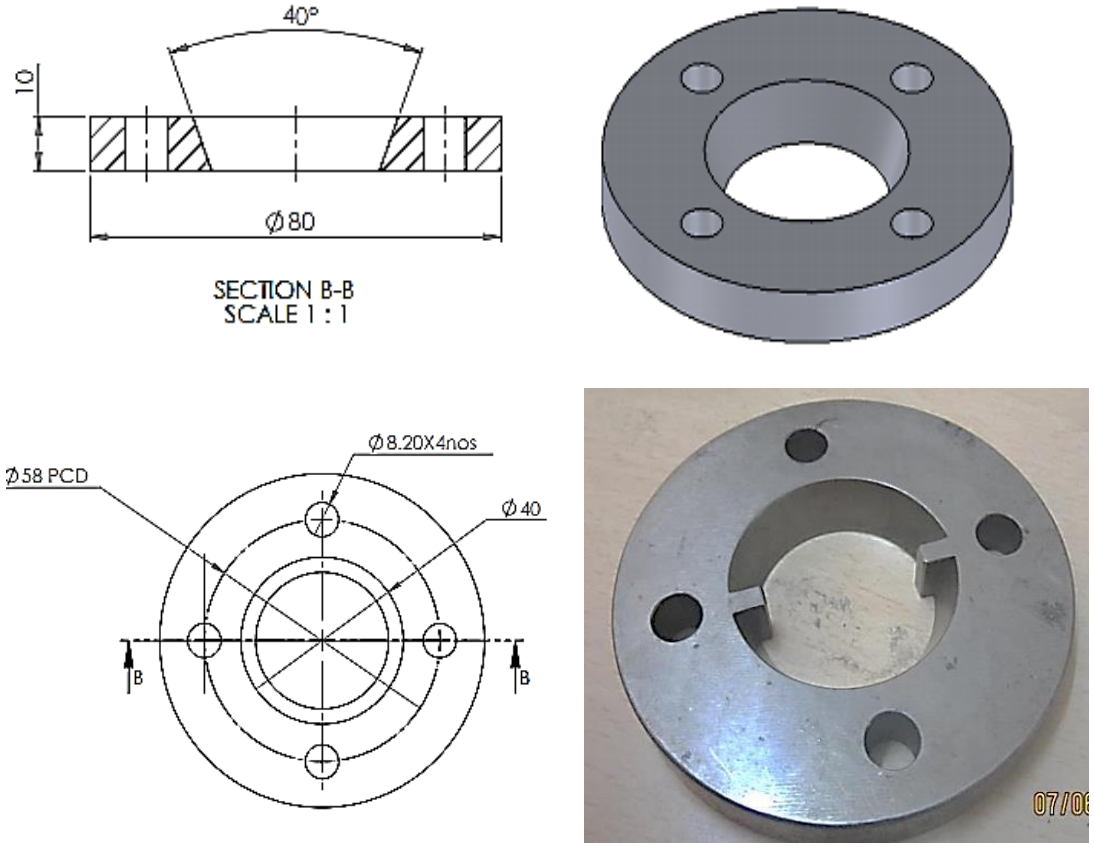

Figure 5.18: Die holder

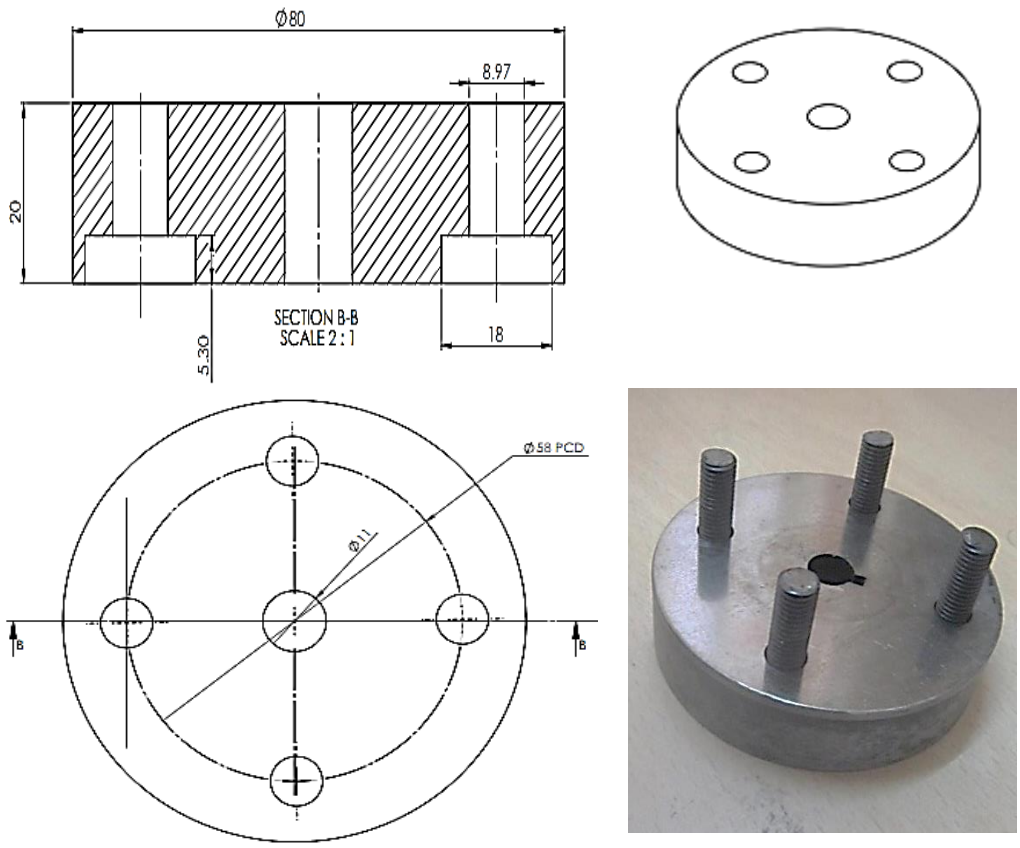

Figure 5.19: Support plate

5.5.2 Experimental procedure

The effective surfaces of the tooling setup are cleaned with acetone to remove external particles. The setup is arranged as per their respective positions and tightened by the allen screw properly. The total setup is covered with glass wool insulation after keeping on the INSTRON® bed. The heat was provided to the setup from an external source and the billet was heated in a resistance furnace very near to the hydraulic press. After a dwell period of 20 minutes at the desired temperature, the press machine is being operational. Experimentation has been carried out for the round to square, simple bar extrusion at a temperature range 400-450℃ for an extrusion ratio of 2.505. The lubricant used for the hot extrusion process is Molykote-1000. The extruded specimens are shown in Figure 5.20.

To compare the simulation results with experiment the simulations were carried at a temperature of 400℃ by considering all other parameters same. It is tough to maintain a constant operating temperature and friction condition at the time of the experiment. So a range of temperature has been mentioned earlier in between which the experiment has been performed. Predicted load versus stroke is in well agreement with the experimental outcome, evident in the Figure 5.21.

Figure 5.20: Extruded specimen

5.5.3 Flow pattern study

To imitate metal flow phenomena encountered in different forming processes grid pattern analysis by FEM is a suitable technique. Experimental flow pattern study was conducted by splitting the billet into two halves along one axis symmetric plane before extrusion. The split billet surface is scratched or inscribed with longitudinal and transverse shallow grooves as shown in Figure 5.22 (a).

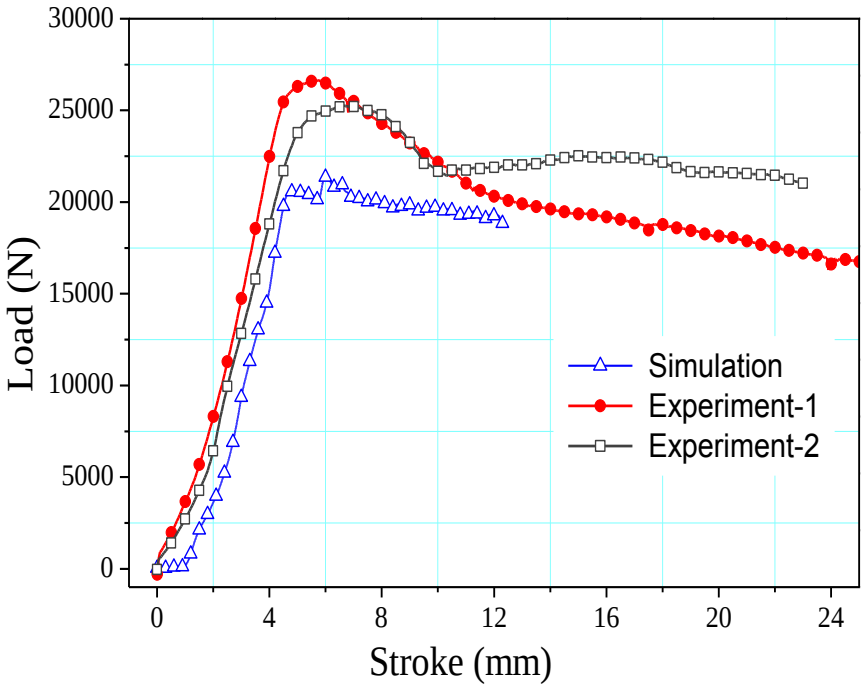

Figure 5.21: Variation of load w.r.t stroke

To avoid welding process in between two scribed surfaces during hot extrusion, a thin layer of graphite powder was spray pasted to act as a parting agent. The dome shaped pattern is clearly visible in the Figure 5.22 (b), split billet extruded through cosine profiled die which is in well agreement with the corresponding flow grid pattern made by FEA shown in Figure 5.23 (a-e). In case of huge reductions, the scratch pattern disappears and fails to show the flow character in case of experimantation due to severe deformations.

The flow pattern of the simulated forward extrusion by all five types die has been observed by the grid pattern analysis of the material model. It is revealed from the Figure 5.23 that the smooth flow of metal occurs in cosine die comparable to other dies. As shown in the comparative flow pattern modelling, there is a dome shape of velocity gradient at the exit cross section in cosine die, but a sharp rise of flow velocity at the centerline is observed in other dies leads to velocity relative difference at the product cross section area.

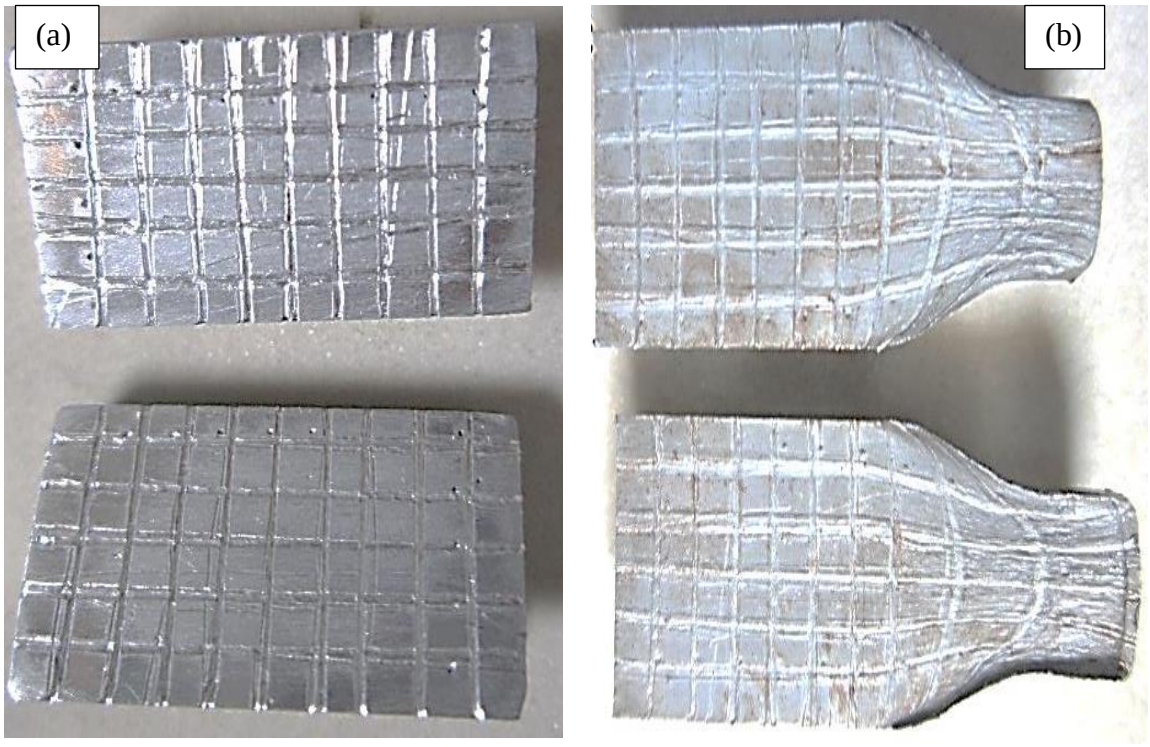

Figure 5.22: Experimental study flow pattern.

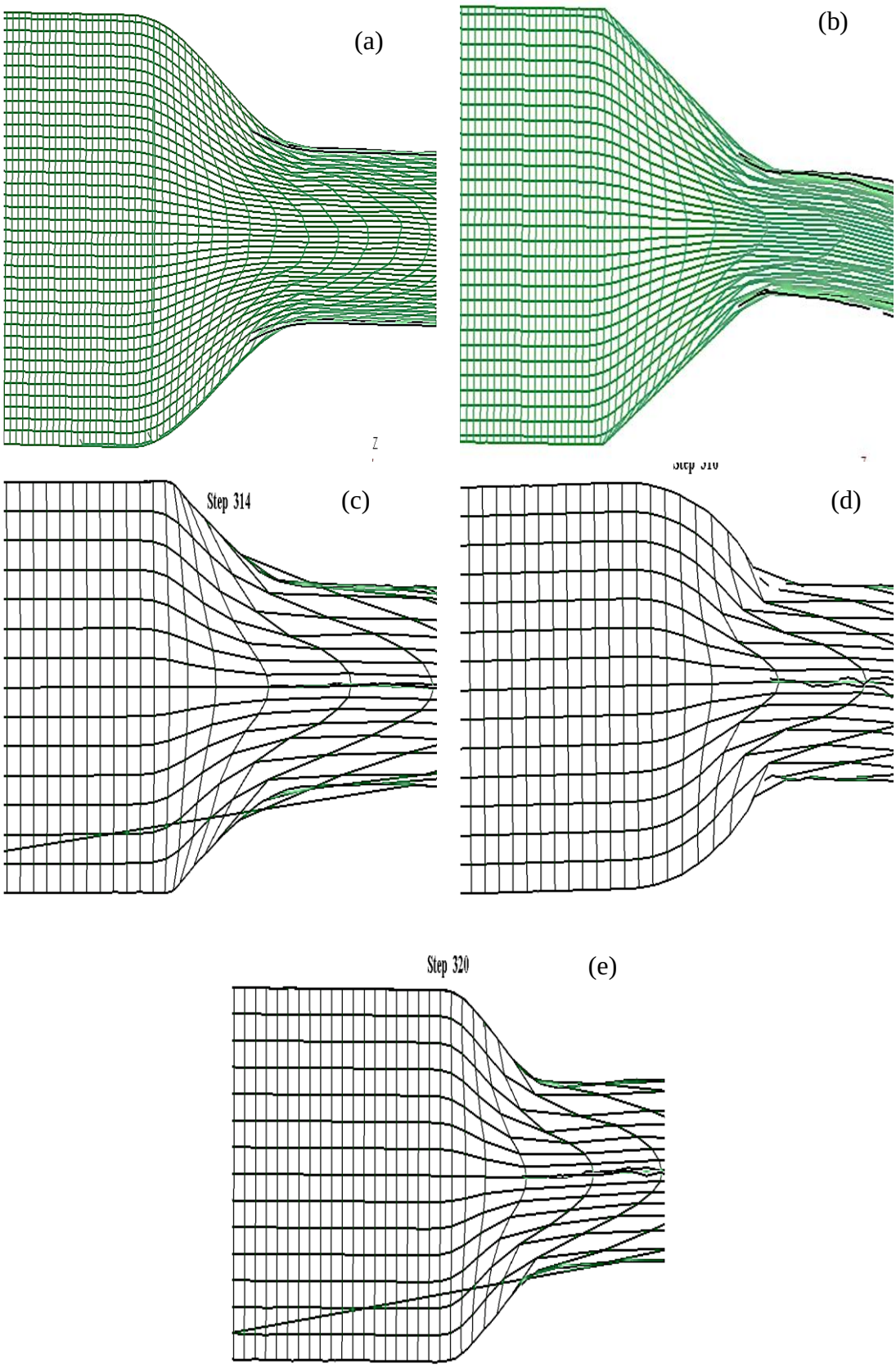

Figure 5.23: Extrusion Flow pattern analysis by FEM grid lines through (a) cosine (b) linear converging (c) hyperbolic (d) elliptic and (e) 3rd order polynomial die.

5.6 Conclusions

In this chapter, three dimensional die profile development for round to square section extrusion following cosine, linear converging, elliptic, hyperbolic and 3rd order polynomial laws has been done to investigate the flow characteristics and suitable die profile. The results uttered from the investigation are as follows:

- A new method to obtain different types of mathematically contoured round to square extrusion die profiles, following cosine, linear converging, hyperbolic, elliptic and 3rd order polynomial laws, have been developed successfully.
- FEM simulations for square bar extrusion from round billet have been performed to study the effect of die profile as well as to study the strain and strain-rate distribution by DEFROM-3D package.
- Effective-strain rate, as well as effective-strain at die entry and exit, was found less in the case of cosine profiled die, results minimum redundant work with less energy consumption and product defects.
- The experimental results of extrusion of the aluminium alloy are in well aggrement with the simulated predictions.

Chapter 6

Extrusion of Aluminium MMC through Cosine Die

6.1 Overview

Aluminium metal matrix composites are the most versatile replacement of other alloys in the sector of automotive, aerospace, defense and sports, because of its high strength to weight ratio, ease and prevalence of processing techniques, good thermal and electrical conductivity and the ability to sustain in uncertain thermal and mechanical loading environment [120]. This emerging area has influenced the researchers to tailor the mechanical, thermal and tribological properties of the composite using different types of reinforcements with various percentages with types of manufacturing process. The endless process of pursuance of mankind needs the material to behave well in critical environments.

Aluminium, iron, titanium and magnesium are the most commonly used matrix elements but other super alloys also have been used. Selection of reinforcement elements principally depends on end uses. The objective of reinforcement is to improve strength, stiffness, wear resistance and ability to absorb thermal shocks with a slight compromise of ductility. The complex and diverse fabrication process of metal matrix composite (MMC) mainly depends on the type of materials. The process is significantly affected by the characteristic of the elements like thermal, mechanical, chemical and structural properties. Depending on the types of processing it is of solid phase and liquid phase fabrication. Both the process has certain advantages and disadvantages over another.

In this chapter, the objective of the work is to fabricate the aluminium MMCs by powder metallurgy route for the further processing. The MMCs were subjected to thermo-mechanical treatment (extrusion) followed by controlled atmospheric sintering, double axial cold compaction and powder blending. Among a number of fabrication techniques like conventional ingot metallurgy, powder metallurgy, squeeze-casting and liquid metallurgy this route is adopted because of its homogeneous distribution of reinforcements of various percentages in the matrix material and the uniformity can be expected in the final product properties. Four different reinforcing elements of 2 wt. % (two metals and two ceramics) were added to Al / 5 wt. % of Mg / 1 wt. % of Gr matrix. The addition of

graphite improves wear resistance compromising with hardness and flexural strength [121, 122]. As the reinforcing components like Ti, soda-lime-silica glass and ZrO_2 have the lower thermal conductivity, hence very small amount of reinforcement is there not to decrease the thermal conductivity of the component significantly [112]. The addition of more amount of zinc reduces the high-temperature performances. So based on the points the composition of graphite and four reinforcing variables remain very less. The prepared specimens of 10 mm diameter were subjected to secondary treatment extrusion to the square billet of 50% reduction in dimension. The mechanical properties after extrusion improve significantly due to the improved density and stronger bond formation after the shearing of the oxide boundary of the particles. The equipment used for the work is listed in Table 6.1. The sample characterization (metallography, spectroscopy, mechanical and tribological testing) were done before and after extrusion. The detailed work plan adopted for this objective is stepwise described in Figure 6.1.

6.2 Sample fabrication and characterisation

6.2.1 Powder selection and characterisation

Since the strength of the aluminium alloy improves significantly due to age hardening, it was decided to consider aluminium as principal matrix material. Magnesium with aluminium is a preferable matrix because of its heat treatability, as well as good strength to weight ratio. As the addition of graphite reduces the hardness of the composite, a minuscule amount of graphite was added to improve the flowability and wear resistance. Aluminium, magnesium, graphite in weight percentages of 92, 5 and 1 respectively were mixed for the matrix composition. Four reinforcements (two metals and two ceramics) were added to the mixture for preparing four types of sample. The basic reasons for choosing the reinforcements are its low cost and easy commercial availability as well as higher hardness. The compositional details of four specimens were tabulated in Table 6.2. A minuscule amount of reinforcements was considered to investigate the changed properties of the composite without affecting the thermal behaviour. The physical characterization of the powders like size, shape, flowability was studied. Particle size and shape was analysed from SEM images.

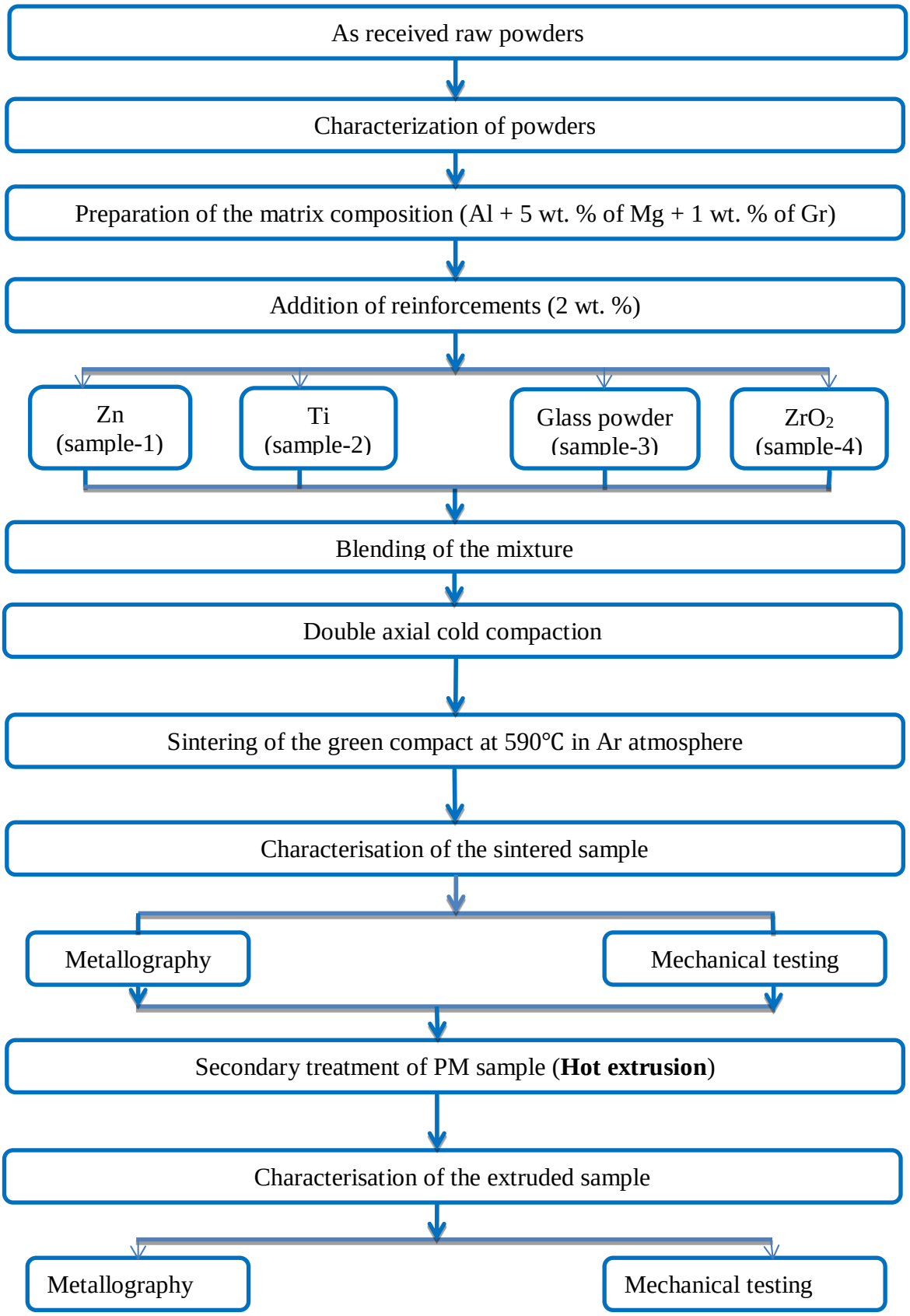

Figure 6.1: Detailed work plan for the study

Table 6.1: List of machineries used during this work

Sl. No	Equipment used	Detailed technical specification	Purpose
1	Centrifugal blender	Mortar pestle	Blending of the mixture.
2	Compression machine	Type: Hydraulic Load Range: 20 tons	To prepare the green sample by double axial compaction.
3	Controlled atmospeheric furnace	Make: Bysakh & Co. Model: 7C T7 Max. Temp.: 1700℃	For sintering the green compact at Ar atmosphere.
4	Universal testing machine	Make: INSTRON Capacity: 600 KN	For secondary treatment (extrusion).
5	Hardness tester	Lecco Vickers microhardness (LV 700)	For checking the hardness of sintered as well as extruded specimen.
6	Scanning electron microscope	Make: JEOL Type: JSM-6480LV	For observing the micrograph of the surfaces.
7	Pin on Disk wear testing machine	Pin-on-disc (DUCOM)	For investigating the wear characteristics of the material.

Table 6.2: Compositional details of the MMC

Specimen	Composition
Type-1	Al (92) + Mg (5)+ Gr (1) + **Zn (2)**
Type-2	Al (92) + Mg (5)+ Gr (1) + **Ti (2)**
Type-3	Al (92) + Mg (5)+ Gr (1) + **glass powder (soda lime silica) (2)**
Type-4	Al (92) + Mg (5)+ Gr (1) + **ZrO_2 (2)**

6.2.2 Blending of the mixture

The mixture was allowed for uniform blending in a centrifugal blender as shown in Figure 6.2. The weight ratio of stainless steel ball to powder was maintained 10 : 1. At an rpm of 200 for 10 hours the mixture was allowed for blending. Flow property of the blended powders was checked by measuring apparent density and tap density for all four types of compositions. Apparent density is the ratio of mass of powders (untapped) to the covered volume and is measured by pouring it into a known volume from a particular height.

Apparent density is also known as bulk density. Measurement of apparent density is very sensitive, because a very slightest change or disturbances in the bed or the powder will make the result vary reportedly. For determining tap density, the container is tapped with a height of near about 3 mm after filling with the powders until there is no visible amount of volume change.

Figure 6.2: Centrifugal blender

6.2.3 Double axial cold compaction

Afore described blended powder was subjected to double axial compression for the preparation of green specimens. Improved fineness with no agglomeration was observed in the blended powders. At the time of compression, the powder inside the container remains in floating condition in between both of the punches. The powders are subjected to a pressure of 275MPa with a very slow rate of rise and kept for a dwell period of 10 minutes. The die at the time of compaction and the 2-D drafting are shown in Figure 6.3. Zinc stearate was used as a lubricant to avoid die sticking. In case of single axial compaction process, the maximum green density of the product will remain just below the punch surface and it gradually decreases towards bottom end. Whereas in double axial compaction, the density at two opposite ends are at higher side and at centre zone it is minimum. Due to the above reason the double axial compaction was chosen for the preparation of the green samples. Green density of the prepared 10 mm diameter specimens was measured and the samples were forwarded for sintering in further processing.

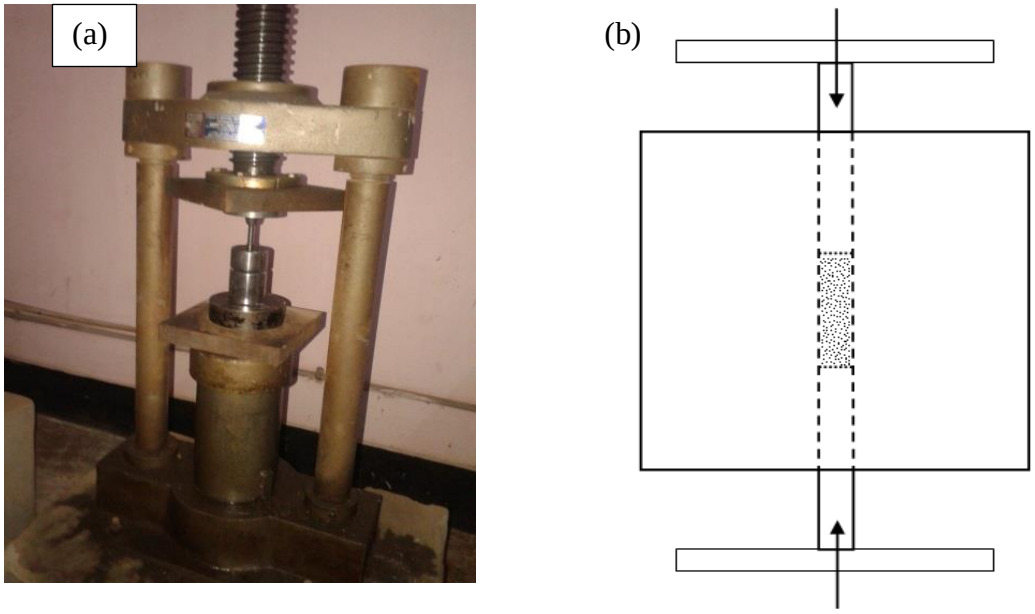

Figure 6.3: (a) Hydraulic press used for compaction (b) 2-D drafting of the process.

6.2.4 Controlled atmospheric sintering

Green specimens were subjected to sintering in a controlled atmospheric tubular furnace (Figure 6.4). The sintering atmosphere was maintained with argon gas to avoid oxidation at high temperature. The ramp rate of $5℃/\,min$ was set for all the temperature-rises. Dwell period of 20 minutes at 110℃ to remove water vapours, 30 minutes at 450℃ to remove lubricants and 90 minutes at 590℃ to form metallic bond are set for the process. Time vs temperature plot is shown in Figure 6.5. After the targeted dwell period the temperature of the sample was allowed for furnace cooling.

Figure 6.4: Controlled atmospheric furnace.

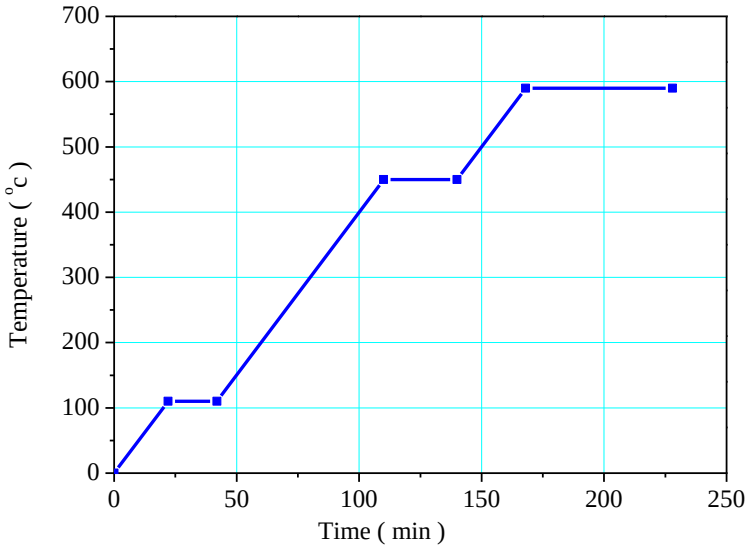

Figure 6.5: Variation of temperature w.r.t time

6.2.5 Characterisation of sintered samples

6.2.5.1 Density

Theoretical density was calculated by the following relation (Rule of mixtures) as follows:

$$\rho_{Theoriticd} = \sum(\rho_i \times m_i) \tag{6.1}$$

ρ_i is the density of individual element and m_i is the mass fraction of the individual element.

Densities of the solid sintered as well as extruded specimen were measured by following Archimedes' principle. In this principle, the mass of the specimen is to be measured in air and in a selected fluid. The relation for calculating the density is presented as follows:

$$\rho_{sample} = \frac{W_A \times \rho_{fluid}}{W_A - W_{fluid}} \tag{6.2}$$

where W_A is the mass of the sample at atmospheric air, W_{fluid} is the mass of the considered sample in a fluid and ρ_{fluid} is the density of the considered fluid. Processed composites were measured five times each to get an accurate density.

The fluid considered for the measurement was distilled water because its density is 1 gm/cc at normal temperature and pressure condition. The density measuring kit is illustrated in Figure 6.6. Contech CB-300 series analytical balance having least count of ± 0.001 g. is utilised.

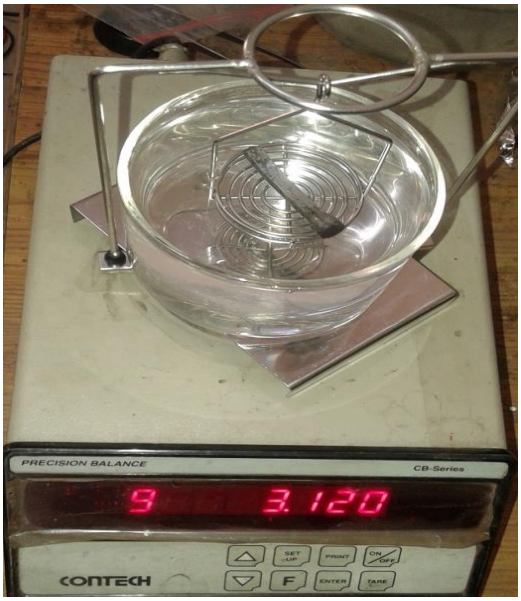

Figure 6.6: Density measurement kit with analytical balance.

Porosity of the specimen was calculated by following the relation mentioned as follows:

$$\gamma = 1 - (\rho_{sample} - \rho_{Theoritical}) \tag{6.3}$$

where ρ_{sample} the density of the sample is found from the Archimedes' principle and $\rho_{Theoritical}$ is the theoritical density estimated by following rule of mixtures.

6.2.5.2 Hardness test

The sample surface was given a fine finish by polishing it through series of emery papers of increasing grit up to 1200. Diamond paste polish with hyphine fluid was performed followed by polishing with 2 μm size alumina powder slurry. Vickers micro hardness of the sintered MMCs was determined by dividing the applied load to the impressed area. The load was applied through a diamond pyramid having the face angle of 136° and a dwell period of 15 seconds was mentained to avoid spring back effects. Lecco Vickers micro hardness (LV 700) was employed for the test.

6.2.5.3 Wear test

Aluminium exhibits inadequate tribological properties. But it is a crucial material to investigate and improve the aforesaid property by reinforcing additional materials having good mechanical and tribological properties because aluminium possesses high thermal conductivity along with low density [123]. There is a wide interest to study and improve the wear characteristics of aluminium MMC in the research fraternity. Engine blocks, drive shaft, brake drums and many more of the automotive components are made by aluminium MMC

manufactured by PM processing route because of their good mechanical, thermal and tribological properties. In this chapter study of wear characteristics was also focused for the MMCs.

Dry sliding wear characteristics of the prepared aluminium MMCs were studied by pin-on-disc wear testing apparatus. Dimensions of the pin were set 10 mm diameter with 25 mm length. The pins were prepared with flat contact surface with smooth corners and kept stationary in the sample holder perpendicular to the counter disc. The rotating EN-31 counter disc is of 160 mm diameter and has the hardness and average surface roughness value of 60 HRC and 2 μm (Ra) respectively. The counter disc and pin surface were cleaned with acetone before the experimentation. A normal load was applied on the MMC specimen through the specimen holder by a leaver attachment. The line diagram of wear testing mechanism is shown in Figure 6.7. The variable parameters like wear path diameter, normal load, RPM of the disc are well facilitated by the machine set-up and all are needed to fix manually anterior to experimentation. The variable parameters chosen for the wear analysis is tabulated in Table 6.3. The 10 min of test duration was adopted for each experiment. With an accuracy of 0.1 mg the MMC pin (specimen) was weighed before and after the wear operation for determining the wear loss in weights. The wear testing apparatus is shown in Figure 6.8.

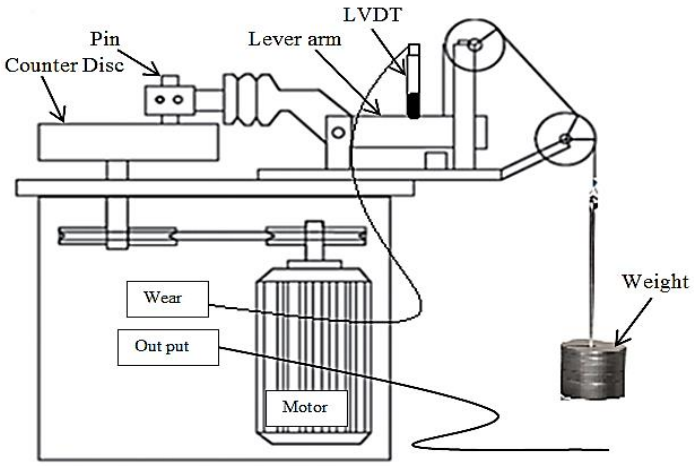

Figure 6.7: Schematic layout of pin-on-disc wear testing apparatus.

Table 6.3: Variable parameters selected for the experimentation

Variable parameters	Level-1	Level-2	Level-3
Wear track dia (D), (mm)	50	70	90
Normal load (L), (N)	40	60	80
Rpm of counter disc (N),	200	400	600

Figure 6.8: Wear testing apparatus

6.2.5.4 Three point flexural test

Three point flexural test has been performed to check the transverse rupture strength (TRS) of the sintered solid cylindrical specimen. The test was executed in UTM (universal testing machine, Instron -5979). A span of 30 mm with a compression rate of 2 mm/min at atmospheric temperature was maintained at the time of operation. The set-up of three point bend test for determining TRS is shown in Figure 6.9.

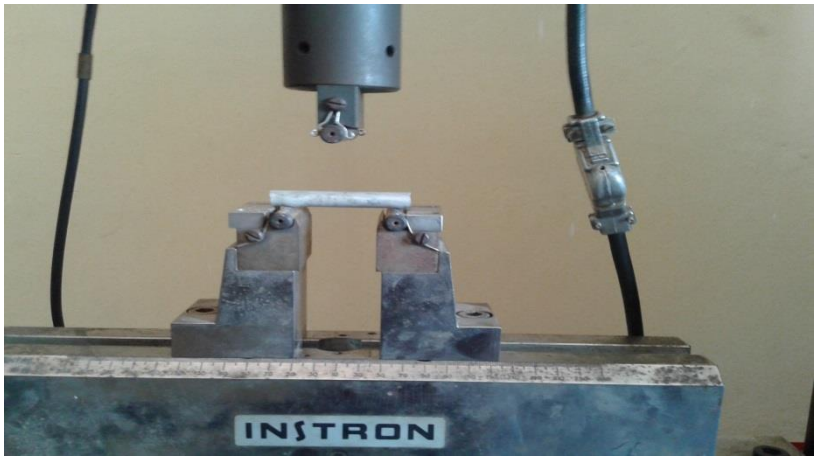

Figure 6.9: 3-point bend test set-up

6.2.5.5 Scanning electronic microscopy

The shapes of the as received loose powders were observed by scanning electron microscope (SEM) (JSM-6480LV). After a standard polishing procedure, the surface of the final product was etched by Keller's reagent (190 ml H_2O, 5 ml HNO_3, 3 ml HCL and 2 ml HF) for the microscopic analysis. The modes of failure of the extruded specimen of the tested fractured surfaces were investigated with the help of scanning electron microscope.

6.3 Secondary Processing (Hot extrusion) and characterisation

Secondary processing of the PM components produced either by cold compaction and sintering or hot compaction process are necessarily required to enhance the properties manifold. The secondary operation like cold or hot rolling, cold or hot forming and cold or hot extrusion etc. processes are commonly followed. By the application of severe compressive stress to generate effective strain in the metal generates are the main cause for the same. Density of the component improves and the same time porosity decreases with improved bond strength. As the component is produced by compaction process, the density of the component is not distributed uniformly. The density near the punch is maximum and at the centre is minimum. There exists a density difference between boundary zone and the centre zone which is removed by the secondary operations. The homogeneous density distribution in the PM component can only be achieved after secondary operations.

The powder surfaces forms oxides due to the use of it in atmospheric conditions, which causes weak bond formation at the inter boundary layers. The hard oxide layers are getting sheared off due to high pressure shearing effect due to secondary operation. The hard oxide particles improve the component properties and removal of it causes a good bond formation between the intermetallic powders.

6.3.1 Hot extrusion

The 10 mm specimen prepared by cold compaction followed by sintering was subjected to thermo-mechanical treatment (Hot extrusion) as a secondary processing. The experiment was carried out to reduce the cross-sectional area of the specimen to 50% at an operating temperature of 400-450℃ with a ram rate of 3 mm/min. Extrusion through shear faced die causes severe surface defects like surface crack and tearing in the extruded product due to velocity relative difference at the die exit. The defects are more prone in the case of extrusion of MMCs synthesised by powder metallurgy route [124]. Hence, a specially designed mathematically contoured cosine die from round to square bar extrusion was used to avoid severe velocity relative difference. The die used for the process is a mathematically contoured cosine die developed for round to square shape extrusion explained in detailed in chapter 5.

6.3.2 Characterisation of extruded specimen

Density, hardness, wear, three point flexural test and scanning electron microscopy have also been performed for the extruded specimen. For comparative wear resistance analysis between

specimen before and after extrusion, the applied load is reduced to 50% as the cross sectional area reduces after extrusion.

6.4 Results and discussion

6.4.1 Physical characteristics of the powders

A better understanding of the physical properties of the powders those essentially affecting product properties are highly desired. Flowability of the blended powders is directly influenced by physical properties like size and shape, as well as environmental conditions of the powders. The properties of the final output material are directly related to flowability. Hence, there is a great importance for the study of physical characterisation such as size, shape and density. Among three most popular techniques like microscopy, LASER diffraction and sieve analysis used for powder size determination, the microscopy and image analysis was utilised for determining the size and shape of the powders. The shape of the powders is idiosyncratic depending on its manufacturing process. The detailed properties of the powders are mentioned in
Table 6.4.

Table 6.4: Physical characteristics of the powders

Powder	Supplier	Size	Shape	Purity / Assay (%)
Aluminium	Loba Chemie	45	Spherical and sub-rounded	98.0
Magnesium		143	Flakey	99.0
Graphite		20	Rounded and Flakey	98.0
Zinc		22	Spherical and sub-rounded	98.0
Ti		85	Very angular and irregular	98
Glass Powder (soda lime silica)		27	Angular	
Zirconia		78	Spherical and rounded	98

6.4.2 Density analysis

Apparent density / bulk density and tap density are recorded from direct measurement. It is depicted from the graph shown in Figure 6.11 that there is an improvement of increase in density of 30-35% by tapping. Green density of the specimen primarily depends on the compaction pressure and flowability. In this case, the double axial cold compaction was carried out at a pressure of 275 MPa. The random distribution of particle size revealed from the SEM immages illustrated in Figure 6.10 supports avoidance of interstitial spacing which results in improved tap density and green density. A good consolidation of metallic particles even in green specimens was observed. After ejection of the green specimen, the density was calculated by dividing the measured volume (with the accuracy of $\pm$2%) with the measured mass (with the accuracy of 0.001gm). The sintered and extruded densities were measured by aforementioned Archimedes' principle. Nondimentional densification parameters were calculated by the following relation illustrated in equation 6.4 [125].

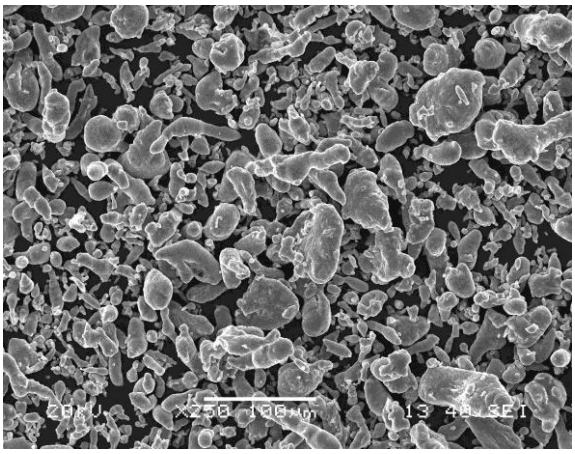

(a)

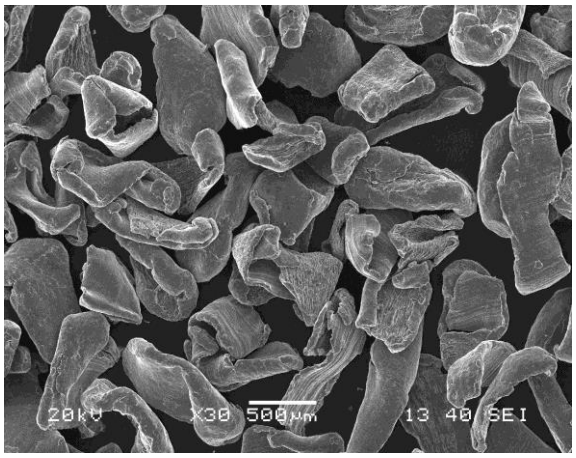

(b)

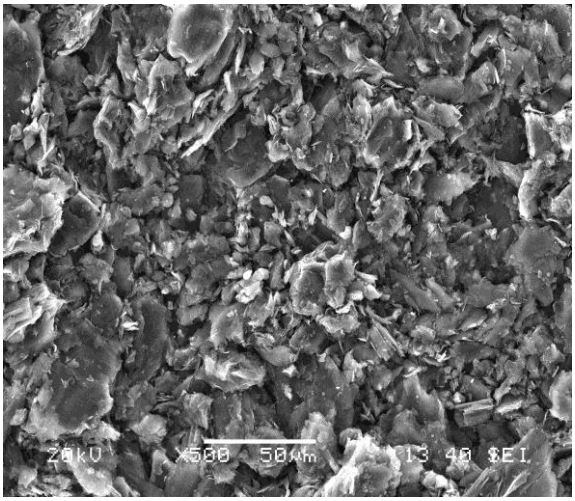

(c)

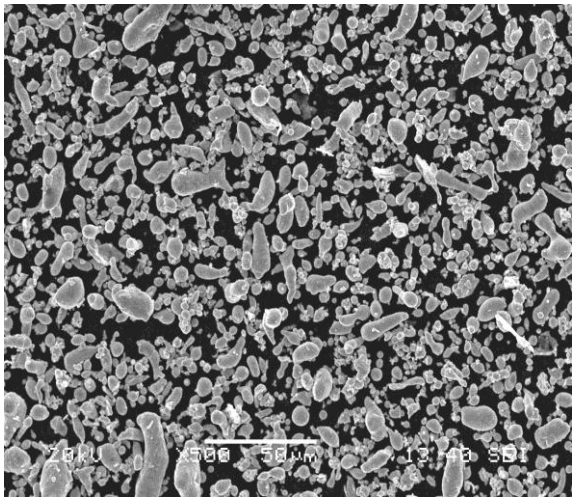

(d)

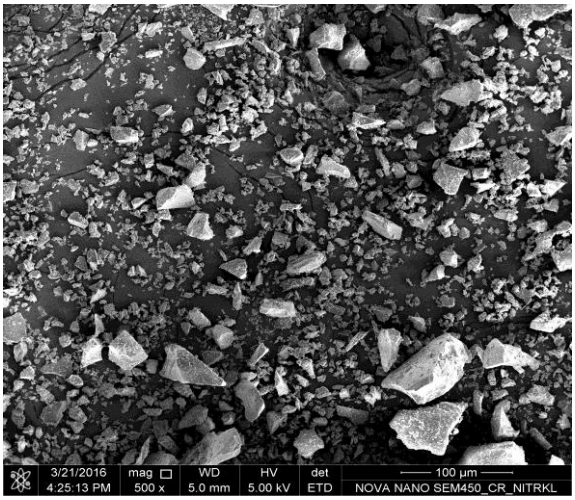

(e)

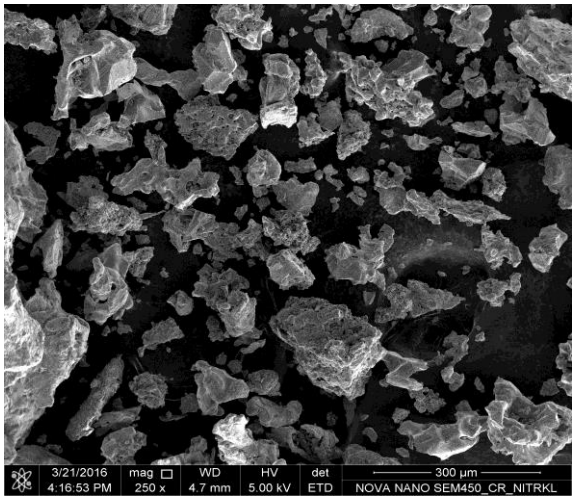

(f)

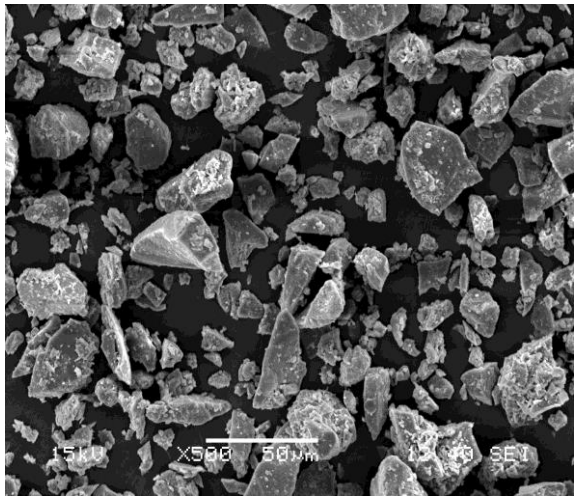

(g)

Figure 6.10: SEM images of (a) Al (b) Mg (c) Gr (d) Zn (e) Glass (f) Ti and (g) ZrO2 powder

$$\text{Densification parameter} = \frac{(\text{sintered density} - \text{green density})}{(\text{theoretical density} - \text{green density})} \tag{6.4}$$

If the above parameters come positive then it indicates shrinkage whereas negative for growth or swelling. All the four samples were showing swelling behaviour during sintering. The percentage improvement in densification by thermo-mechanical treatment (extrusion) is calculated by the relation illustrated as follows:

$$\text{Percentage improvement in densification} = \frac{\text{extruded density} - \text{sintered density}}{\text{sintered density.}} \tag{6.5}$$

It was found that there was an improvement of 15-20% of density after extruding the sintered billet with 50% reduction.

The porosity of the sintered, as well as extruded specimen, has been determined by using equation 6.3 and presented in Figure 6.12. There is a significant amount of decrease in

porosity level after extrusion. Decrease in porosity level causes improved mechanical strength which is discussed latter on.

Table 6.5 Density analysis for four specimen

Sample	Sample-1	Sample-2	Sample-3	Sample-4
Densification factor	-0.597	-0.742	-0.489	-0.48
percentage improvement in densification (after extrusion)	20.32	17.35	16.46	17.30
Porosity before extrusion (%)	23.7	22	20.37	22.13
Porosity after extrusion (%)	8.15	8.53	7.26	8.65

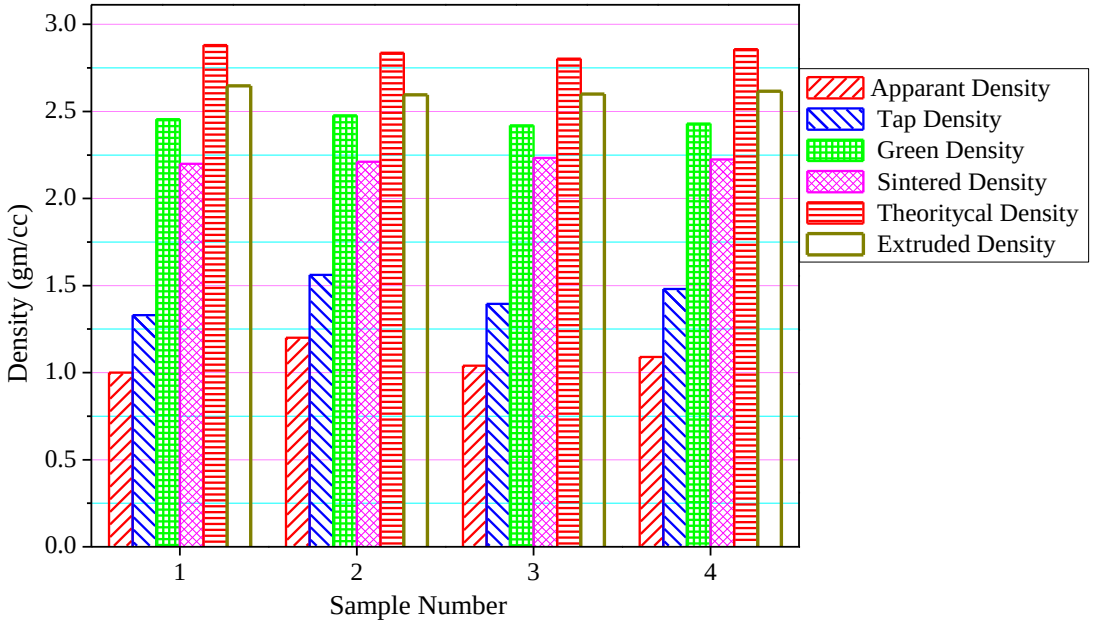

Figure 6.11: Comparative density analysis

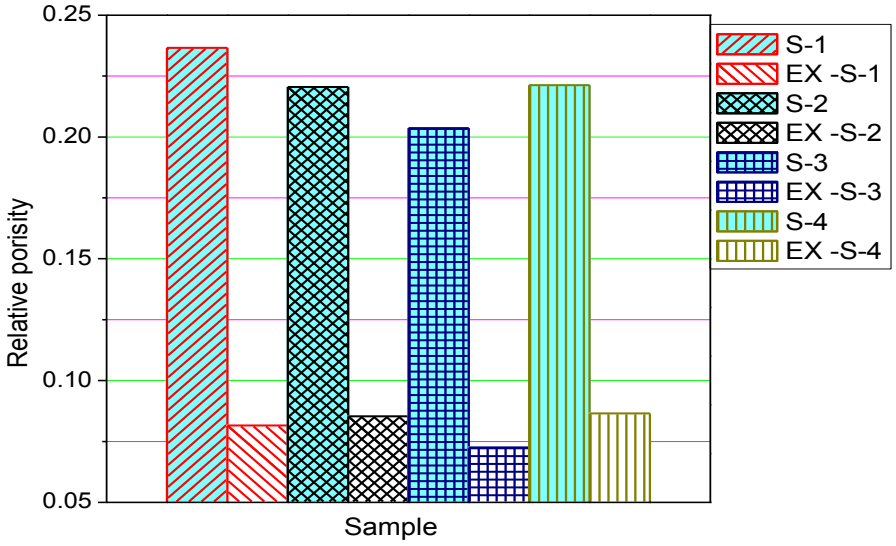

Figure 6.12: Relative porosity of the specimen

6.4.3 Microstructural studies

Figure 6.13 depicts the scanning electron micrographs of all four types of specimen after the thermo-mechanical treatment at different magnifications. A minuscule amount of porosity still remains in the material after extrusion which is evident from the Figure 6.12. After extrusion operation the improved density and decreased volume of porosity are illustrated in Figure 6.11 and Figure 6.12 respectively. The distribution of reinforced particles in the extruded product is uniform It also shows good dispersion of reinforcements in matrix elements. Figure 6.13 (a & b) shows very fine distribution of graphite and other reinforcements. In case of sample type 1 there is very less probability of breaking of the reinforced particles due to persistence of liquid phase at high temperature. In sample type -2 there is an existence of good bond in between Ti with the matrix element due to the very angular or the irregular particle shape. In Figure 6.13 (e & f) scanning electron microscopic image of extruded soda-lime-silica glass reinforced AMC is evident.

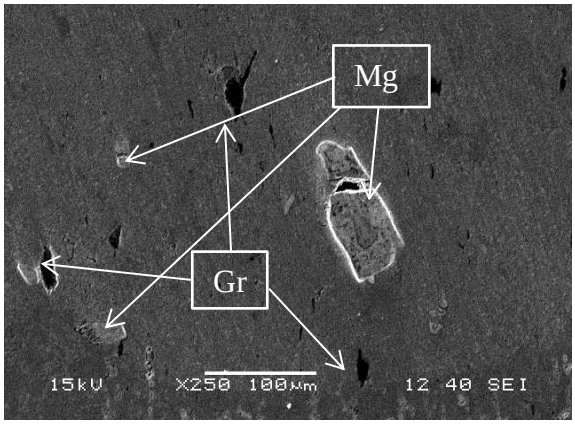

(a) S_1

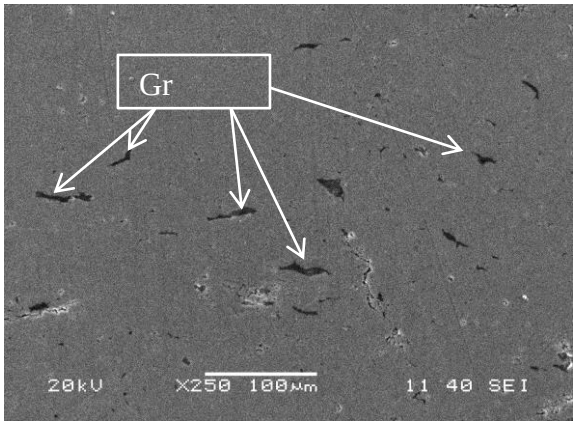

(b) S_1

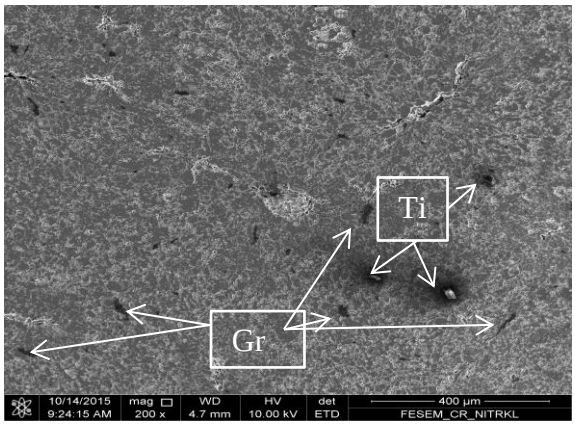

(c) S_2

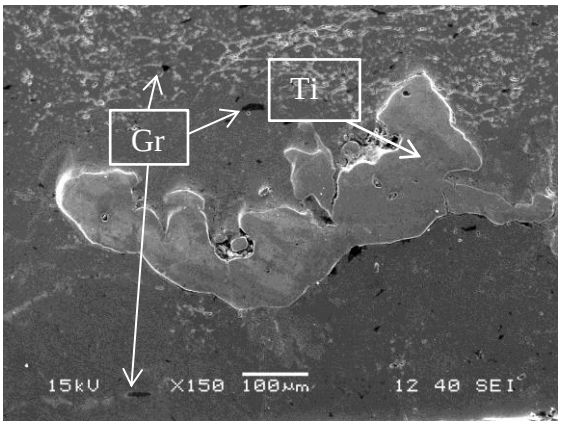

(d) S_2

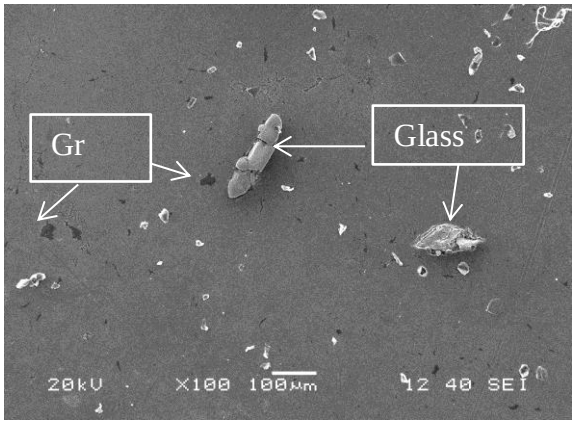

(e) S_3

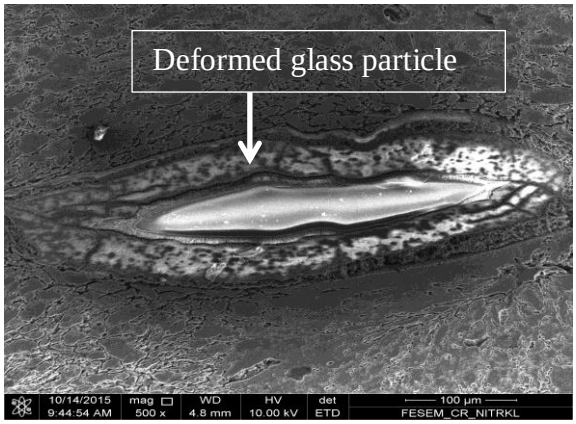

(f) S_3

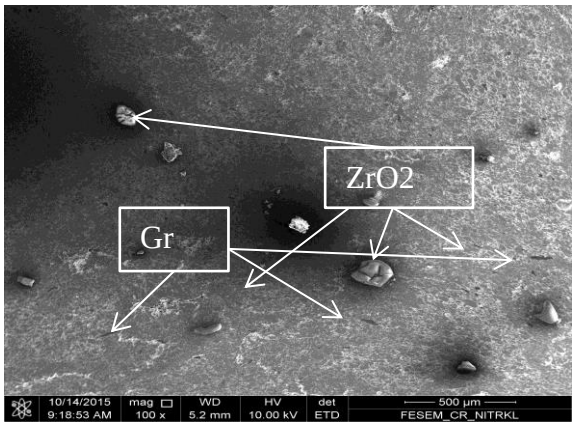

(g) S_4

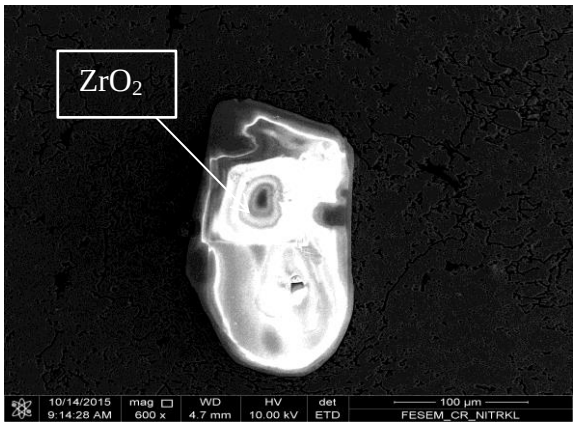

(h) S_4

Figure 6.13: Microstructures of materials after extrusion

In first case glass particle is found broken due to excessive extrusion pressure which could be attributed to the existence of lesser temperature, whereas in second the glass particle achieved plastic deformation at high temperature and pressure condition. At the operating temperature the pressure required to deform soda-lime-silica glass particles plastically is a bit higher side which was anticipated from the squeezed matrix particle distribution around the deformed glass particle along extrusion direction. As the glass transition temperature of soda-lime-silica glass is 575℃, it forms a good bond with the aluminium matrix at high pressure in hot working conditions which causes ameliorated mechanical and tribological properties. As the size of zirconia particle is on higher side there exists some pores at its boundary.So a weak bonding exists which deteriorates the mechanical property and responsible for crack initiation. Due to the size effect at high pressures, some of the particles also arrested brittle fracture.

6.4.4 Mechanical testing

6.4.4.1 Compression test of sintered specimen

Compression test of all the four types of specimen were conducted by the UTM (Instron-setec series). From the output results stress versus strain curve is plotted in the Figure 6.14 (a, b, c, d). The average ultimate stress of the four samples is 409, 381, 416 and 404 MPa for sample type 1, 2, 3 and 4 respectively. The addition of zinc as well as of hard ceramic reinforcements with aluminium improves compression strength significantly [126].

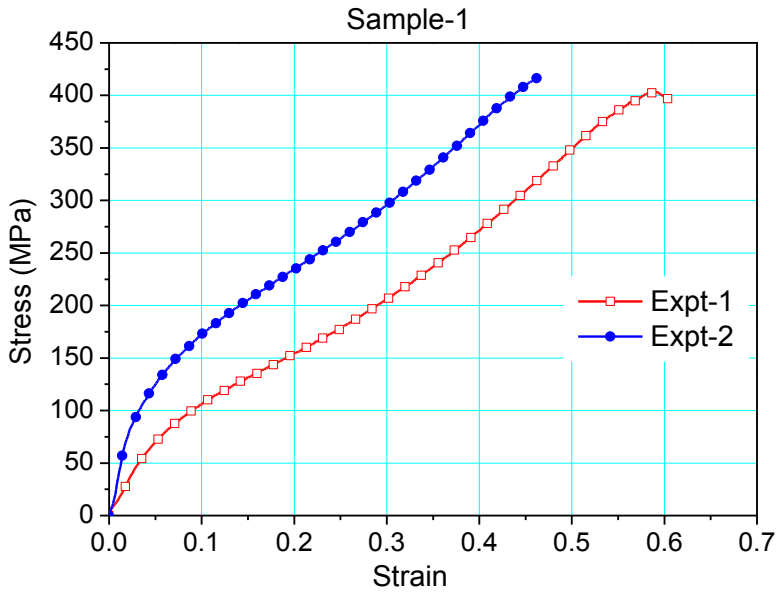

(a)

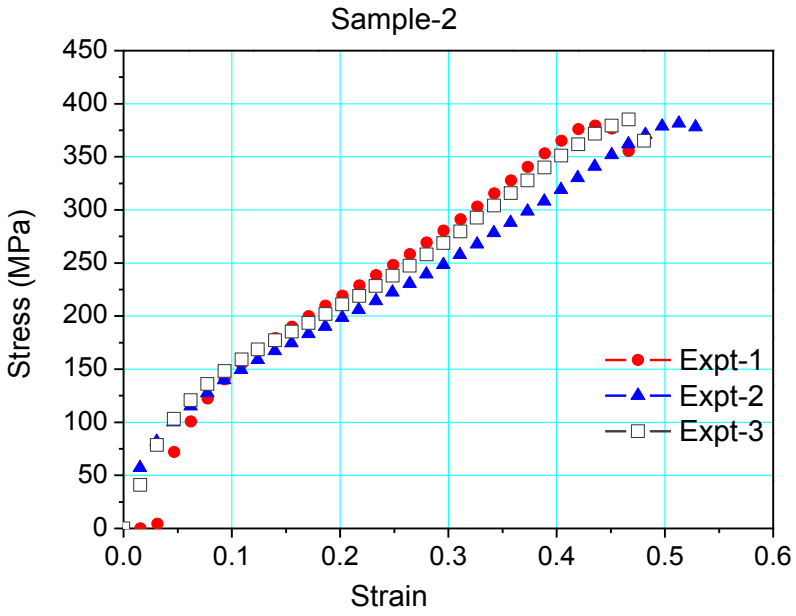

(b)

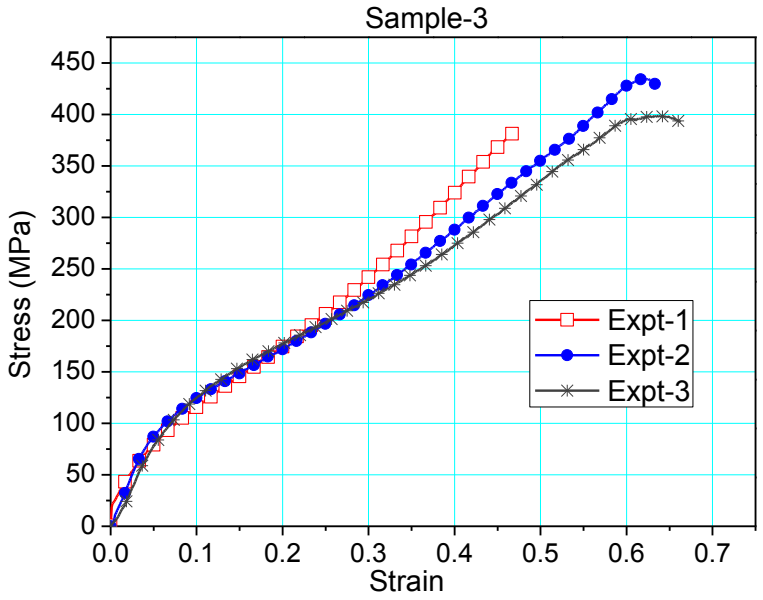

(c)

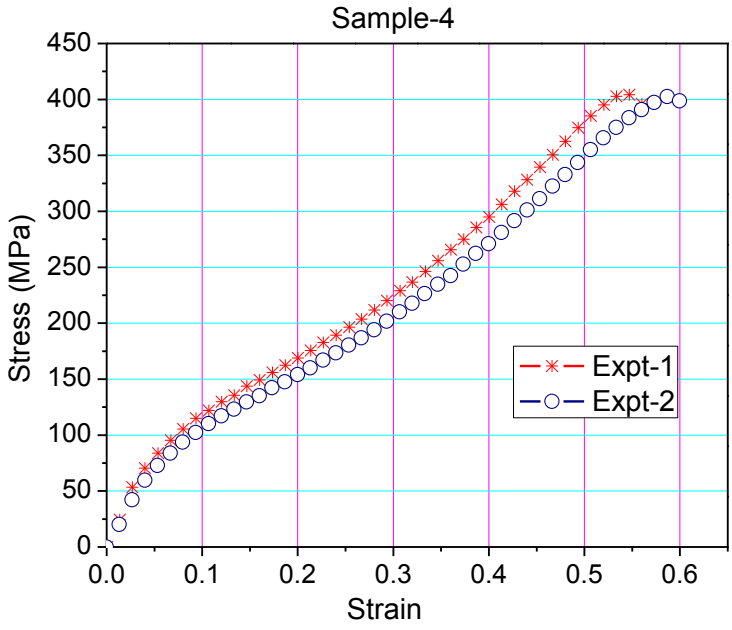

(d)

Figure 6.14: Stress strain plot for (a) sample-1, (b) sample-2, (c) sample-3, (d) sample-4

The structure of zinc is hexagonal closed packing, which is not having a good formability property which improves the compressive strength. The reinforcement of hard and brittle ceramic particles up-to some limit improves the compressive strength significantly.

6.4.4.2 Micro-hardness

The average micro-hardness was calculated from the ten readings taken for both sintered and extruded products. Figure 6.15 shows the improvement of hardness in the material after extrusion. There exist 28.85, 26.13, 35.76 and 16.14% of improvement of hardness in the material type-1, 2, 3 and 4 respectively after extrusion, prepared by the above procedure. Hard ceramic particles are surrounded by soft matrix, so there is a variation in hardness. As the percentage of ceramic reinforcement is very less the standard deviation of value of hardness is very less.

The improvement of hardness of the extruded AMCs can be attributed to principally the hardness of the reinforcements. It can also be attributed to the higher dislocation density around the reinforcement particles due to the difference of mechanical property and thermal mismatch [127, 128]. The mismatch of the properties between the matrix and reinforcements causes the storage of massive internal and thermal stress and engenders improved mechanical properties.

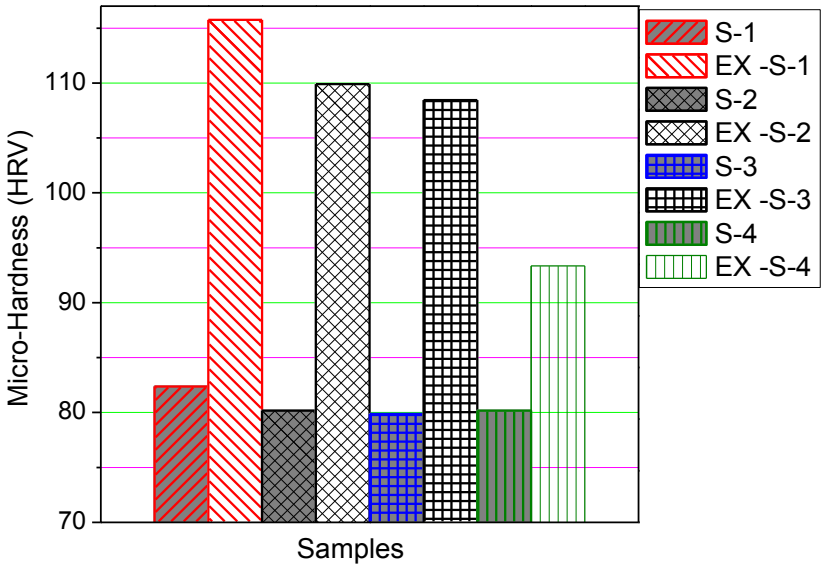

Figure 6.15: Micro-Hardness of the samples

6.4.4.3 3-point bend test and factography

The TRS in MPa found of the specimens was estimated for sintered as well as extruded specimen by following the relations mentioned in the equation as follows:

For cylindrical sintered specimen, TRS = $8Pl/\Pi D^3$ (6.6)

For extruded square bar, TRS = $3Pl/2d^3$ (6.7)

where P = the maximum load (N)

l = length of the sample (mm)

D = Diameter of the sintered specimen (mm)

d = depth = width of the extruded square specimen (mm)

Average TRS for all sintered sample is presented in Figure 6.16 and for all extruded sample in Figure 6.17. Reinforcement of ceramic particles decreases TRS. For the case of sample type 1 presence of zinc having melting point 420℃ causes liquid phase sintering at temperature of 600℃. Liquid zinc passes to intermetallic gaps of the composite at the time of sintering and extrusion due to capillary effect which improves the bond strength. In the case of other three sample types there exist high-stress concentration at the boundary zone of the reinforcements.

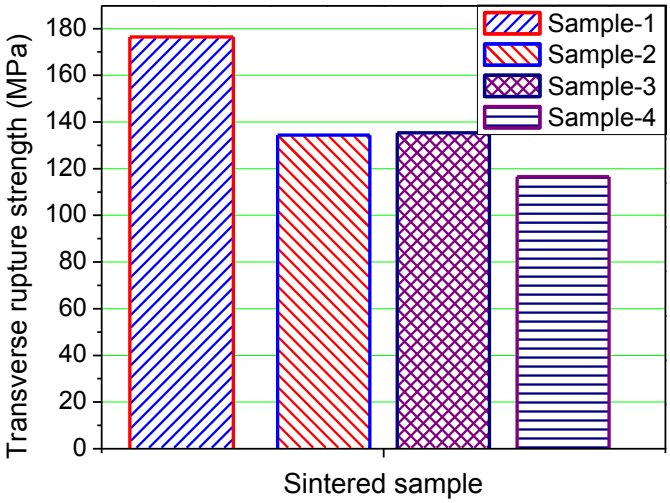

Figure 6.16: TRS of the sintered specimen

In case of sample type-3 the glass transition temperature of soda-lime-silica glass is 575℃. In extruded specimen, TRS of soda-lime-silica glass reinforced AMC is higher which can be attributed to the higher bond strength and the deformation in glass particles caused due to the pressure and temperature. The strength of sample type-4 is found minimum because of the improper bonding due to defects and stress concentration around the larger sized ZrO_2 particles which led to crack initiation.

Factography of the 3-point bend test specimen was performed by SEM analysis to investigate the fracture behavior of the extruded specimen shown in Figure 6.18. Apparently mixed mode of fracture (cleavage and ductile) is evident in the composites. The soft and ductile aluminium are bonded by oxides and form harder boundaries which causes intergranular fracture confronted in.

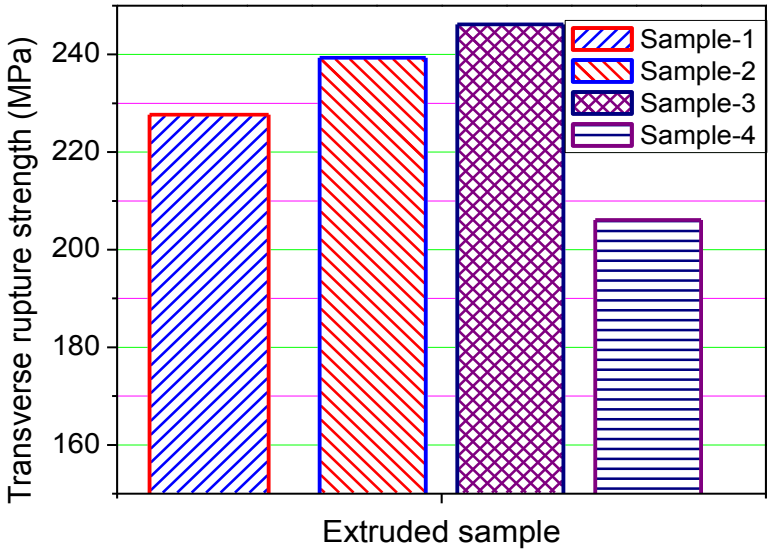

Figure 6.17: TRS of the extruded specimen

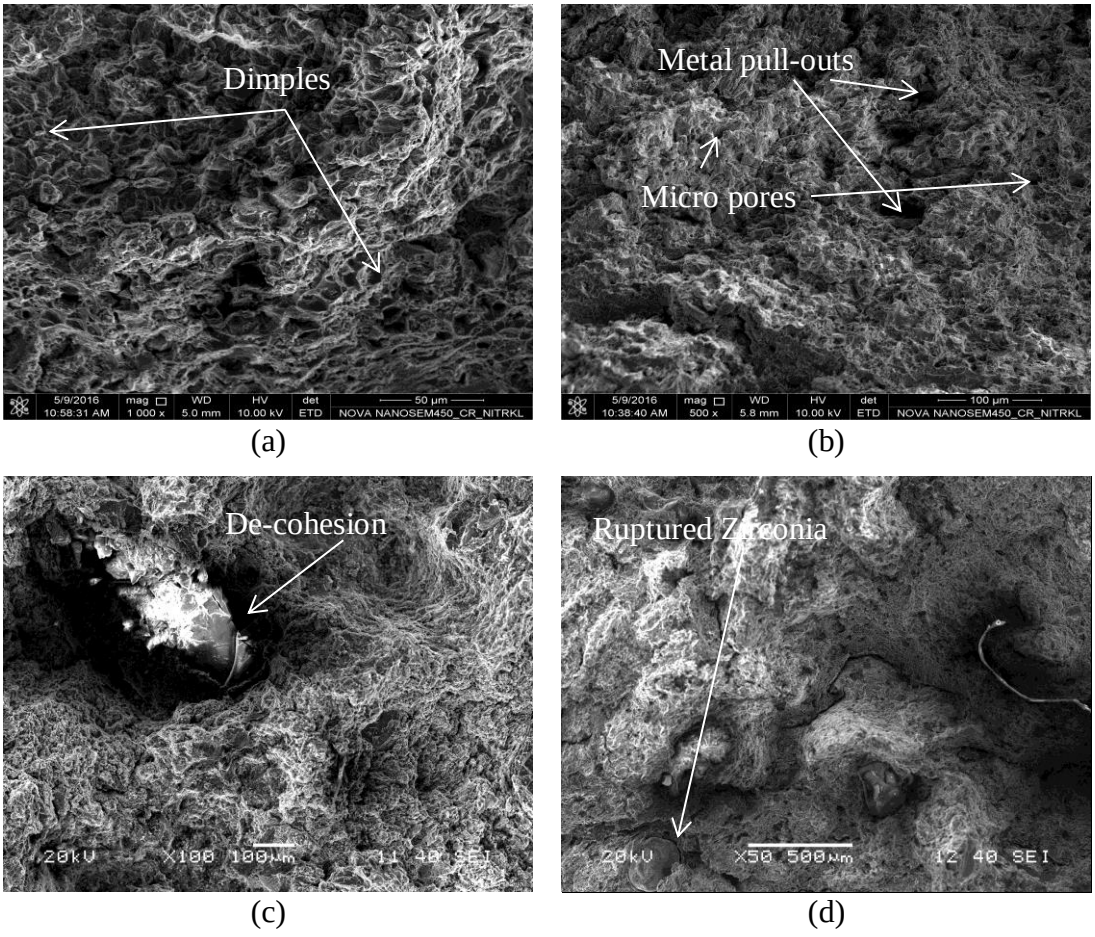

Figure 6.18 Factography of the extruded specimen (a) for sample-1(b) for sample-2 (c) for sample-3 (d) for sample-4

There exists some fine pores on the fracture surfaces. The dimple morphology present on the surface indicates the ductile mode of fracture. Moreover, the dimple size, depth and distribution decide the quality of ductile fracture. The surface also exhibits micro-void coalescence, rupture of the hard reinforced particles and de-cohesion of the matrix-particle interface [129]. Cracking of the ZrO_2 particle and the formation of the oxide around the particle surface causes weak cohesion bonding is apparent in the figure beneath that causes the initiation of fracture.

6.4.4.4 Wear test

Aluminium MMCs are used in the automotive industries and emerging as a promising friction resistive materials. Commonly the MMCs used in the breaking systems need to be investigated deeply about its resistances againest different variables [130]. Considering the aforementioned three variables with three levels, an orthogonal array (

Table 6.6) has been designed for experimentation of extruded and sintered samples. The variation of wear rates of sintered, as well as extruded specimen for four types of composites, are presented in Figure 6.19, Figure 6.20, Figure 6.20 and Figure 6.21. Mass loss of the pin was estimated from the recorded mass of the sample before and after wear test. The mass loss the test is defined as follows:

$$\Delta w = (w_a - w_b) \tag{6.8}$$

where w_a and w_b are the mass of the sample before and after the test respectively.

Table 6.6 L9 orthogonal array for wear test

Run	Load (N)	Track Dia (mm)	RPM of counter disc
1	20	50	200
2	20	70	400
3	20	90	600
4	40	50	400
5	40	70	600
6	40	90	200
7	60	50	600
8	60	70	200
9	60	90	400

The volume loss of the AMCs is estimated as follows:

$$\text{Volume loss } (mm^3) = \text{Mass loss } (g) / \text{Density } (g/mm^3) \quad (6.9)$$

The volumetric wear rate W_r (mm^3/Km) was estimated by following the relation

W_r = Volume loss (mm^3) / Sliding distance (Km)

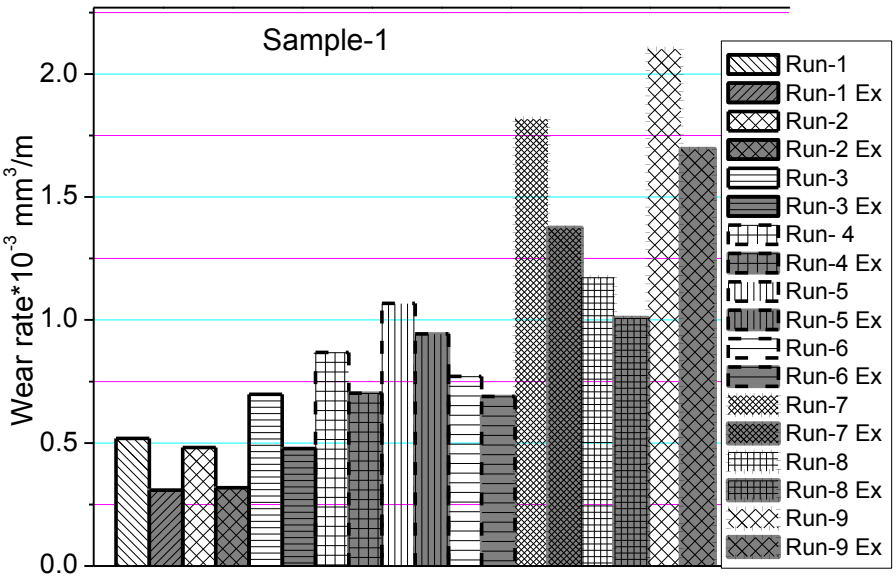

Figure 6.19: Wear rate for sample type-1

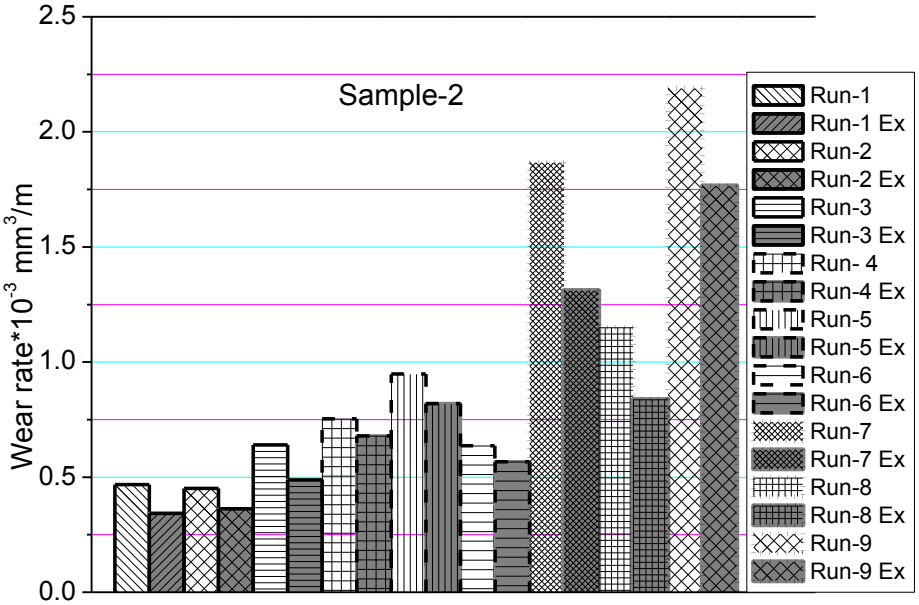

Figure 6.20: Wear rate for sample type-2

It was found that a steady state wear regime was observed after a certain time period as wear increased linearly with distance. Due to the addition of hard reinforcements the

average bulk hardness of the AMCs increases which has a significant impact on the wear resistance. Increased sliding velocity and increased applied load causes increased wear rate which was observed from the figures.

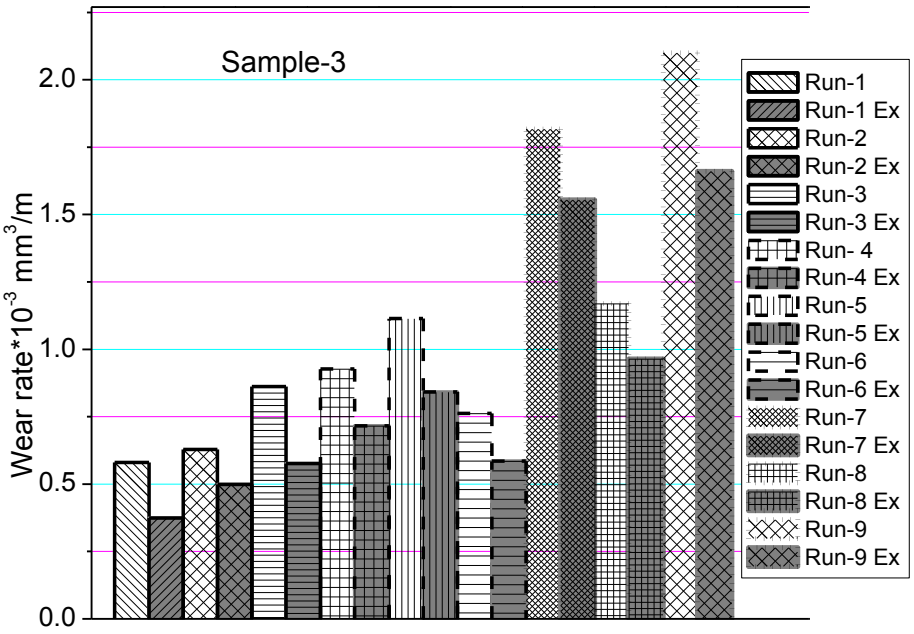

Figure 6.21: Wear rate for sample type-3

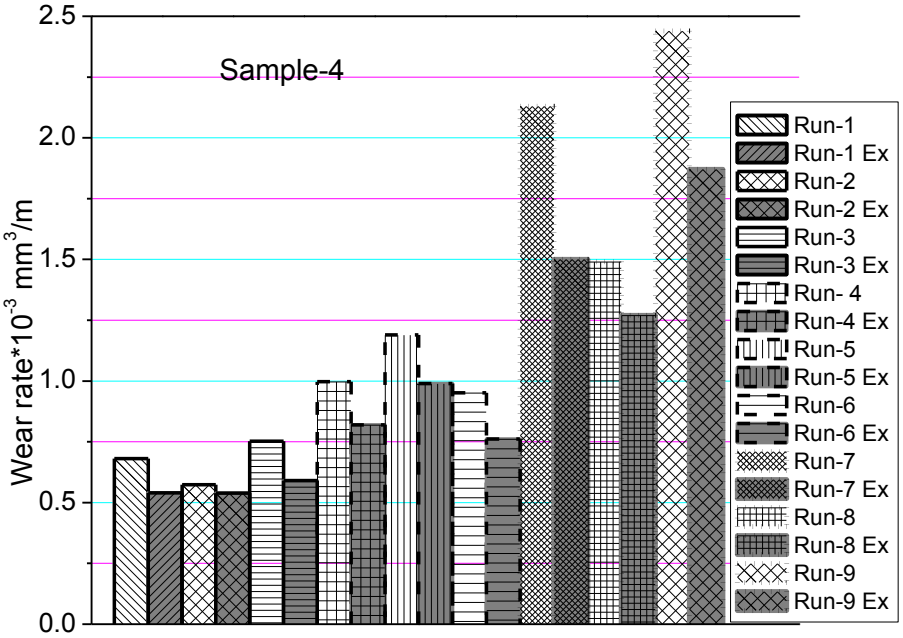

Figure 6.22: Wear rate for sample type-4

The reduction in ductility is due to the presence of hard phase of reinforcements that is responsible for the localised crack initiation and increased embrittlement effect on the composite due to local stress concentration at the interface between reinforcement and matrix

material. The reinforcements also act as load bearing agents which oppose adhesion and plastic deformation at the initial stage but after the crack formation, along with the contacted boundary matrix elements get dislodged and form creators.

After thermo-mechanical treatment of the composite, there is a significant amount of decrease in porosity and increase in hardness. Several researchers have reported the direct proportionality relation of hardness with wear resistance. The bond strength between matrix and reinforcement material improves after extrusion which improves wear resistance. It also avoids three body abrasive wear [131]. For sample type 4 the size of the reinforcement ZrO_2 is larger compared to other reinforcements so the particles got cracked at high pressure and relative sliding velocity condition. Hence a higher wear rate is observed. Among the four types of specimen type 1 and type 2 possess better wear resistance. Addition of Zn causes a semi-liquid phase sintering at the temperature of 590℃

6.4.4.5 Wear microscopy

High magnification FESEM images of the worn surfaces of the sample at two different runs (run-2 and run-7) before and after extrusion condition are shown in Figure 6.23. Run-2 is the case for lower loading and sliding velocity condition whereas, Run-7 constitutes with higher loading and sliding velocity.

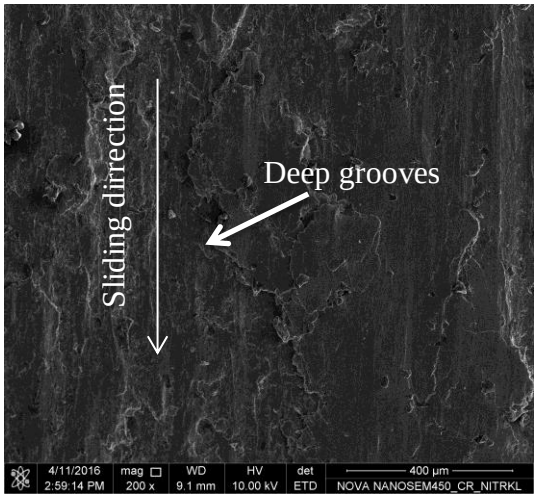

(a) S_1 run 2

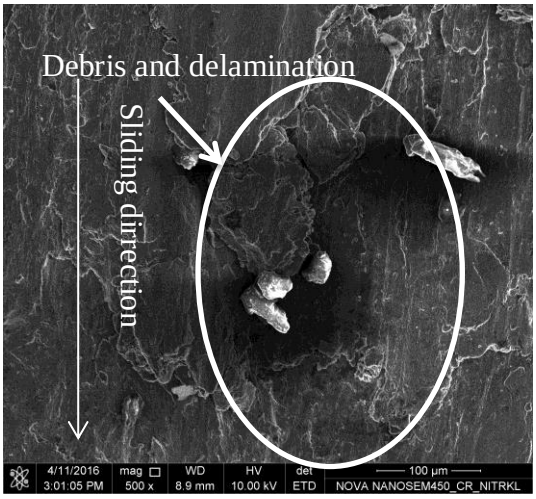

(b) S_1 run7

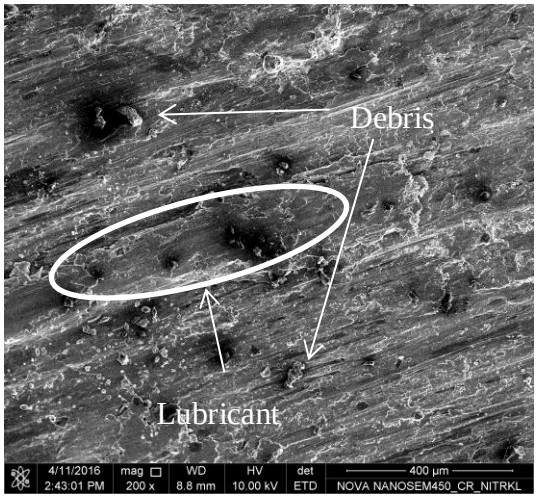

(c) S_1 extruded run-2

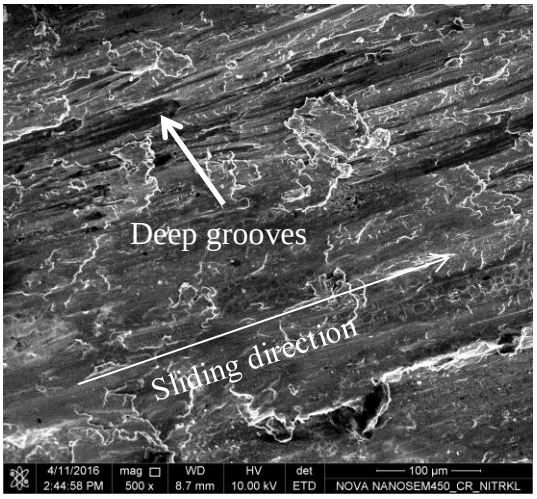

(d) S_1 extruded run-7

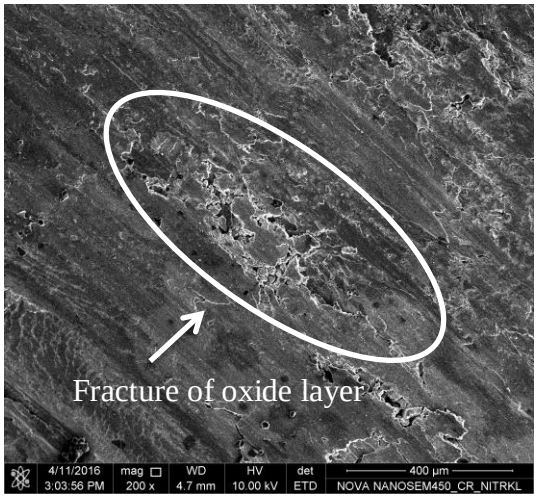

(e) S_2 run-2

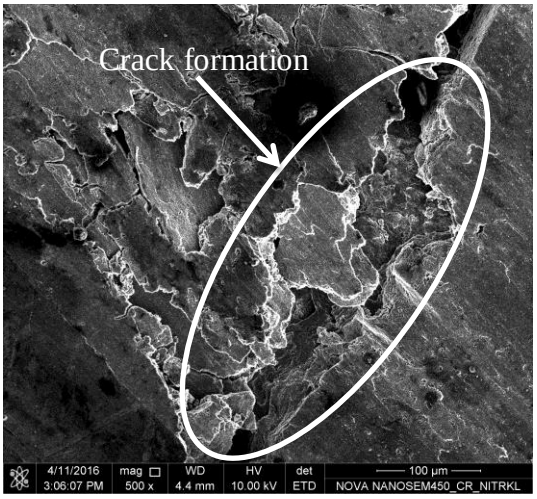

(f) S_2 run-7

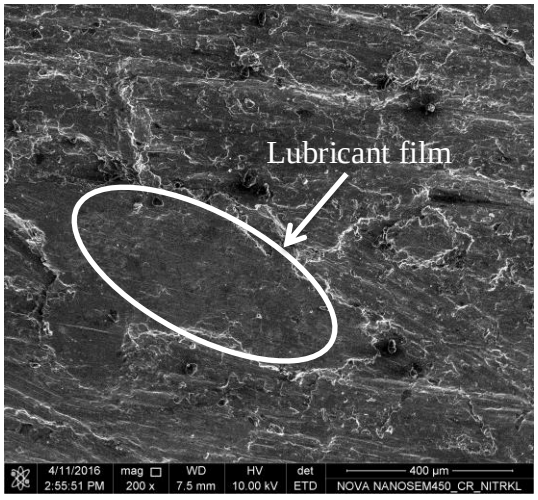

(g) S_2 extruded run-2

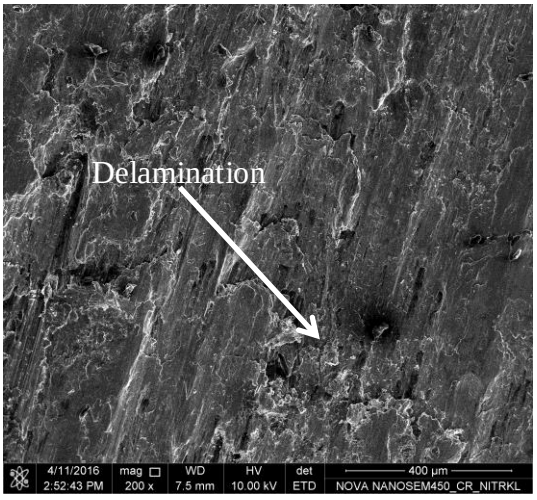

(h) S_2 extruded run-7

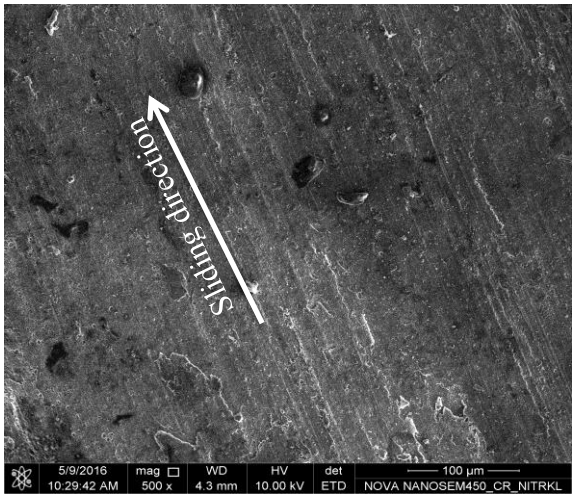

(i) S_3 run 2

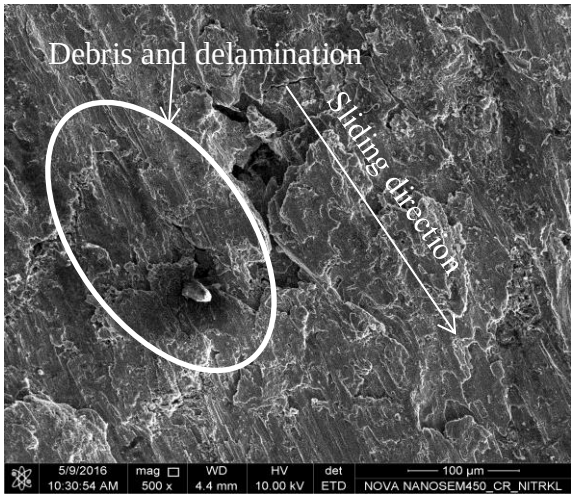

(j) S_3 run7

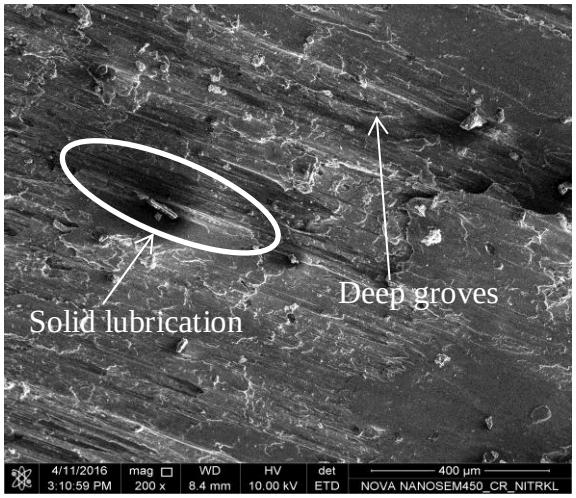

(k) S_3 extruded, run-2

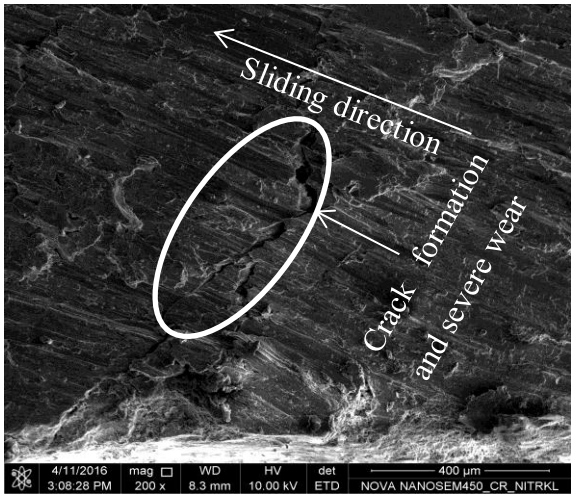

(l) S_3 extruded, run-7

(m) S_4 run-2

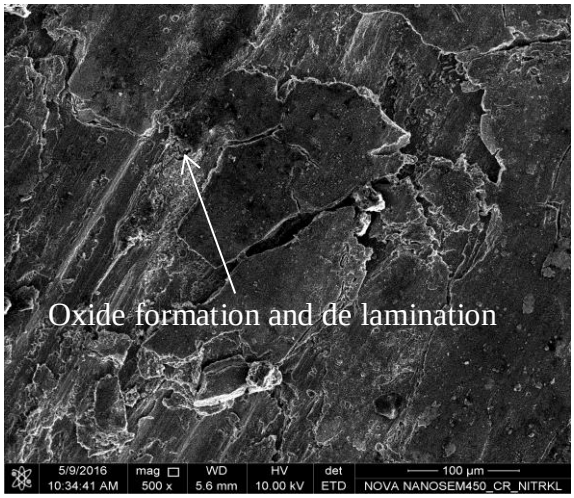

(n) S_4 run-7

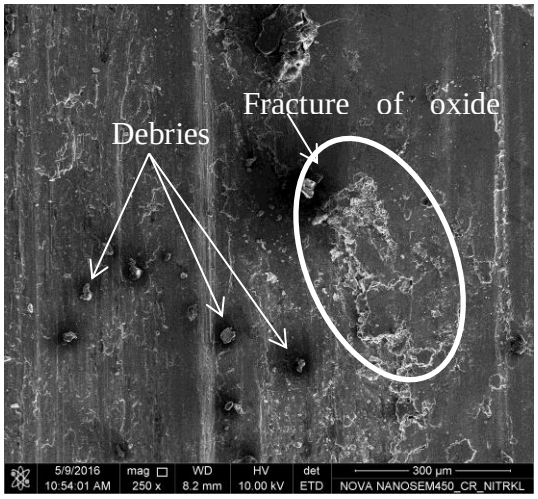

(o) S_4 extruded, run-2

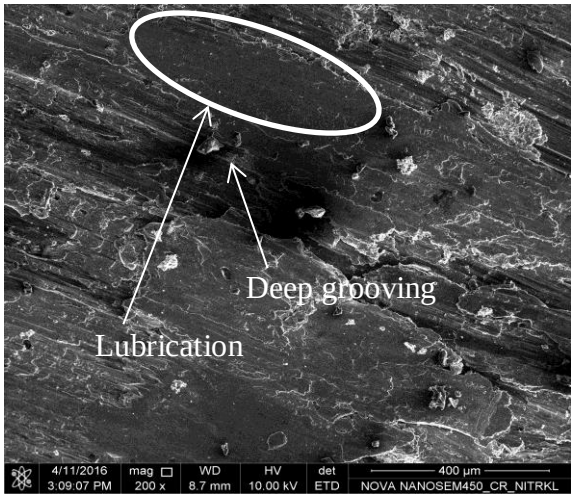

(p) S_4 extruded, run-7

Figure 6.23: FESEM immages of the worn surfaces

At very high loading and high-velocity condition delamination and combination of abrasion, delamination and adhesion mechanism of wear came into the picture. Due to frequent repetitive sliding behaviour subsurface crack has been induced due to the fatigue failure of the pin. These subsurface cracks grow with increasing travel distance and eventually shear deformation occur to the surface. Moreover at the adverse conditions melting, thermal softening and adhesion takes the predominant role to cause plastic deformation. In the case of AMCs, the mechanism of wear is less severe than the base metal alloys. Metal/graphite composite forms a lubricating layer on the tribosurface due to the shearing of graphite particles which prevents the metal to metal contact that causes the reduction of friction and wear.

In case of lower loading conditions the harder ceramic particles causes the wear of the counter surface and the asperities in between contact surface plough and cut into the pin material. The images showing a large amount of white particles present at the tribosurface which can be attributed to oxidation of the surface due to frictional heating as aluminium surface is highly prone to oxide. In case of AMCs the mechanism of wear is less severe than the base metal alloys.

6.4.4.6 Load requirement

The average Load-stroke plot for extrusion of four types of specimen is presented in Figure 6.24. Load required for extrusion of PM sample reinforced with ceramic particles are maximum, whereas for the samples having metal reinforcement are minimum. Effect of zinc on the maximum load requirement is clear in the above figure. Due to the low glass transition temperature (575℃) of soda-lime-silica glass, it also deforms along the extrusion direction.

Ceramic particle reinforced composites require more load for the deformation due to its decreased ductility and improved hardness. The reinforced particles also restricts inter boundary slip and causes sticking effect.

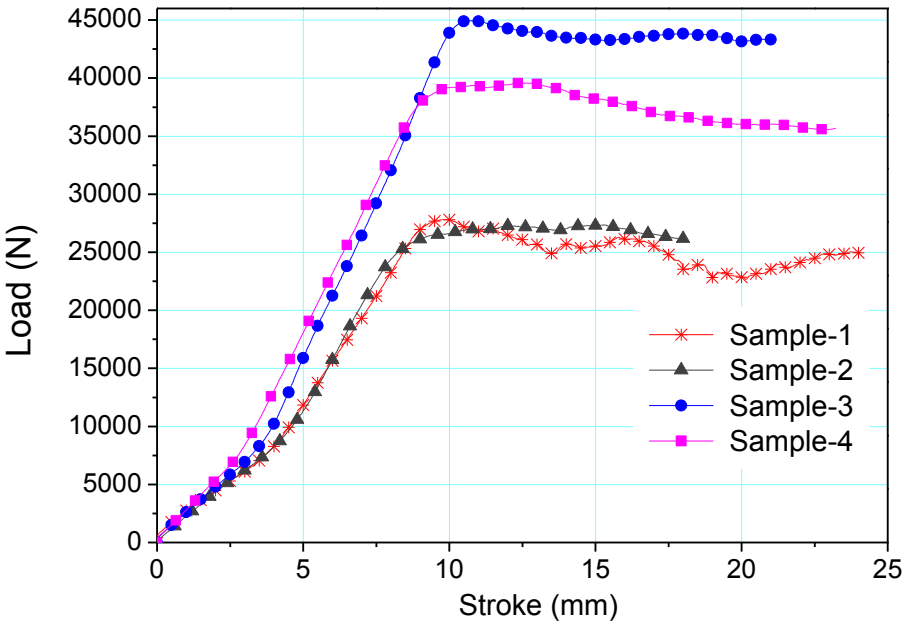

Figure 6.24: Variation of load w.r.t stroke

6.5 Conclusions

Effect of extrusion on the improvement of the mechanical and tribological properties of the AMCs was investigated. The results of this investigation are summarised as follows:

- Significant improvement of mechanical properties of all of the AMCs is observed which can be attributed to improved bond strength and grain refinement after extrusion through mathematically contoured cosine profiled die.
- The minimal product defects (few cracks at the corner zone and fine pores) in the extruded samples are observed, which support the improvement of flexural strength and tribological properties. The wear rate of the extruded specimen is lesser compared to the sintered specimen for each trial.
- Shearing of the homogeneously dispersed graphite particles at the tribosurface acts as a lubricant. So the addition of graphite particle improves the wear resistance by compromising with little amount of hardness.
- Influence of sliding speed on wear rate at less loading conditions is profound whereas at higher loading conditions it reduces the co-efficient of friction. So the rate of rise of wear rate decreases comparably.

- At higher loading and sliding velocity condition a mixed type of wear mechanism (oxidative, delamination, adhesive and abrasion) takes place. But oxidative and delamination is the predominating wear mechanism found on the surface for this investigation

Chapter 7

Closure

7.1 Concluding remarks

Due to huge demand for production of aluminium extrusion, there is a strong desire to minimise the expences associated with the production. The two major areas like tooling cost and processing cost need to be concentrated equally on improving the efficiency of manufacturing. The cost reduction can be achieved by avoiding the trial experiments, using the optimised tooling setups and using most favourable process parameters. In this dissertation a finite element model has been utilised for investigating the influence of process parameters to decide the optimum setup. The mathematical contoured die profiles were analysed for achieving the favourable flow conditions. The improved billet material type (PM composites) was also investigated by extruding them by using the optimum setups.

In the previous chapters, the aforementioned investigations were reported. This chapter contributes the description of the summary of the research, conclusion and future scope of the present research.

7.2 Contributions of the thesis

The contributions of the present work are reported as follows:

- The first and foremost contribution to the present work is to study the effect of the variable process parameters for the square to square extrusion of Al-6XXX by FEA, which supports to avoid the trial experiments for the prediction. A comparative analysis between linear converging die, cosine die and shear die profile is also performed.
- Finite Element tool was utilised to study the effect of the process parameters involved with round to square shape extrusion of Al-6XXX. The precess was validated with experimentation.
- For investigating the effect of die profile, three-dimensional solid dies following cosine, linear converging, elliptic, hyperbolic and 3^{rd} order polynomial laws has been developed for the FEA investigation. The best-suited die is manufactured indigenously to validate the simulated results

- The extruded product quality can be ameliorated by improving the billet material properties by producing it through powder metallurgy route and extruding it by following the optimum combinational setups. Extrusion of aluminium based MMC has been performed through the optimal combinational setup and the improvement is studied.

7.3 Conclusions

The results incurred from the series of finite element simulations and experimental investigations in the previous chapters are presented as follows:

- The simulation results obtained by DEFORM-3D are in good agreement with experimental outcomes. So it can be accepted as a good predictor before final production.
- Effect of ram velocity which directly influence the strain rate, in the case of cold extrusion is very less, but it is not negligible. In the case of shear faced die due to higher ram velocity, the temperature generation becomes maximum compared to other dies that directly affects the product quality.
- Cosine dies require less load for the extrusion operation of AA-6063 at room temperature condition compared to linear converging and shear faced die profile for square to square extrusion condition. At an optimum die length, maximum load required for extrusion by cosine die is 3-5% less than linear converging die.
- Load requirement improves with the increase of extrusion ratio logarithmically. At higher extrusion ratios, cosine die with optimum die length is more preferable than the linear converging profile.
- Friction and die profile bears the principal role for velocity relative difference of metal flow at die exit for which cosine profiled die with minimum friction condition is the best recommendation.
- There is a significant effect of punch shape on the flow behaviour of metal inside the container, conical and inner cone punch creates two different types of flow inside the container chamber which counteracts and favours frictional effect respectively. The volume of metal deformed per stroke varies up to the commencement of extrusion that is why the slope to achieve the peak load varies by using various types of punch.
- A new method to obtain different types of mathematically contoured round to square extrusion die profiles, following cosine, linear converging, hyperbolic, elliptic and 3rd order polynomial laws, have been developed successfully. Effective-strain rate, as well as effective-strain at die entry and exit, was found less in the case of extrusion through

cosine profiled die. The redundant work is less so comparatively less energy consumption and product defects in the process.

- Significant improvement of mechanical properties of all of the AMCs observed, which can be attributed to improved bond strength and grain refinement after extrusion through mathematically contoured cosine profiled die.
- It was found that minimal product defects were observed (few cracks at the corner zone and fine pores) in the extruded product, which supported the improvement of flexural strength and tribological properties. The wear rate of the extruded specimen was less compared to the sintered specimen for each trial.
- Shearing of the homogeneously dispersed graphite particles at the tribosurface acts as a lubricant. So the addition of graphite particle improves the wear resistance by compromising with minimum amount of hardness.
- At higher loading and sliding velocity condition a mixed type of wear mechanism (oxidative, delamination, adhesive and abrasion) takes place. But oxidation and delamination is the predominating wear mechanism found on the surface for this investigation.

7.4 Future scope of the work

- In this thesis, the analysis was performed for the simple bar extrusion. For the similar investigations, the complex shapes can be focused .
- The die profile design for the simple bar extrusion process was successful. The design methodology can be extended for the complex shape extrusion.
- Finite element analysis was performed to investigate the effect of various state variables, but the analysis can be increased to the microstructural changes due to the variables.
- The extrusion process can be investigated by employing ultrasonic vibrations for minimising the load requirements and improving the product quality.
- For improving the product quality, different kinds of twist extrusions can be performed to have a significant change in the microstructural level.

References

[1] W. S. Miller, L. Zhuang, J. Bottema, A. J. Wittebrood, P. De Smet, A. Haszler, *et al.*, "Recent development in aluminium alloys for the automotive industry," *Materials Science and Engineering: A*, vol. 280, pp. 37-49, 3/15/ 2000.

[2] A. Heinz, A. Haszler, C. Keidel, S. Moldenhauer, R. Benedictus, and W. S. Miller, "Recent development in aluminium alloys for aerospace applications," *Materials Science and Engineering: A*, vol. 280, pp. 102-107, 3/15/ 2000.

[3] T. Altan, S.-I. Oh, and G. Gegel, "Metal forming fundamentals and applications," *American Society for Metals, 1983*, p. 353, 1983.

[4] M. Bauser and K. Siegert, *Extrusion: Second Edition*: ASM International, 2006.

[5] C. Zhang, G. Zhao, H. Chen, Y. Guan, and F. Kou, "Numerical simulation and metal flow analysis of hot extrusion process for a complex hollow aluminum profile," *The International Journal of Advanced Manufacturing Technology*, vol. 60, pp. 101-110, 2012.

[6] H. Zhao, H.-n. Wang, M.-j. Wang, and G.-y. Li, "Simulation of extrusion process of complicated aluminium profile and die trial," *Transactions of Nonferrous Metals Society of China*, vol. 22, pp. 1732-1737, 2012.

[7] C. Labergere, P. Lestriez, K. Saanouni, and A. Rassineux, "Numerical simulation of bursting in extrusion process using finite viscoplasticity with ductile damage and thermal effects," *International Journal of Material Forming*, vol. 2, pp. 89-92, 2009/08/01 2009.

[8] M. Ketabchi, H. Mohammadi, and M. Izadi, "Finite-element simulation and experimental investigation of isothermal backward extrusion of 7075 Al alloy," *Arabian Journal for Science and Engineering*, vol. 37, pp. 2287-2296, 2012.

[9] T. Chanda, J. Zhou, and J. Duszczyk, "FEM analysis of aluminium extrusion through square and round dies," *Materials & Design*, vol. 21, pp. 323-335, 2000.

[10] F. Li, J. Lin, S. Yuan, and X. Liu, "Effect of inner cone punch on metal flow in extrusion process," *The International Journal of Advanced Manufacturing Technology*, vol. 42, pp. 489-496, 2009.

[11] J. Lof, *Developments in finite element simulations of aluminium extrusion*, 2000.

[12] T. Sheppard, *Extrusion of aluminium alloys*: Springer Science & Business Media, 2013.

[13] D.-C. Chen, S.-K. Syu, C.-H. Wu, and S.-K. Lin, "Investigation into cold extrusion of aluminum billets using three-dimensional finite element method," *Journal of Materials Processing Technology*, vol. 192–193, pp. 188-193, 10/1/ 2007.

[14] D.-C. Chen, S.-K. Syu, C.-H. Wu, and S.-K. Lin, "Investigation into cold extrusion of aluminum billets using three-dimensional finite element method," *Journal of materials processing technology*, vol. 192, pp. 188-193, 2007.

[15] S. Syahrullail, C. Azwadi, and Y. Najib, "The influences of the die half angle of taper die during cold extrusion process," *Arabian Journal for Science and Engineering*, vol. 38, pp. 1201-1207, 2013.

[16] P. Karami and K. Abrinia, "An analytical formulation as an alternative to FEM software giving strain and stress distributions for the three-dimensional solution of extrusion problems," *The International Journal of Advanced Manufacturing Technology*, vol. 71, pp. 653-665, 2014.

[17] O. Gbenebor, O. Fayomi, A. Popoola, A. Inegbenebor, and F. Oyawale, "Extrusion die geometry effects on the energy absorbing properties and deformation response of 6063-type Al–Mg–Si aluminum alloy," *Results in Physics,* vol. 3, pp. 1-6, 2013.

[18] A. Khosravifard and R. Ebrahimi, "Investigation of parameters affecting interface strength in Al/Cu clad bimetal rod extrusion process," *Materials & Design,* vol. 31, pp. 493-499, 1// 2010.

[19] X. Ma, M. De Rooij, and D. Schipper, "Modelling of contact and friction in aluminium extrusion," *Tribology International,* vol. 43, pp. 1138-1144, 2010.

[20] L. Wang, J. Zhou, J. Duszczyk, and L. Katgerman, "Friction in aluminium extrusion—part 1: a review of friction testing techniques for aluminium extrusion," *Tribology International,* vol. 56, pp. 89-98, 2012.

[21] Q. Zhang, E. Felder, and S. Bruschi, "Evaluation of friction condition in cold forging by using T-shape compression test," *Journal of Materials Processing Technology,* vol. 209, pp. 5720-5729, 2009.

[22] Z. Chen, S. Xu, and X. Dong, "Deformation behavior of AA6063 aluminium alloy after removing friction effect under hot working conditions," *Acta Metallurgica Sinica (English Letters),* vol. 21, pp. 451-458, 2008.

[23] A. Buschhausen, K. Weinmann, J. Y. Lee, and T. Altan, "Evaluation of lubrication and friction in cold forging using a double backward-extrusion process," *Journal of materials processing technology,* vol. 33, pp. 95-108, 1992.

[24] G. Shen, A. Vedhanayagam, E. Kropp, and T. Altan, "A method for evaluating friction using a backward extrusion-type forging," *Journal of Materials Processing Technology,* vol. 33, pp. 109-123, 1992.

[25] Y.-J. Hwu, C.-T. Hsu, and F. Wang, "Measurement of friction and the flow stress of steels at room and elevated temperatures by ring-compression tests," *Journal of Materials Processing Technology,* vol. 37, pp. 319-335, 1993/02/01 1993.

[26] A. T. Male, "A method for the determination of the coefficient of friction of metals under conditions of bulk plastic deformation," *J. Inst. Metal.,* vol. 93, pp. 38-46, 1964.

[27] R. S. Hartley, T. J. Cloete, and G. N. Nurick, "An experimental assessment of friction effects in the split Hopkinson pressure bar using the ring compression test," *International Journal of Impact Engineering,* vol. 34, pp. 1705-1728, 10// 2007.

[28] S. Orangi, K. Abrinia, and R. Bihamta, "Process Parameter Investigations of Backward Extrusion for Various Aluminum Shaped Section Tubes Using FEM Analysis," *Journal of Materials Engineering and Performance,* vol. 20, pp. 40-47, 2011// 2011.

[29] L. Wang and H. Yang, "Friction in aluminium extrusion—part 2: A review of friction models for aluminium extrusion," *Tribology International,* vol. 56, pp. 99-106, 2012.

[30] X. Ma, M. de Rooij, and D. Schipper, "Friction conditions in the bearing area of an aluminium extrusion process," *Wear,* vol. 278, pp. 1-8, 2012.

[31] A. Farhoumand and R. Ebrahimi, "Analysis of forward–backward-radial extrusion process," *Materials & Design,* vol. 30, pp. 2152-2157, 6// 2009.

[32] M. Bakhshi-Jooybari, "A theoretical and experimental study of friction in metal forming by the use of the forward extrusion process," *Journal of Materials Processing Technology,* vol. 125–126, pp. 369-374, 9/9/ 2002.

[33] L. R. Allen, "Process for the extrusion of fine wire," ed: Google Patents, 1964.

[34] R. Ebrahimi and A. Najafizadeh, "A new method for evaluation of friction in bulk metal forming," *Journal of Materials Processing Technology,* vol. 152, pp. 136-143, 10/20/ 2004.

[35] W. Evans and B. Avitzur, "Measurement of friction in drawing, extrusion, and rolling," *Journal of Lubrication Technology,* vol. 90, pp. 72-80, 1968.

[36] H. S. Valberg, *Applied metal forming: including FEM analysis*: Cambridge University Press, 2010.

[37] S. Bikass, B. Andersson, and A. Pilipenko, "Simulation of distortion due to non-uniform cooling in aluminium extrusion process," *International Journal of Material Forming,* vol. 3, pp. 813-816, 2010/04/01 2010.

[38] M.-j. Wang, Z. He, X.-x. Wu, C.-w. Li, and G.-y. Li, "Deformation simulation of low-temperature high-speed extrusion for 6063 Al alloy," *Journal of Central South University of Technology,* vol. 17, pp. 881-887, 2010.

[39] L.-x. Li, J. Zhou, and J. Duszczyk, "Prediction of temperature evolution during the extrusion of 7075 aluminium alloy at various ram speeds by means of 3D FEM simulation," *Journal of Materials Processing Technology,* vol. 145, pp. 360-370, 2004.

[40] L. Chen, G. Zhao, J. Yu, and W. Zhang, "Constitutive analysis of homogenized 7005 aluminum alloy at evaluated temperature for extrusion process," *Materials & Design,* vol. 66, pp. 129-136, 2015.

[41] Y. Zhao, B. Song, J. Pei, C. Jia, B. Li, and G. Linlin, "Effect of deformation speed on the microstructure and mechanical properties of AA6063 during continuous extrusion process," *Journal of Materials Processing Technology,* vol. 213, pp. 1855-1863, 2013.

[42] G. Liu, J. Zhou, and J. Duszczyk, "Predicting the variation of the exit temperature with the initial billet temperature during extrusion to produce an AZ31 profile," *International Journal of Material Forming,* vol. 2, pp. 113-119, 2009// 2009.

[43] T. Sheppard, "Temperature and speed effects in hot extrusion of aluminium alloys," *Metals Technology,* vol. 8, pp. 130-141, 1981.

[44] G. Fang, J. Zhou, and J. Duszczyk, "Extrusion of 7075 aluminium alloy through double-pocket dies to manufacture a complex profile," *Journal of Materials Processing Technology,* vol. 209, pp. 3050-3059, 3/19/ 2009.

[45] N. Jin, H. Zhang, Y. Han, W. Wu, and J. Chen, "Hot deformation behavior of 7150 aluminum alloy during compression at elevated temperature," *Materials Characterization,* vol. 60, pp. 530-536, 6// 2009.

[46] R. J. Immanuel and S. K. Panigrahi, "Transformation of cast A356 ingots to wrought sheets with enhanced mechanical and tribological properties by different thermo-mechanical processing routes," *Materials & Design,* vol. 101, pp. 44-55, 7/5/ 2016.

[47] K. Maity, P. Kar, and N. Das, "A class of upper-bound solutions for the extrusion of square shapes from square billets through curved dies," *Journal of materials processing technology,* vol. 62, pp. 185-190, 1996.

[48] K. P. Maity, A. K. Rout, and K. Majhi, "Computer-Aided Simulation of Metal Flow through Curved Die for Extrusion of Square Section from Square Billet," *Key Engineering Materials,* vol. 424, pp. 181-188, 2010.

[49] R. Narayanasamy, P. Srinivasan, and R. Venkatesan, "Computer aided design and manufacture of streamlined extrusion dies," *Journal of materials processing technology,* vol. 138, pp. 262-264, 2003.

[50] A. K. Rout and K. Maity, "Numerical and experimental study on the three-dimensional extrusion of square section from square billet through a polynomial shaped curved die," *The International Journal of Advanced Manufacturing Technology,* vol. 54, pp. 495-506, 2011.

[51] P. Ulysse, "Optimal extrusion die design to achieve flow balance," *International journal of machine tools and manufacture,* vol. 39, pp. 1047-1064, 1999.

[52] W. Xutang, J. Qijian, and X. Shueisheing, "Elasto-Plastic Finite Element Analysis of Hydrostatic Extrusion with Various Mathematically Contoured Dies," in *Proceedings of the Twenty-Fourth International Machine Tool Design and Research Conference*, B. J. Davies, Ed., ed London: Macmillan Education UK, 1984, pp. 51-57.

[53] C. Zhang, G. Zhao, H. Chen, Y. Guan, and H. Li, "Optimization of an aluminum profile extrusion process based on Taguchi's method with S/N analysis," *The International Journal of Advanced Manufacturing Technology,* vol. 60, pp. 589-599, 2012.

[54] M. F. Erinosho, S. O. Ojo, J. S. Ajiboye, and E. T. Akinlabi, "Effect of punch diameters on shear extrusion of 6063 aluminium alloy," 2015.

[55] F. Halvorsen and T. Aukrust, "Studies of the mechanisms for buckling and waving in aluminum extrusion by use of a Lagrangian FEM software," *International Journal of Plasticity,* vol. 22, pp. 158-173, 1// 2006.

[56] T. Altan, S. I. Oh, and H. L. Gegel, *Metal forming: fundamentals and applications*: American Society for Metals, 1983.

[57] T. Sheppard, *Extrusion of Aluminium Alloys*: Springer, 1999.

[58] C. Zhang, G. Zhao, Z. Chen, H. Chen, and F. Kou, "Effect of extrusion stem speed on extrusion process for a hollow aluminum profile," *Materials Science and Engineering: B,* vol. 177, pp. 1691-1697, 2012.

[59] C. Venkatesh and R. Venkatesan, "Design and analysis of optimal die profile for the extrusion of round SiC DRMM Al 6061 composite billet into hexagonal section," *Journal of the Brazilian Society of Mechanical Sciences and Engineering,* vol. 37, pp. 1687-1700, 2015// 2015.

[60] R. Narayanasamy, R. Ponalagusamy, R. Venkatesan, and P. Srinivasan, "An upper bound solution to extrusion of circular billet to circular shape through cosine dies," *Materials & design,* vol. 27, pp. 411-415, 2006.

[61] R. Ponalagusamy, R. Narayanasamy, and P. Srinivasan, "Design and development of streamlined extrusion dies a Bezier curve approach," *Journal of Materials Processing Technology,* vol. 161, pp. 375-380, 2005.

[62] R. Ponalagusamy, R. Narayanasamy, R. Venkatesan, and S. Senthilkumar, "Computer-aided metal flow investigation in streamlined extrusion dies," *Materials & Design,* vol. 29, pp. 1228-1239, 2008.

[63] W. Gordon, C. Van Tyne, and Y. Moon, "Overview of adaptable die design for extrusions," *Journal of materials processing technology,* vol. 187, pp. 662-667, 2007.

[64] A. Farjad Bastani, T. Aukrust, and S. Brandal, "Optimisation of flow balance and isothermal extrusion of aluminium using finite-element simulations," *Journal of Materials Processing Technology,* vol. 211, pp. 650-667, 2011.

[65] N. H. Kim, C. G. Kang, and B. M. Kim, "Die design optimization for axisymmetric hot extrusion of metal matrix composites," *International Journal of Mechanical Sciences,* vol. 43, pp. 1507-1520, 6// 2001.

[66] S. K. Lee, D. C. Ko, and B. M. Kim, "Optimal die profile design for uniform microstructure in hot extruded product," *International Journal of Machine Tools and Manufacture,* vol. 40, pp. 1457-1478, 8// 2000.

[67] M. Noorani-Azad, M. Bakhshi-Jooybari, S. J. Hosseinipour, and A. Gorji, "Experimental and numerical study of optimal die profile in cold forward rod extrusion of aluminum," *Journal of Materials Processing Technology,* vol. 164–165, pp. 1572-1577, 5/15/ 2005.

[68] M. Saboori, M. Bakhshi-Jooybari, M. Noorani-Azad, and A. Gorji, "Experimental and numerical study of energy consumption in forward and backward rod extrusion," *Journal of Materials Processing Technology*, vol. 177, pp. 612-616, 7/3/ 2006.

[69] M. Bakhshi-Jooybari, M. Saboori, M. Noorani-Azad, and S. J. Hosseinipour, "Combined upper bound and slab method, finite element and experimental study of optimal die profile in extrusion," *Materials & Design*, vol. 28, pp. 1812-1818, // 2007.

[70] C. Lin and R. S. Ransing, "An innovative extrusion die layout design approach for single-hole dies," *Journal of Materials Processing Technology*, vol. 209, pp. 3416-3425, 4/1/ 2009.

[71] G.-A. Lee, D.-Y. Kwak, S.-Y. Kim, and Y.-T. Im, "Analysis and design of flat-die hot extrusion process 1. Three-dimensional finite element analysis," *International Journal of Mechanical Sciences*, vol. 44, pp. 915-934, 5// 2002.

[72] K. H. Min, S. P. Kang, D.-G. Kim, and Y. D. Kim, "Sintering characteristic of Al2O3-reinforced 2xxx series Al composite powders," *Journal of Alloys and Compounds*, vol. 400, pp. 150-153, 9/1/ 2005.

[73] J. M. Torralba, C. E. da Costa, and F. Velasco, "PM aluminum matrix composites: an overview," *Journal of Materials Processing Technology*, vol. 133, pp. 203-206, 2/1/ 2003.

[74] F. Thummler and R. Oberacker, "Introduction to powder metallurgy," *Oxford Science Publications, 1993. 346*, 1993.

[75] J. Pickens, "Aluminium powder metallurgy technology for high-strength applications," *Journal of Materials Science*, vol. 16, pp. 1437-1457, 1981.

[76] F. L. Alves, A. Baptista, and A. Marques, "Metal and ceramic matrix composites in aerospace engineering," *Advanced Composite Materials for Aerospace Engineering: Processing, Properties and Applications*, p. 59, 2016.

[77] T.-G. Nieh, J. Wadsworth, and O. D. Sherby, *Superplasticity in metals and ceramics*: Cambridge university press, 2005.

[78] A. Mazahery and M. O. Shabani, "Application of the Extrusion to Increase the Binding between the Ceramic Particles and the Metal Matrix: Enhancement of Mechanical and Tribological Properties," *Journal of Materials Science & Technology*, vol. 29, pp. 423-428, 5// 2013.

[79] O. El-Kady and A. Fathy, "Effect of SiC particle size on the physical and mechanical properties of extruded Al matrix nanocomposites," *Materials & Design*, vol. 54, pp. 348-353, 2// 2014.

[80] T. Rajmohan, K. Palanikumar, and S. Ranganathan, "Evaluation of mechanical and wear properties of hybrid aluminium matrix composites," *Transactions of Nonferrous Metals Society of China*, vol. 23, pp. 2509-2517, 2013.

[81] M. Alizadeh and M. M. Aliabadi, "Synthesis behavior of nanocrystalline Al–Al2O3 composite during low time mechanical milling process," *Journal of Alloys and Compounds*, vol. 509, pp. 4978-4986, 4/14/ 2011.

[82] C. Nie, J. Gu, J. Liu, and D. Zhang, "Investigation on microstructures and interface character of B4C particles reinforced 2024Al matrix composites fabricated by mechanical alloying," *Journal of Alloys and Compounds*, vol. 454, pp. 118-122, 4/24/ 2008.

[83] K. Tavighi, M. Emamy, and A. R. Emami, "Effects of extrusion temperature on the microstructure and tensile properties of Al–16 wt% Al4Sr metal matrix composite," *Materials & Design*, vol. 46, pp. 598-604, 4// 2013.

[84] M. A. Jabbari Taleghani, E. M. Ruiz Navas, and J. M. Torralba, "Microstructural and mechanical characterisation of 7075 aluminium alloy consolidated from a premixed powder by cold compaction and hot extrusion," *Materials & Design*, vol. 55, pp. 674-682, 3// 2014.

[85] A. Abdollahi, A. Alizadeh, and H. R. Baharvandi, "Dry sliding tribological behavior and mechanical properties of Al2024–5 wt.%B4C nanocomposite produced by mechanical milling and hot extrusion," *Materials & Design,* vol. 55, pp. 471-481, 3// 2014.

[86] N. Soltani, H. R. Jafari Nodooshan, A. Bahrami, M. I. Pech-Canul, W. Liu, and G. Wu, "Effect of hot extrusion on wear properties of Al–15 wt.% Mg2Si in situ metal matrix composites," *Materials & Design,* vol. 53, pp. 774-781, 1// 2014.

[87] W. Schatt, E. P. M. Association, and K. P. Wieters, *Powder metallurgy: processing and materials*: European Powder Metallurgy Association, 1997.

[88] M. Adamiak, J. B. Fogagnolo, E. M. Ruiz-Navas, L. A. Dobrzañski, and J. M. Torralba, "Mechanically milled AA6061/(Ti3Al)P MMC reinforced with intermetallics – the structure and properties," *Journal of Materials Processing Technology,* vol. 155–156, pp. 2002-2006, 11/30/ 2004.

[89] D. R. Kumar, R. Narayanasamy, and C. Loganathan, "Effect of Glass and SiC in Aluminum matrix on workability and strain hardening behavior of powder metallurgy hybrid composites," *Materials & Design,* vol. 34, pp. 120-136, 2// 2012.

[90] D. R. Kumar, C. Loganathan, and R. Narayanasamy, "Effect of glass in aluminum matrix on workability and strain hardening behavior of powder metallurgy composite," *Materials & Design,* vol. 32, pp. 2413-2422, 4// 2011.

[91] Y. H. Seo and C. G. Kang, "Effects of hot extrusion through a curved die on the mechanical properties of SiCp/Al composites fabricated by melt-stirring," *Composites Science and Technology,* vol. 59, pp. 643-654, 4// 1999.

[92] L. E. G. Cambronero, E. Sánchez, J. M. Ruiz-Roman, and J. M. Ruiz-Prieto, "Mechanical characterisation of AA7015 aluminium alloy reinforced with ceramics," *Journal of Materials Processing Technology,* vol. 143–144, pp. 378-383, 12/20/ 2003.

[93] M. Rajabi, M. M. Khodai, and N. Askari, "Microwave-assisted sintering of Al–ZrO2 nano-composites," *Journal of Materials Science: Materials in Electronics,* vol. 25, pp. 4577-4584, 2014.

[94] R. Goswami, R. Sikand, A. Dhar, O. Grover, U. Jindal, and A. Gupta, "Extrusion characteristics of aluminium alloy/SiCpmetal matrix composites," *Materials science and technology,* vol. 15, pp. 443-449, 1999.

[95] C. Zhang, G. Zhao, H. Chen, Y. Guan, and H. Li, "Optimization of an aluminum profile extrusion process based on Taguchi's method with S/N analysis," *The International Journal of Advanced Manufacturing Technology,* vol. 60, pp. 589-599, 2012// 2012.

[96] C. Zhang, G. Zhao, H. Chen, Y. Guan, and F. Kou, "Numerical simulation and metal flow analysis of hot extrusion process for a complex hollow aluminum profile," *The International Journal of Advanced Manufacturing Technology,* vol. 60, pp. 101-110, 2012// 2012.

[97] D. Svyetlichnyy, J. Majta, and J. Nowak, "A flow stress for the deformation under varying condition—internal and state variable models," *Materials Science and Engineering: A,* vol. 576, pp. 140-148, 2013.

[98] A. Mihelič and B. Stok, "Tool design optimization in extrusion processes," *Computers & structures,* vol. 68, pp. 283-293, 1998.

[99] G. Li, J. T. Jinn, W. T. Wu, and S. I. Oh, "Recent development and applications of three-dimensional finite element modeling in bulk forming processes," *Journal of Materials Processing Technology,* vol. 113, pp. 40-45, 6/15/ 2001.

[100] J. Zhou, L. Li, and J. Duszczyk, "3D FEM simulation of the whole cycle of aluminium extrusion throughout the transient state and the steady state using the updated Lagrangian approach," *Journal of Materials Processing Technology,* vol. 134, pp. 383-397, 3/20/ 2003.

[101] L. Li, J. Zhou, and J. Duszczyk, "Prediction of temperature evolution during the extrusion of 7075 aluminium alloy at various ram speeds by means of 3D FEM simulation," *Journal of Materials Processing Technology,* vol. 145, pp. 360-370, 2/1/ 2004.

[102] G. Fang, J. Zhou, and J. Duszczyk, "FEM simulation of aluminium extrusion through two-hole multi-step pocket dies," *Journal of Materials Processing Technology,* vol. 209, pp. 1891-1900, 2/19/ 2009.

[103] L. Peng, F. Liu, J. Ni, and X. Lai, "Size effects in thin sheet metal forming and its elastic–plastic constitutive model," *Materials & Design,* vol. 28, pp. 1731-1736, // 2007.

[104] C. Zhang, G. Zhao, H. Chen, Y. Guan, and F. Kou, "Numerical simulation and metal flow analysis of hot extrusion process for a complex hollow aluminum profile," *The International Journal of Advanced Manufacturing Technology,* vol. 60, pp. 101-110, 2011// 2011.

[105] N. Biba, S. Stebounov, and A. Lishiny, "Cost effective implementation of forging simulation," *Journal of Materials Processing Technology,* vol. 113, pp. 34-39, 6/15/ 2001.

[106] Z. Hu, L. Zhu, B. Wang, Z. Liu, Y. Miao, P. Xie, *et al.*, "Computer simulation of the deep extrusion of a thin-walled cup using the thermo-mechanically coupled elasto-plastic FEM," *Journal of Materials Processing Technology,* vol. 102, pp. 128-137, 5/15/ 2000.

[107] J. Lof and Y. Blokhuis, "FEM simulations of the extrusion of complex thin-walled aluminium sections," *Journal of Materials Processing Technology,* vol. 122, pp. 344-354, 3/28/ 2002.

[108] X. Duan, X. Velay, and T. Sheppard, "Application of finite element method in the hot extrusion of aluminium alloys," *Materials Science and Engineering: A,* vol. 369, pp. 66-75, 3/25/ 2004.

[109] M. Noorani-Azad, M. Bakhshi-Jooybari, S. Hosseinipour, and A. Gorji, "Experimental and numerical study of optimal die profile in cold forward rod extrusion of aluminum," *Journal of materials processing technology,* vol. 164, pp. 1572-1577, 2005.

[110] A. Khosravifard, M. Jahedi, and A. H. Yaghtin, "Three dimensional finite element study on torsion extrusion processing of 1050 aluminum alloy," *Transactions of Nonferrous Metals Society of China,* vol. 22, pp. 2771-2776, 2012.

[111] Y. Meng, J. Cui, Z. Zhao, and Y. Zuo, "Effect of vanadium on the microstructures and mechanical properties of an Al–Mg–Si–Cu–Cr–Ti alloy of 6XXX series," *Journal of Alloys and Compounds,* vol. 573, pp. 102-111, 2013.

[112] L. Cambronero, E. Sanchez, J. Ruiz-Roman, and J. Ruiz-Prieto, "Mechanical characterisation of AA7015 aluminium alloy reinforced with ceramics," *Journal of Materials Processing Technology,* vol. 143, pp. 378-383, 2003.

[113] K. Tavighi, M. Emamy, and A. Emami, "Effects of extrusion temperature on the microstructure and tensile properties of Al–16wt% Al< sub> 4</sub> Sr metal matrix composite," *Materials & Design,* vol. 46, pp. 598-604, 2013.

[114] H.-P. Liermann, S. Merkel, L. Miyagi, H.-R. Wenk, G. Shen, H. Cynn, *et al.*, "Experimental method for in situ determination of material textures at simultaneous high pressure and high temperature by means of radial diffraction in the diamond anvil cell," *Review of scientific instruments,* vol. 80, p. 104501, 2009.

[115] I. Flitta and T. Sheppard, "Nature of friction in extrusion process and its effect on material flow," *Materials science and technology,* vol. 19, pp. 837-846, 2003.

[116] T. Sundararajan and G. Lai, "Viscoplastic Deformation Analysis and Extrusion Die Design by FEM," *Transactions,* vol. 37, p. 3, 1991.

[117] C. Venkatesh and R. Venkatesan, "Design and analysis of streamlined extrusion die for round to hexagon using area mapping technique, upper bound technique and finite element method," *Journal of Mechanical Science and Technology,* vol. 28, pp. 1867-1874, 2014.

[118] Z. Lin, X. Juchen, W. Xinyun, and H. Guoan, "Optimization of die profile for improving die life in the hot extrusion process," *Journal of Materials Processing Technology*, vol. 142, pp. 659-664, 2003.

[119] X. S. W. Zutang, "Numerical simulation and experimental investigation of the effect of die profiles on the flow during metal extrusion," *Chinese Journal of Mechanical Engineering*, 1989.

[120] B. S. Yigezu, P. Jha, and M. Mahapatra, "The key attributes of synthesizing ceramic particulate reinforced Al-based matrix composites through stir casting process: a review," *Materials and Manufacturing Processes*, vol. 28, pp. 969-979, 2013.

[121] S. Suresha and B. Sridhara, "Wear characteristics of hybrid aluminium matrix composites reinforced with graphite and silicon carbide particulates," *Composites Science and Technology*, vol. 70, pp. 1652-1659, 2010.

[122] A. Baradeswaran and A. E. Perumal, "Wear and mechanical characteristics of Al 7075/graphite composites," *Composites Part B: Engineering*, vol. 56, pp. 472-476, 1// 2014.

[123] M. Ramachandra and K. Radhakrishna, "Effect of reinforcement of flyash on sliding wear, slurry erosive wear and corrosive behavior of aluminium matrix composite," *Wear*, vol. 262, pp. 1450-1462, 5/10/ 2007.

[124] V. B. Prasad, B. Bhat, Y. Mahajan, and P. Ramakrishnan, "Effect of extrusion parameters on structure and properties of 2124 aluminum alloy matrix composites," 2001.

[125] C. Padmavathi, A. Upadhyaya, and D. Agrawal, "Effect of microwave and conventional heating on sintering behavior and properties of Al–Mg–Si–Cu alloy," *Materials chemistry and physics*, vol. 130, pp. 449-457, 2011.

[126] G. Abouelmagd, "Hot deformation and wear resistance of PM aluminium metal matrix composites," *Journal of Materials Processing Technology*, vol. 155–156, pp. 1395-1401, 11/30/ 2004.

[127] I. Ozdemir and M. Toparli, "An investigation of Al-SiCp composites under thermal cycling," *Journal of composite materials*, vol. 37, pp. 1839-1850, 2003.

[128] C. Ramesh, R. Keshavamurthy, and G. Naveen, "Effect of extrusion ratio on wear behaviour of hot extruded Al6061–SiC p (Ni–P coated) composites," *Wear*, vol. 271, pp. 1868-1877, 2011.

[129] X. Xia, H. J. McQueen, and H. Zhu, "Fracture Behavior of Particle Reinforced Metal Matrix Composites," *Applied Composite Materials*, vol. 9, pp. 17-31, 2002// 2002.

[130] K. M. Shorowordi, A. S. M. A. Haseeb, and J. P. Celis, "Velocity effects on the wear, friction and tribochemistry of aluminum MMC sliding against phenolic brake pad," *Wear*, vol. 256, pp. 1176-1181, 6// 2004.

[131] C. S. Ramesh, S. K. Seshadri, and K. J. L. Iyer, "A model for wear rates of composite coatings," *Wear*, vol. 156, pp. 205-209, 1992/07/30 1992.